GENERAL ATOMIC
DIVISION OF GENERAL DYNAMICS

GA-3872

RADIATION EFFECTS ON SILICON SOLAR CELLS

by

V. A. J. van Lint, J. W. Harrity, H. Horiye
S. W. Kurnick, D. K. Nichols, D. P. Snowden,
E. G. Wikner, and M. E. Wyatt, Jr.

FINAL REPORT

Contract NAS7-91

National Aeronautics and Space Administration

February 15, 1963

GENERAL ATOMIC

DIVISION OF

GENERAL DYNAMICS

JOHN JAY HOPKINS LABORATORY FOR PURE AND APPLIED SCIENCE

P.O. BOX 608. SAN DIEGO 12. CALIFORNIA

GA-3872

Copy No.

RADIATION EFFECTS ON SILICON SOLAR CELLS

FINAL REPORT

Work done by:

V. A. J. van Lint
S. K. Boehm
D. M. J. Compton
C. M. Faulkner
R. F. Goff
J. W. Harrity
H. Horiye
N. Hubble
S. W. Kurnick
D. K. Nichols
D. P. Snowden
E. G. Wikner
M. E. Wyatt, Jr.

Report written by:

V. A. J. van Lint
J. W. Harrity
H. Horiye
S. W. Kurnick
D. K. Nichols
D. P. Snowden
E. G. Wikner
M. E. Wyatt, Jr.

Contract NAS7-91
Covering period of December 1, 1961, through December 31, 1962
National Aeronautics and Space Administration
General Atomic Project No. 258

February 15, 1963

ABSTRACT

Experiments have been performed to study the defects introduced into silicon by high energy (~ 30 Mev) electron irradiation. These defects are expected to be similar to those produced by high-energy protons. The diagnostic tools used include measurements of galvanomagnetic coefficients, excess carrier lifetime, electron-spin resonance, and infrared absorption. The results indicate that the A center in quartz-crucible-grown silicon is not the primary excess-carrier recombination center. Instead, recombination in quartz-crucible-grown and floating-zone refined silicon appears to be dominated by the same center. This center exhibits a strong dependence of the excess-carrier lifetime on excess-carrier density, with increasing lifetime at higher densities. The temperature dependence of the excess carrier lifetime appears to indicate an ionization energy of approximately 0.12 ev, and this same level is seen in the galvanomagnetic measurements. However, this activation energy may not be real, due to a strong temperature dependence of the recombination cross sections. A variety of other energy levels have been identified by the galvanomagnetic measurements and the rates of introduction of defects have been measured.

CONTENTS

CONTENTS (CONT.)

FIGURES

FIGURES (CONT.)

FIGURES (CONT:)

FIGURES (CONT.)

I. INTRODUCTION

This is the final report on National Aeronautics and Space Administration Contract NAS7-91, "Radiation Effects on Silicon Solar Cells," and covers work performed during the period December 1, 1961 through December 31, 1962.

The purpose of this research program was to study displacement defects introduced in silicon by high-energy nuclear radiation, with emphasis on those defects responsible for changes in the excess carrier lifetime in silicon. The decrease in carrier lifetime is generally responsible for the degradation of silicon solar cells exposed to a radiation environment, such as that found in space applications. Of particular concern is the effect of high-energy protons ($E > 10$ Mev) on silicon, because such protons are the predominant defect-producing radiation in the inner Van Allen belt. The present program has been concerned primarily with providing an understanding of the nature of the defects and the manner in which they are produced by a combination of radiation and annealing processes. The aim of the program is to develop, through this understanding, a method of doping silicon so that the defects, after they have undergone thermal motion and have formed a stable secondary defect, are inactive as far as producing carrier lifetime changes is concerned.

This problem has been attacked by utilizing a number of diagnostic tools to investigate the defects introduced. It is known that high energy radiation, particularly high-energy protons and electrons that produce small clusters of defects, produces a number of different defect-energy states and that the interpretation of any particular experimental measurement in terms of a simple one-level model is likely to be unsuccessful. On the other hand, to be able to untangle the effects of a number of defects acting simultaneously, it is necessary to have fairly specific diagnostic tools so that the multiplicity of data may be used to determine the multiplicity of parameters associated with simultaneous defects.

The diagnostic techniques which have been used include the following:

1. Galvanomagnetic measurements,
2. Excess carrier lifetime measurements,
3. Electron spin resonance measurement, and
4. Infrared absorption measurements.

Of these techniques, the most emphasis was placed upon the galvanomagnetic and lifetime measurements. The ESR studies were restricted to a measurement of the concentration of A centers. The infrared absorption measurements were also performed to detect A centers and to confirm the presence of oxygen in the quartz-crucible-grown silicon. In terms of sensitivity to a small concentration of defects, the excess carrier lifetime measurements are the most sensitive; the galvanomagnetic studies are next in sensitivity; the ESR technique, third; and the infrared absorption measurements are the least sensitive.

In Section II of this report, we will present the background for this research program, including the present understanding of the processes of displacement radiation effects, particularly as it relates to a comparison of the effects of the different types of primary radiations, and an analysis of previously published experimental work on radiation effects produced by electrons in silicon. Section III discusses the experimental techniques used. The various types of experimental measurement are then discussed separately in Sections IV through VII. A summary and conclusion section (Section VIII) will discuss the over-all results deduced by comparing the results of the different experimental measurements. Section IX presents a list of personnel who have contributed to this research program, together with brief statements of their duties.

II. BACKGROUND

2.1 DISPLACEMENT RADIATION EFFECTS

The processes which occur when high energy nuclear radiation bombards a single crystal of silicon can be described by the following sequence of events:

1. A bombarding particle collides with an atom in the crystal.
2. The atom recoils from its lattice position and moves through the crystal, losing energy by collision with other atoms and displacing some of them.
3. When the kinetic energy imparted to the initial recoil atom and the subsequent secondary recoil atoms is dissipated, the displacements may produce temporary defects such as vacancies, interstitials, and, possibly, aggregates of these. The defects may not be thermally stable unless the temperature of the sample is very low.
4. The defects undergo thermal motion unless the temperature of the sample is maintained very low, and, as a result of the thermal motion, secondary stable defects are formed which are not significantly mobile at the sample temperature.
5. These stable defects affect the physical properties of the material.

We will now discuss briefly our present understanding of each of the steps in this sequence of events.

2.1.1 Primary Collisions

The collisions between a fast-moving primary particle, such as a high energy electron, proton, or neutron, and a crystal can validly be described as a collision with a single atom, without taking into detailed account the fact that the target atom occupies a position in a crystalline lattice. The energy binding the target atom to the crystal lattice can be approximated by an effective threshold energy. If, during the two-body collision, energy greater than the threshold energy is imparted to the atom, it will be displaced from its lattice site. If the imparted energy is less than the threshold energy, it will be dissipated as vibrational energy of the lattice. In describing the interaction of the primary particle with the atom, no further account need be taken of the other atoms in the lattice. The impact parameters significant for this interaction, if displacements are to result, are very much smaller than the average distance between atoms in a crystal and, hence, multibody collisions are not significant.

The cross sections for this primary collision process are well known. They have been studied by nuclear physicists for more than twenty years and are certainly sufficiently well known for displacement radiation effects analysis. In particular, the interaction between a charged particle, such as an electron or proton, and an atom, can be described by the Coulomb electrostatic interaction between the moving charge of the particle and the charge of the atomic nucleus. Since, to produce a displacing collision, the impact parameter has to be much shorter than the radius of the K electron orbit, the shielding effect of the orbital electrons can be neglected. This interaction has a cross section, given by the familiar Rutherford formula, which, for non-relativistic velocities, is proportional to the reciprocal of the energy of the incident particle. At relativistic velocities, such as those achieved by high energy electrons, the cross section becomes approximately independent of the primary energy. The energy spectrum of the recoil atoms for charged primaries is roughly proportional to $1/E^2$, where E is the recoil energy. This energy spectrum is heavily peaked for energies just above the threshold energy for diplacement of a recoil atom, and the average of this energy spectrum increases only logarithmically with increasing upper limits on the recoil energy.

If neutrons are the incident particles, the interaction must occur via the short-range strong nuclear force field. This interaction can be described reasonably well by a billiard ball type of collision (hard sphere) with a cross section of a few barns. The cross section is comparatively insensitive to both energy and the nature of the target foil. The energy spectrum of the secondary recoil in this case is approximately uniform between the minimum and maximum displacement energy transfer. The maximum possible energy transfer is approximately equal to 4/A times the energy of the incident neutron, where A is the mass number of the target atom.

As seen from the foregoing arguments, the average energy imparted by a charged particle, such as a proton, to a recoil atom is very much less than the average energy imparted by a neutron, even though the maximum possible energy transfer, which corresponds to a head-on collision between the incident particle and the nucleus, may be the same for a proton and neutron. It can be shown, as in Table 1, that the average energy transfer for the collision of a high energy proton with a silicon target nucleus is much closer to the average energy transfer for a high energy electron collision than it is for a high energy neutron collision.

Table 1

PERTINENT INTERACTION PARAMETERS
FOR RADIATION EFFECTS IN SILICON

Bombarding Particle	Energy Loss $\left(\frac{\text{Mev cm}^2}{\text{g}}\right)$	Range (g/cm^2)	Scattering Length (g/cm^2)	Displacement Cross Section (b)	Average Number Displaced Atoms Per Collision	Maximum Number Displaced Atoms Per Collision
Electrons						
0.02 Mev	44	8×10^{-4}		0	0	0
0.2 Mev	7.7	4.5×10^{-2}		16	1	1.6
40 Mev	3.0	15		75	5	5000
Gammas						
0.1 Mev			8			
0.7 Mev			14			
2 Mev			25			
Protons						
10 Mev	35	0.16		3500	6	5×10^{4}
100 Mev	5.9	10		350	7	5×10^{5}
500 Mev	2.4	143		75	8	2.5×10^{6}
Neutrons						
0.025 ev			20	0	0	0
1 Mev			10	4	2.5×10^{3}	5×10^{3}
14 Mev			25	2	3.5×10^{4}	7×10^{4}

2.1.2 Motion of the Recoil Atom

Once a recoil atom of a particular energy has been produced in the primary collision, it can be assumed that the subsequent events are determined by the energy spectrum of this recoil. For high-energy recoils (> 1 kev), the pertinent interaction processes are now reasonably well understood, at least up to the point at which appreciable ionization occurs. A silicon atom having an energy less than 100 kev is moving at velocities appreciably less than the classical orbital velocity of its most loosely bound electrons. Hence, one would expect that the atom would retain all of its electrons during its motion through the lattice and that its energy loss would primarily be due to elastic collisions with other neutral atoms during which the respective electron clouds interpenetrate.

Recent experimental results at General Atomic indicate that some ionization may occur for energies as low as 25 kev. However, for energies up to at least 100 kev in silicon, the primary mechanism of energy loss probably remains elastic scattering, producing secondary displaced atoms. By the same argument, based upon relative velocities of orbital electrons and colliding particles, it can be assumed that the interactions for these recoil atoms with other atoms should be described by a velocity-independent potential. Measurements of the range-energy relation of recoil atoms in solids at General Atomic have established a form for the appropriate interatomic potential. These measurements indicate that an interatomic potential, calculated from a variational approach to the Thomas-Fermi-Dirac model by Abrahamson, et al.,[1] leads to agreement with the range-energy experiments.

At low energies (< 1 kev), more complicated effects are expected to become dominant because the pertinent impact parameters become comparable to interatomic distances in a crystalline lattice. In this region, we might expect multibody collisions to become important, with such manifestations as focusing chains.[2] Of course, the silicon lattice is probably open enough so that the long-range focusing observed in close-packed lattices such as copper and gold will not be effective. This low energy region of the recoil atom motion is not well understood at present, although reasonably good models are available for the high-energy motion. It should be noted that most of the recoils resulting from charged particle bombardment are in this low-energy region, whereas most of the displacement production by neutrons occurs in a higher energy region. At very high energies (> 100 kev), the recoil atom velocity becomes comparable to or greater than the classical orbital velocity of the more loosely bound electrons, and the recoil is likely to be charged for an appreciable fraction of a motion. In this case, the Coulomb field of the atom has a long range and can produce appreciable electronic ionization in atoms at significant distances from the recoil path. The energy lost in these ionization processes will not appear as a relatively permanent displacement radiation effect; it will only serve to change temporarily, the electronic properties of the material. For example, this ionization would generate excess carriers which may temporarily affect the conductivity of the silicon, particularly the reverse conductance across a rectifying junction. Since the relaxation time for the excess carriers is rather short, it is expected that, in a relatively steady-state radiation environment, such as space radiation, the manifestation of the transient radiation effect will be a function primarily of the dose rate. In practical electronic devices, dose rates of less than 10^3 rad/sec will probably not produce significant transient radiation effects. Hence, these effects will be ignored in the present analysis, which is applicable to silicon solar cells in a space radiation environment.

2.1.3 Formation of Temporary Temperature Defects

When the energy imparted to the recoil atoms by collision with the incident particles has been dissipated by secondary collisions within the solid lattice, temporary defects are formed. The simplest version of these defects is interstitial atoms and vacancies. A vacancy is defined as an unoccupied lattice site. The interstitial atom is located between occupied lattice sites. In many materials either one or both of these members of a Frenkel pair are thermally unstable at room temperature. There is evidence to suggest that in silicon the vacancy is mobile above 160°K. The annealing kinetics of interstitital atoms are not known; hence, in an irradiation at room temperature, some of these defects are not expected to persist but are expected to undergo thermal motion. Of course, it is possible, by performing irradiations and subsequent measurements at very low temperatures, to stabilize the temporary defects by minimizing the thermal energy available to them.

2.1.4 Thermal Motion of Defects and Formation of a Stable Defect

Thermal motion of many of the simpler radiation-induced defects is known to occur at temperatures below room temperature. Again, the simplest model assumes that the motion of either an interstitial or a vacancy would result in the recombination of one of these with the other and the subsequent annihilation of both defects. Unfortunately, in practice, the annealing kinetics are rarely this simple, and the usual result of thermal motion of the defect is the formation of a thermally-stable secondary defect. One example of secondary defects is the divacancy, which can be formed by the agglomeration of two vacancies during their migration. Another example, frequently seen in silicon, is the association of the mobile defect with an impurity or defect originally present in the lattice before irradiation. An example of this in silicon is the A center, which is the association of a mobile vacancy with an interstitial oxygen atom to form a thermally-stable substitutional oxygen. Another example is the migration of a vacancy to a position next to a phosphorus donor where it forms a thermally-stable E center. These examples illustrate that many of the secondary defects involve original chemical impurities which, as in the case of the A center, are frequently unintentional and unsuspected. It is this feature of radiation effects, in which a chemical impurity present in the lattice before irradiation plays a controlling factor in the nature of the thermally-stable resultant defect, that gives hope for radiation-hardening of the material. One needs to deliberately insert chemical impurities which act as sinks for the mobile defects, such as vacancies, and result in a thermally-stable secondary defect which is inactive as a recombination center.

2.1.5 Effect of Stable Defects on Properties of a Material

An important consideration is the magnitude of the effect a particular stable defect has on the pertinent properties of a material. To make a device resistant to radiation, it is not necessary to eliminate defects from the material entirely. Instead, it is much more feasible to form defects which have a minimum effect on the physical properties important to the operation of a device. For example, in the case of silicon used in solar cells, the important physical property is the carrier-recombination lifetime. For example, an A center in n-type silicon is expected to be a very effective carrier-recombination center; hence, its formation by radiation must be inhibited. On the other hand, an A center in p-type silicon is expected to be much less effective as a recombination center and, therefore, the choice of p-type silicon over n-type silicon may not change the rate of production of these defects but may improve the radiation resistance simply by minimizing the effect of the defect. However, in p-type silicon, donors are introduced by high-energy radiation, and these donors may act as effective recombination centers. Other manifestations of stable secondary defects in silicon include change of net acceptor or donor density, change of optical transmission, and change of the carrier mobility. However, these changes are not expected to have a major effect on the operation of a silicon solar cell. These changes do furnish valuable laboratory tools to diagnose the nature of the defects introduced and, hence, these properties are used in this measurement program.

2.2 COMPARISON OF DIFFERENT PRIMARY RADIATIONS

Of particular interest in this research program is a comparison of the effects produced by different types of primary radiation and different energies of each type. This comparison can be effected most readily by considering the first step in the processes discussed in Section 2.1; that is, the primary collision between the incident particle and a single atom. Considering the sequence of events, it is reasonable to expect that the radiation effect produced by a recoil atom of a given energy will be independent of the means whereby this recoil atom was created. A comparison of the cross sections for production of recoil atoms and the average energies of these recoil atoms has been shown in Table 1.

For example, as shown in Table 1, the average total number of displaced atoms per primary displacement collision, for 40-Mev electrons, is quite similar to that for 10- to 100-Mev protons. The maximum number of displaced atoms per displacing collision is much larger for protons because the proton is more massive than the high-energy electron. However, this maximum number does not appreciably affect the nature of

the displacement damage produced, since a collision with such a large energy is unlikely. As a result of these calculations, it is shown that the cross section for producing a recoil by a 10-Mev proton is approximately 50 times the cross section for producing a recoil by a 40-Mev electron. These calculations also show that the energy spectrums of the recoils produced in these interactions are very similar. It is therefore reasonable to expect that a flux of 40-Mev electrons 50 times greater than a flux of 10-Mev protons would produce the same degree of radiation displacement effects within the irradiated volume. Of course the absorption length for the 10-Mev protons is very much smaller than for 40-Mev electrons; hence, in practical devices, the gradient in damage production as a function of distance from the surface would have to be considered. However, the nature of the damage produced would be the same in both cases.

Very high-energy protons ($\sim$ 500-Mev) will produce nuclear stars, in addition to the Rutherford scattering interaction summarized in Table 1. The recoils of the residual nuclei from these nuclear stars can, in turn, produce a significant amount of displacement radiation effects. It can be shown that these recoil-produced displacements are reasonably similar to those produced by high-energy neutrons from a nuclear reactor. In both cases, the number of displaced atoms per displacing collision amounts to at least 1000, although the number for the nuclear-star-induced recoils is significantly larger than for the neutron-induced recoils. Nevertheless, the structure of the diplacement cascade is such that it would be unlikely for a qualitative difference to occur between the larger displacement cascades from star recoils and the displacement cascades from fast neutron collisions. Only a quantitative difference should relate the total size of the cascade,and the total number of displaced atoms should be apparent.

In the research program conducted under this contract, high energy electrons were used exclusively as the irradiating particle. This choice was based upon reasonable simulation of high-energy proton damage by the electrons, as well as the experimental convenience of using electrons rather than protons. These electrons can irradiate uniformly samples of appreciable thickness. The electrons are available in the direct beam from a linear accelerator at either high or low intensities. The electron beam in its single pulsed mode can also be used to measure the excess carrier lifetime in the material. Hence, the same accelerator and irradiation equipment used for measuring this lifetime can be used for producing the damage.

2.3 CALCULATION OF THE TOTAL DEFECT INTRODUCTION RATE

As a specific example of the foregoing discussion, the total rate at which defects are introduced into silicon by high energy electron

irradiation can be calculated from the following assumptions:

1. Energy transfer between a high energy electron and a silicon atom occurs via the Coulomb electrostatic interaction.
2. The displacement of atoms can be characterized by a threshold energy, T_d. The atom is not displaced for energies imparted to it that are less than T_d. For energies greater than T_d, the atom is always displaced.
3. The motion of the primary recoil atoms through the lattice can be characterized by hard sphere scattering for purposes of calculating the total number of displacements produced. The probability that secondary displacements occurred can be evaluated by assuming that the distribution of energies imparted to the secondaries is uniform between zero and the maximum possible energy transfer.
4. The interstitials and vacancies produced are isolated and do not interact to form more complicated defects.
5. No secondary annealing reactions take place.

Obviously, assumptions 4 and 5 do not apply for silicon irradiated at room temperature. However, this calculation estimates the total number of defects produced and affords a comparison with the experimental results whereby one can deduce the fraction of the defects actually seen in a given experiment.

The calculation of the total number of displaced atoms has been described by Seitz and Koehler.[3] The cross section for displacing an atom from its lattice, σ_d, in which it must receive an energy of at least T_d, is given by the following expression:

$$\sigma_d = \frac{\pi}{4} b'^2 \left[\left(\frac{T_m}{T_d} - 1 \right) - \beta^2 \log \frac{T_m}{T_d} + \pi\alpha\beta \left\{ 2\left[\sqrt{\frac{T_m}{T_d}} - 1 \right] - \log \frac{T_m}{T_d} \right\} \right]$$

where $b' = \dfrac{2Z_2 e_o^2 c^2}{m_o \lambda \beta^2}$,

$T_m = 2E/Mc^2 (E + 2m_e c^2)$,

E, v are the kinetic energy and velocity of the electron,

$\beta = v/c$, $\gamma = (1 - v^2/c^2)^{-\frac{1}{2}}$,

$\alpha = Z_2/137$,

Z_2, M_2 are the atomic number and mass number of the target atom, and

e_o, m_o are the charge and mass of the electron.

For large T_m/T_d, the formula approaches

$$\sigma_d \approx \pi Z_2^2 \left(e_o^2/m_o c^2\right) \left(\beta^4 \gamma^2\right)^{-1} \left(T_m/E_d - 1\right)$$

The threshold energy T_d has been chosen at two possible values: 12.9 ev and 25 ev. The absolute threshold for which silicon atoms can be displaced from their lattice has been measured to be 12.9 ev by Lofersky and Rappaport.[4] However, it is probably not true that an atom receiving more than 12.9 ev will always be displaced from its lattice position. Instead, it is quite likely that an ever increasing probability of displacement is associated with increasing energies above this threshold. The value 25 ev has been chosen as an effective threshold for multiple displacement production by high energy electrons. The assumption is that a displacement probability equal to zero for energy < 25 ev and equal to one for energies > 25 ev is a reasonable approximation to the continuously increasing displacement probability curve which has its threshold at 12.9 ev.

The total displacement primary cross section calculated from the above formula for electrons of energy 30 Mev is 75 barns for the 12.9 ev threshold, and 39 barns for the 25 ev threshold. The average total number of displaced atoms in collisions resulting from Rutherford scattering cross section has been given in Ref. 3 by the following formula:

$$\bar{\nu} = \left[0.885 + 0.561 \log\left(\frac{T_m}{4T_d}\right)\right] \frac{T_m}{T_m - E_d} .$$

Evaluated for 30-Mev electrons on silicon, $\bar{\nu} = 4.94$ for the 12.9 ev threshold, and $\bar{\nu} = 4.57$ for the 25 ev threshold.

The total number of displaced atoms, N_d, per unit volume per electron per cm^2, is equal to the product of the displacement cross section, σ_d, the average number of total displacements per displacing collision, and the number of atoms per unit volume. N_d is calculated to be 18.5 for the 12.9-ev threshold, and 8.9 for the 25-ev threshold.

It should be noted that this calculated rate at which diplacements are produced by high energy electrons is greater by approximately an order of magnitude than the measured rate of introduction of the A centers in pulled silicon. This fact has important implications. In our simplest analysis, we assume that all vacancies produced by irradiation migrate at room temperature to an interstitial oxygen atom, forming the substitutional oxygen or A center. On the other hand, it appears from this fact that only ~10 percent of the vacancies suffer this fate, and the other ~90 percent must be accounted for by some other annealing mechanism.

2.4 ANALYSIS OF PREVIOUS EXPERIMENTAL WORK

Previously published work on electron irradiation of silicon has been analyzed in terms of three known defect centers. The following subsections discuss the measurements which we ascribe to the A center, the E center, the J-C center, as well as some measurements which cannot be fitted into any of these categories and, hence, must be considered as evidence for other defect centers.

2.4.1 The A Center

The A center has been identified as a substitutional oxygen atom in the silicon lattice.[5] It is presumably formed by the thermal motion of a lattice vacancy created by irradiation until it migrates to an interstitial oxygen atom which drops in substitutionally. The A center is an acceptor state approximately 0.17 ev below the energy level of the conduction band. Hall coefficient measurements indicated the ionization energy to be $0.16 + 1.1 \times 10^{-4}$ T.[6] Its acceptor status is deduced from its action in removing carriers from the conduction band and also from the fact that mobility measurements indicate that it is singly charged for the Fermi level above the defect energy level and is neutral for the Fermi level below the defect energy level.[6]

The model proposed for the A center has been verified in detail by electron spin resonance and infrared measurements,[5, 7] including studies of the effect of a lattice distortion on the relaxation rate of the interatomic bonds. For example, it was observed that the thermally activated switching of the oxygen bonds from one pair of silicon atoms to another requires an activation energy of 0.38 ± 0.04 ev.[5]

The introduction rate of the A centers in pulled silicon crystals by 1-Mev electrons is approximately 0.072/cm to 0.14/cm. The introduction rate appears to decrease for the more heavily doped samples ($>10^{16}$ donors/cm^3), indicating that these donor atoms may compete with the oxygen atoms for the vacancies.[8] The A center production rate in floating zone-refined material is much smaller than it is in pulled silicon. Furthermore, a sample irradiated at 20°K, and subsequently annealed up to 300°K, exhibited only 2.5 percent of the A centers produced in similar material irradiated at 300°K.[8]

The A centers can be studied by infrared techniques utilizing a 12-micron vibrational absorption band ascribed to the substitutional oxygen.[7] This absorption can also be compared with the 9-micron band associated with the vibrational resonance of interstitial oxygen. Infrared measurements are best adapted to the higher concentrations of A centers in that it is difficult to see less than 10^{16} A centers/cm^3 by the 12-micron

band absorption.

The annealing of the A centers, as observed by either its 12-micron infrared absorption or electron spin resonance, is the same, indicating an activation energy of about 1.3 ev. The anneal occurs at 330°K.[7]

Studies of excess carrier recombination rates in p-type silicon indicated that the A center was dominant in this recombination and that the cross sections for both hole and electron capture were near 2×10^{-15} cm^2.[6] The equality between these two cross sections is surprising because usually one of them is associated with an attractive Coulomb potential, and the other with a neutral defect site. More recent studies of lifetime in n-type silicon[9] indicate that degradation could be explained by a hole-capture cross section of 4×10^{-14} and an electron-capture cross section of 1×10^{-15}, evaluated at 300°K. These observations, if confirmed, will eliminate the need for the close-spaced pair model proposed to interpret the earlier data.[10] The role of the A center in lifetime changes is also confirmed by early annealing studies[11] which indicate that the activation energy for annealing of lifetime changes in both n- and p-type pulled silicon crystals was 1.3 ev, in agreement with the subsequent studies utilizing infrared absorption and electron spin resonance.

The presence of the A center can also be detected by a 5.5-micron infrared absorption band associated with the excitation of electrons from the A center to the conduction band. This absorption and its associated photoconductivity are observed only in n-type silicon with the Fermi level above the A center position.

Irradiation of silicon by Co^{60} gamma rays also produces A centers. The production rate observed in 2 ohm-cm pulled silicon was 1.3×10^{-3}/cm. In floating zone-refined material of the same resistivity, the production rate was only 0.8×10^{-3}/cm.[12] In 12 ohm-cm pulled material, the carrier removal rate was less than in 2 ohm-cm silicon, amounting to 1×10^{-3}/cm.[13]

Wertheim has offered an explanation for the lack of production of A centers during the anneal following a low temperature irradiation.[14] His model discusses the interatomic potential between a latice vacancy and the interstitial atom as it leaves. He assumes that, in the first nearest position, the potential barrier for annealing the interstitial back to its original vacancy is slightly lower than for moving farther away. The lower temperature annealing would give preference to interstitial-vacancy recombination, whereas the high temperature anneal associated with room temperature irradiation would lead to a higher probability of escape of the interstitial resulting in A center formation.

2.4.2 The E Center

The E center is an acceptor state reported to have an energy either 0.43 ev[8] or 0.38 ev[15] below that of the conduction band. It is produced predominantly in floating zone n-type silicon in lieu of the A center. For example, the carrier removal rate associated with the E center in floating-zone n-type silicon was 0.26/cm for 1-Mev electrons, whereas, for similar pulled silicon crystals, the E center contribution was only 0.005/cm.[15] It does not appear to be a primary radiation-induced defect because irradiation of floating-zone refined silicon at 78°K produced a lower rate of formation of the E center of 0.07/cm.[15] Electron spin resonance studies have indicated that the E center consists of a vacancy next to a substitutional phosphorus donor.[8]

Although no detailed studies of the annealing characteristics of the E center have been reported, it was noted that lifetime changes anneal faster in floating-zone material than in pulled silicon crystals.[11]

In 2 ohm-cm floating zone silicon, the carrier removal rate associated with the E center by Co^{60} gamma rays was 1.0×10^{-3} cm^{-1}.

2.4.3 The J-C Center

Electron spin resonance measurements have suggested that the energy of the J center, previously observed in the lower half of the energy gap, was possibly one of the two or three energy levels associated with different charge states of the same defects (C center).[16] Early observations located the J center energy level at $[0.268 + 5 \times 10^{-5} T]$ ev above the energy of the valence band.[15] Recombination rates in n-type silicon were ascribed to this level, resulting in cross sections for electron capture and for hole capture of 10^{-14} cm^2, and 8×10^{-13} cm^2 respectively, assuming an introduction rate of 5×10^{-3}.[6] The introduction rate was deduced from the carrier removal rate in p-type silicon of 5×10^{-3}.[17] Recent experiments on lifetime changes in n-type silicon[9] seem to indicate that the A center is responsible and the cross sections quoted above are probably incorrect. Hence, the necessity for another close pair model to explain both the carrier removal and the recombination rates for the J center[10] is probably also removed.

Mobility changes in p-type silicon are consistent with a model of a singly-charged center if the Fermi level is below the energy level of the center, and, under these conditions, there are no other charged sites of comparable density. This fact, together with the carrier removal by this center in p-type silicon, indicates that it is a donor which has a positive charge if the Fermi level is below its energy level. The other

centers mentioned, A and E centers, would be neutral with the Fermi level below them and are not expected to contribute to the mobility decrease.

As mentioned previously, the lifetime changes in p-type silicon are probably due to the A center. An attempt to calculate the contributions of the lifetime change from the J center, utilizing the cross sections previously computed from n-type silicon experiments, predicts a much larger effect from the J center than was observed experimentally.[6] However, since these cross sections are probably in error, this discrepancy may no longer be significant.

The 3.9-micron infrared absorption band observed in p-type silicon with the Fermi level below that of the J center is probably associated with the photoionization of electrons from the valence into the J center state.[18] It is associated with photoconductivity which can be ascribed to the holes left in the valence band by this process. The carrier removal rate of J centers in p-type silicon appears to increase from 0.05/cm for 0.7-Mev electrons to 0.3/cm for 4.5-Mev electrons.[19]

2.4.4 Other Centers

In addition to the centers already discussed, there are observations which indicate the presence of other defect centers produced by electron irradiation in silicon. Some very shallow states have been observed by Hill[19] who locates an acceptor at 0.03 ev below the conduction band with an effective introduction rate of 11/cm for 4.5-Mev electrons. He also locates a donor 0.05 ev above the valence band with an introduction rate of 13/cm for 4.5-Mev electrons. These introduction rates are surprisingly large because they are even greater than would be expected from the Seitz-Koehler model with no annealing. At 0.7 Mev, the introduction rates were lower by approximately a factor of 3. The same work indicates that there is an anomalously large mobility change for the Fermi level more than 0.1 ev from either band, since the calculated rate of introduction of ionized impurity is an order of magnitude greater than the carrier removal rate. Wertheim[15] has also searched for shallow levels by irradiating 0.01 ohm-cm n-type and p-type silicon. A spectrum of levels was observed in n-type silicon between 0.05 and 0.16 ev below the conduction band. The carrier removal rate associated with these levels was 0.5/cm, a value significantly lower than the observations of Hill. Irradiation of degenerate p-type silicon produced a carrier removal rate 300 times larger than previously observed in higher resistivity p-type material, suggesting a level quite near the valence band. However, the carrier removal rate observed by Wertheim is still much less than that reported by Hill.

Various infrared absorption bands have been noted which have not been identified with one of the centers discussed before.[18] These include the following:

1. An 8-micron absorption band seen when the Fermi level is more than 0.2 ev below the conduction band. It annealed with an activation energy of 0.8 ev in an apparent mono-molecular fashion. There is no photoconductivity associated with this absorption peak and its introduction seems to be independent of the oxygen content of the sample.[20]
2. A 3.3-micron absorption band is observed if the Fermi level is closer than 0.2 ev to the conduction band. At low temperatures this absorption splits into a triplet at 0.343 ev, 0.359 ev and 0.374 ev. Its production also seems to be independent of the oxygen content of the sample.[20] It is associated with a photoconductivity rise at the high energy side.
3. A 6-micron absorption band is seen in p-type silicon after the 3.9-micron band identified with the electron transition to the J center has annealed. It was seen only when the Fermi level was closer to the valence band than 0.13 ev. Its production was rather erratic and it may be associated with the presence of an unknown impurity in the material.

III. EXPERIMENTAL TECHNIQUES

3.1 ELECTRON LINEAR ACCELERATOR

The irradiation experiments were performed with the General Atomic electron linear accelerator (LINAC). It is a three-section, L-band traveling wave-type with an electron-energy range of 3 to 45 Mev. Pulse widths of from 0.01 to 14 μsec and beam currents of up to 700 ma are available. In addition to single pulse operation, repetition rates of 7.5, 15, 30, 60, 120, 180, 360 and 720 pulses per second are available. For most of these experiments, low current densities (< 10 ma / cm^2) and pulse repetition rates of ≤ 30 pps were used. No dependence of displacement radiation effects on irradiation rate has been observed at these levels. The geometry for a typical irradiation experiment is shown in Fig. 1.

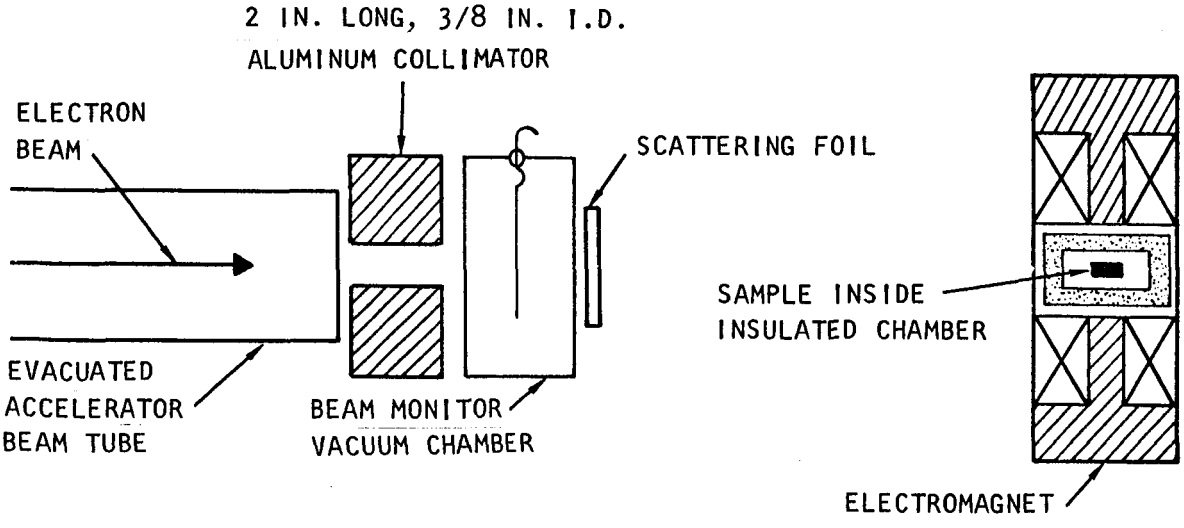

Fig. 1--Irradiation geometry

3.2 DOSIMETRY

During electron irradiations the accelerator beam was continuously monitored by observing the current due to secondary electrons knocked out of a 0.0008-in. titanium foil mounted in an evacuated chamber situated behind a 3/8-in. collimator at the accelerator beam window.

A wide-band amplifier transmitted the signal to the remote monitoring station, where it was displayed on an oscilloscope. During a steady-state irradiation an integrating circuit and a strip chart recorder were used to record the average rate at which the beam was delivered.

To calibrate the beam intensity at the sample position in terms of the titanium foil monitor reading, a Faraday cup could have been used as an absolute standard. A thin calorimeter, which is a much more convenient secondary standard, was used for all calibrations in experiments reported here. The thin calorimeter consists of a small copper block, to which a copper-constantan thermocouple is attached, mounted in one of our standard sample boxes. The rate at which the temperature of the copper block changes when the beam is incident on it provides a measure of electron beam intensity.

3.3 MATERIAL AND SAMPLE PREPARATION

The silicon boules were obtained from a number of different suppliers. The quartz-crucible pulled crystals were grown by Mono Silicon, Inc., Knapic Electro Physics, Inc. and Merck and Co. The crystals from the latter two suppliers were all phosphorus doped and were obtained through the Hughes Aircraft Co. The floating-zone grown crystals, both phosphorus and boron doped, were obtained from Merck and Co. The arsenic-doped floating-zone grown crystals were obtained from Sylvania Electric, Inc. All crystals were grown along the $[111]$ axis.

The silicon crystal boules were first sliced with a diamond wheel into samples with dimensions of 1 by 2.5 by 12 mm. These samples were then lapped successively with 400 grit, 600 grit, 2/0, and 4/0 emery papers. Next they were etched with a mixture of equal parts of glacial acetic acid, concentrated nitric acid and hydrofluoric acid, after which they were washed in alcohol. The procedure then varied according to the type of silicon being prepared.

3.3.1 Preparing n-type Silicon

For n-type silicon, the following method was used. The ends of the sample were roughened with 600-grit emery paper and electroplated with nickel using a solution of 105 parts by weight of nickel ammonium sulfate, 15 parts of ammonium chloride and 15 parts boric acid.[21] The sample was then washed in alcohol and carbon tetrachloride and placed in a quartz jig for the gold bonding operation. The jig held 4 small dots of 0.5 percent antimony-doped gold against the sample at the voltage and Hall lead positions. It was spring-loaded to allow for contractions due to the melting of the gold dots during the bonding. The jig and sample

were placed in an oven and heated for about 10 minutes in a flow of forming gas to 450°C and then cooled slowly. The sample was then taken from the jig and additional nickel was plated onto the current ends. The nickel was masked with enamel and etched again, after which the masking was removed and the sample washed in alcohol. It was then tinned with cerroseal solder.

One mil copper wires were soldered to the gold buttons. A copper-constantan thermocouple was soldered to one gold button and used both as a thermocouple and as a Hall lead. Soldering to the gold buttons was accomplished by first tinning the copper wire, leaving a small ball of solder on the end. The solder ball was then heated in contact with the gold button with a small jet of hot helium gas. Usually a little flux was needed to fuse the solder to the gold. Next the current leads were soldered to the end of the sample which was then washed in electronic grade alcohol to complete the preparation of the sample.

3.3.2 Preparing p-type Silicon

The following method was developed for attaching leads to p-type silicon. After the sample was etched, the ends were roughened with 600-grit emery paper and electroplated with a rhodium plating solution obtained from Englehard Industries, Inc. The ends were tinned with indium solder and the current leads attached. The thermocouple was also attached to one end. The sample was then washed with electronic grade alcohol. The point contact voltage leads consisted of phosphor-bronze spring wire probes whose ends were fused with aluminum tips. Usually a small amount of sparking with a Tesla coil was needed to obtain a low resistance contact with the sample.

The samples for the electron spin resonance (ESR) and the optical infrared (IR) studies were cut with an ultrasonic cutter. The ESR samples were cylinders, 0.125 in. diameter by 0.250 in. length, with a 0.050 in. hole along the axis which was used as an aid to hold the sample in place during the ESR measurements. The IR samples were cylinders 10 - 20 mm in diameter and about 6 mm in length. The ends of these samples were optically polished.

3.4 IRRADIATION TECHNIQUES

For electron irradiation experiments the sample was mounted in an aluminum sample container (See Fig. 2), placed in a styrofoam insulating box and put between the poles of an electromagnet directly in line with the accelerator beam tube (See Fig. 1). The sample chamber was then evacuated and a slight excess pressure of helium was admitted to the chamber to aid in cooling the sample. The electrical leads were

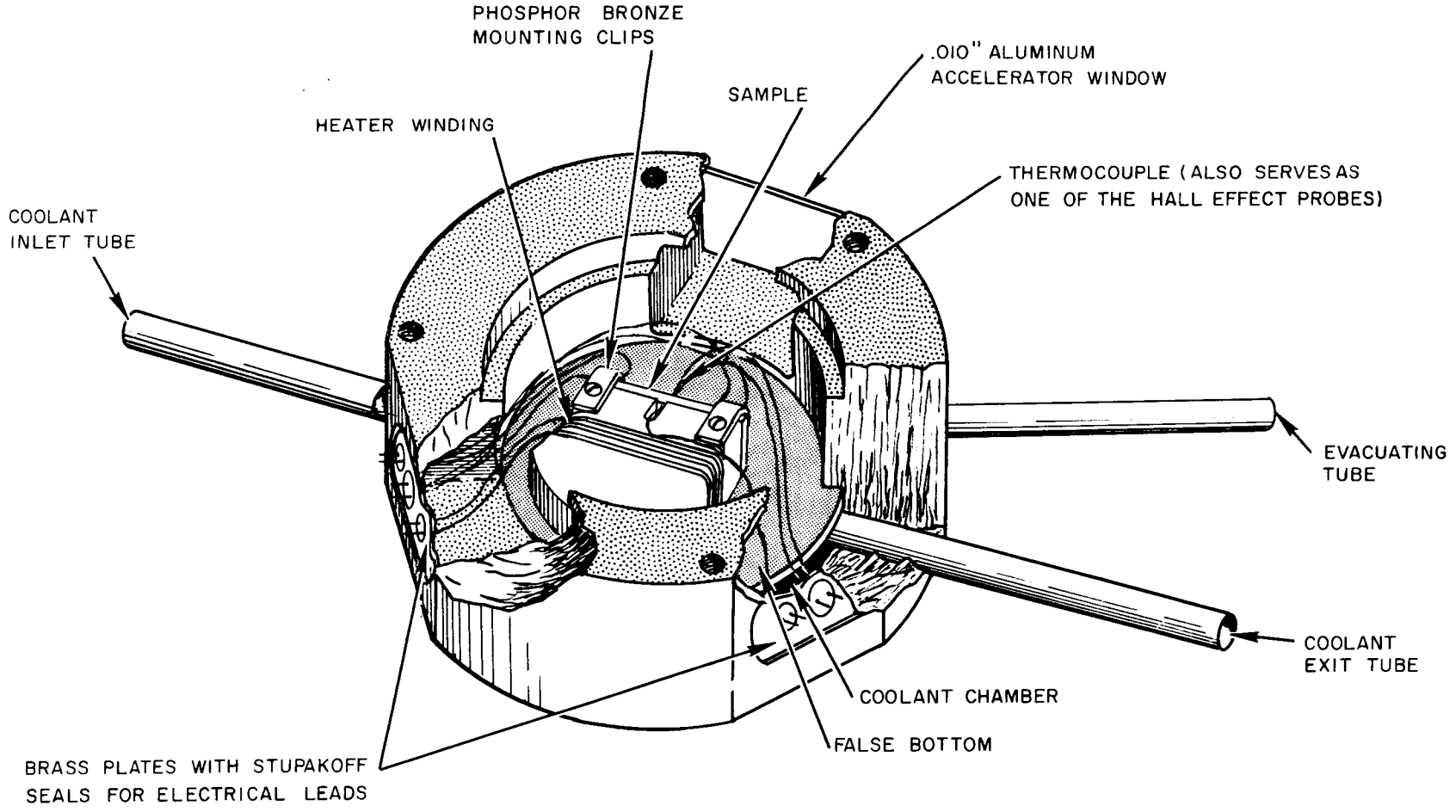

Fig. 2--Improved electron-irradiation sample container

connected to cables running to the monitor station. Sample temperature was monitored by a copper-constantan thermocouple soldered to the middle of the sample. This thermocouple also acted as one of the Hall probes when needed.

For room temperature irradiations, a flow of water was run through the coolant chamber to keep the sample from becoming too warm. When measurements were needed as a function of temperature a flow of liquid nitrogen was run through the coolant chamber. A heater was used to produce temperatures between liquid nitrogen and room temperature and also to make measurements at higher than room temperature.

3.5 LIFETIME AND HALL COEFFICIENT MEASUREMENTS

Figure 3 shows the circuit used to perform lifetime conductivity and/or Hall coefficient measurements. The voltage source, V_o, provides the current through the sample. The resistor, R_m, together with a voltmeter located at the remote monitoring station, measures the steady-state sample current. The 1 K series resistor and 0.1 μf capacitor provide a filter circuit located physically near the sample chamber to minimize rf noise induced in the measuring circuits. The 100 K current-limiting series resistors are located near the sample to minimize the capacitance between the resistors and the sample. The steady state value of the potential between two voltage probes on the sample is monitored with the assistance of a remotely-located differential voltmeter. When the ac measuring circuit is used, relays disconnect the dc voltage measuring circuit and the thermocouple to eliminate the capacitance and rf noise induced in the long measuring leads. The change in voltage across the sample during and after a radiation pulse is observed with a differential amplifier having a push-pull output driving two identical RG-62U triaxial cables to the remotely located recording oscilloscope. The wave-forms were photographed with a camera mounted on the oscilloscope.

The differential amplifier with push-pull output is the standard amplifier system used for our radiation effects experiments. It consists of a Tektronix Type G input, a main amplifier consisting of a replacement vertical amplifier for a Tektronix 545 oscilloscope, and a specially designed pair of high-current cathode-follower output stages. This system has a rise time of 30 mμsec when utilized with a Tektronix 551 oscilloscope having another Type G differential preamplifier. It also has the capability of performing measurements out to dc, although the noise level makes it wise to perform accurate low-level dc measurements with a separate voltmeter, as shown in Fig. 3. The use of the push-pull feature of the main amplifier and cable driver minimizes rf noise in the measuring circuit.

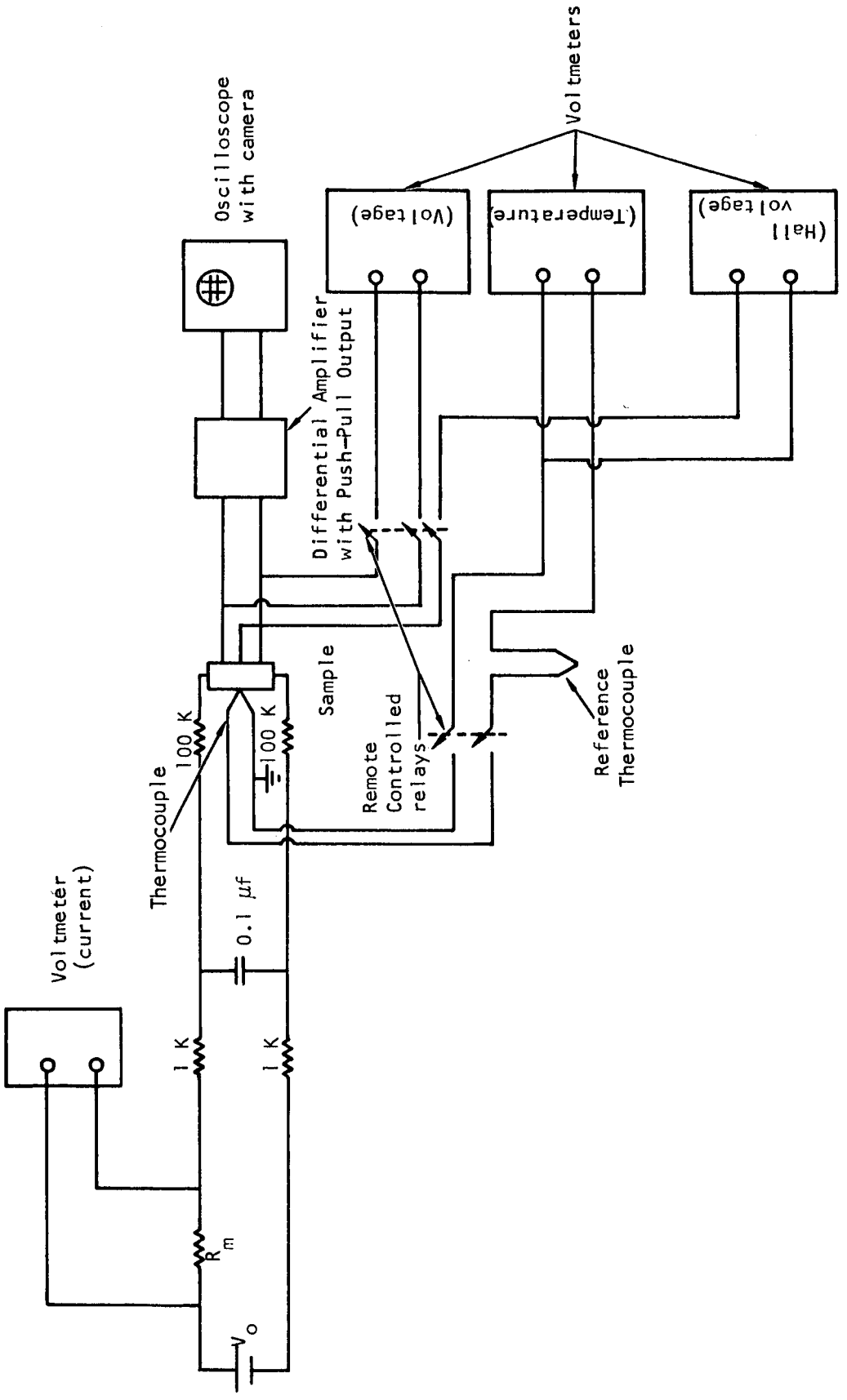

Fig. 3--Circuit used to perform lifetime, conductivity and/or Hall coefficient measurements

For all dc measurements of sample current, voltage, and Hall voltage, Hewlett-Packard Model 425A voltmeters were used. The outputs of these meters were fed to Varian Model G-11A strip-chart recorders to give a continuous record of changes during irradiation.

Two electromagnets were used in the course of our investigations. One, used at the LINAC during bombardment, has 2-in. diameter pole faces and a gap adjustable from 1/2 in. to 2-1/2 in. The field of this magnet can be reversed by remote control and is continuously variable up to 4000 gauss at a gap of 1-1/2 in. During irradiations, the magnet was positioned so that, when the magnetic field was off, the beam passed between the pole faces. The sample container was then placed in the magnet so that the sample was in the center of the magnetic field. The field was turned on during brief recesses in the irradiation to measure the Hall coefficient.

The other electromagnet, situated in the laboratory, was used for Hall effect measurements in temperature runs before and after irradiation. It has 3-in. diameter shaped pole pieces and a fixed 1-3/4-in. gap. It is water-cooled and is capable of producing fields up to 12 kilogauss.

3.6 INFRARED ABSORPTION

The infrared absorption measurements were made with a Perkins-Elmer 112 spectrometer. This instrument may be used interchangeably as a prism spectrophotometer or a grating spectrophotometer with the grating used interchangeably in the Littrow mirror mount. As a prism spectrophotometer, the instrument is capable of operating between 0.2 and 35 microns, dependent on the prism material chosen. As a grating spectrophotometer with a diamond window-detector (Golay cell), the instrument can be operated up to about 125 microns. Available with the Perkins-Elmer instrument is a helium-temperature cryostat mounted at the exit port of the spectrophotometer. During the present measurements, the cryostat was used only as a sample mount, and the sample was maintained at room temperature.

Shown in Fig. 4 is a block diagram of the optical equipment used. It is noted that the sample is always inserted at the exit port to avoid the full radiation energy hitting the sample (when measured at the entrance to the spectrophotometer). Since we are particularly interested in the measurement of small absorption coefficients ($\mu < 2/\text{cm}$), the samples were sufficiently thick ($t \sim 0.6$ cm) so that the absorption would be detectable even by rough visual inspection. Of course, the introduction of such a thick sample would alter the focusing of the infrared energy on the sample, but this error has been shown to be negligible by direct

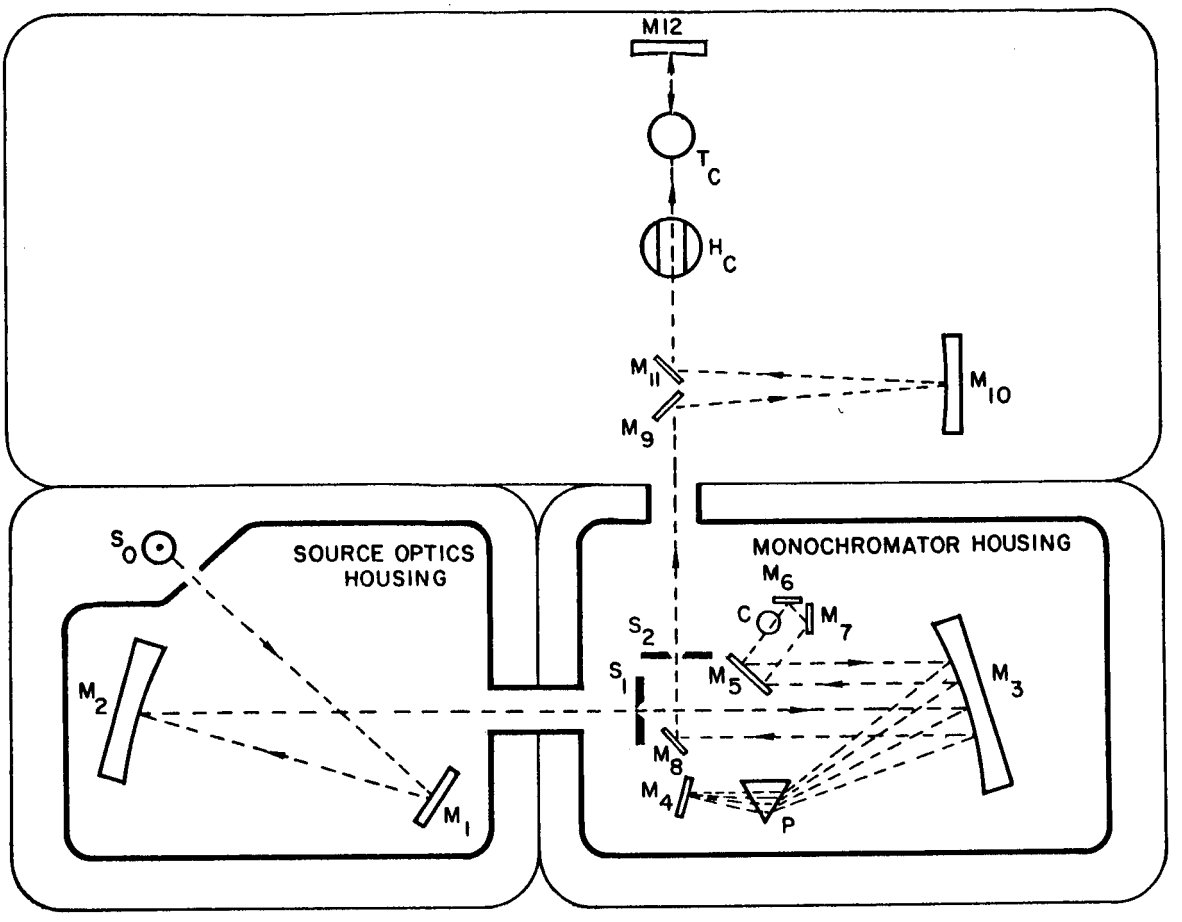

S_0 GLOBAR SOURCE

$M_1, M_4, M_5, M_6, M_7, M_8, M_9, M_{11}$, = PLANE MIRRORS

M_2, M_{10}, M_{12} = CONCAVE MIRRORS

M_3 14° OFF AXIS PARABALOID MIRROR

P= PRISM

H_C = HELIUM CRYOSTAT

S_1, S_2 = SLITS

T_C = THERMOCOUPLE DETECTOR

C = 13 CYCLE CHOPPER

Fig. 4--Optical equipment used for infrared absorption measurements

comparison of the absorption curve of an unirradiated sample with that provided in the literature.

3.7 ESR MEASUREMENTS

The ESR experiments were performed using superheterodyne crystal detection and field modulation.[22] A block diagram of the spectrometer is shown in Fig. 5. The internally stabilized X-band signal generator feeds power into the magic-T which is split between arms 2 and 3. Arm 2 has the reflection cavity with the sample. The reflection from the cavity is bucked out in arm 4 by the reflection from arm 3 which is adjusted by the precision attenuator and phase shifter in that arm. The signal appearing in arm 4 is fed into a balanced mixer which receives the local oscillator power from the second internally stabilized supply. The output of the mixer then passes through the 60 Mc amplifier, second detector, audio-amplifier and lock-in detector to the strip chart recorder.

For oscilloscopic observation of the frequency dependence of the power reflected from the cavity (as monitored in arm 2) the signal klystron is frequency-modulated by application of a saw-tooth voltage derived from the oscilloscope sweep and applied to the klystron. Unloaded cavity Q is measured by subtracting from the signal proportional to the power reflected from the cavity, a second signal proportional to the incident power. In this manner a signal proportional to the power absorbed in the cavity is obtained. From this latter signal the cavity resonant frequency and width at half-power is obtained. Frequency is measured roughly by means of a cavity wavemeter and more precisely by means of a transfer oscillator and high speed counter.

In the conventional manner, a small low-frequency ac magnetic field is superposed on the dc field so that ac detection techniques may be employed, thereby eliminating dc drifts which occur after the second detector in the i.f amplifier. The field modulation coils which provide this ac field are mounted on the pole faces inside the shims of a Varian 6 in. electromagnet. The field coils are driven by a 60-watt power amplifier providing up to 70 gauss peak to peak at 1 Kc and 80 gauss peak to peak at 100 cps. A signal from the oscillator which drives the power amplifier is also fed to the phase-sensitive lock-in detector which provides the output. Resonance signals are displayed by slowly sweeping the dc magnetic field through the value for resonance and displaying the output of the lock-in detector on a strip chart recorder.

The microwave cavity is a right circular cylinder and oscillates in a TE_{011} mode. The silicon samples used were 1/8 in. in o. d. and 1/4 in. in length and were mounted on nylon rods with a sleeve of

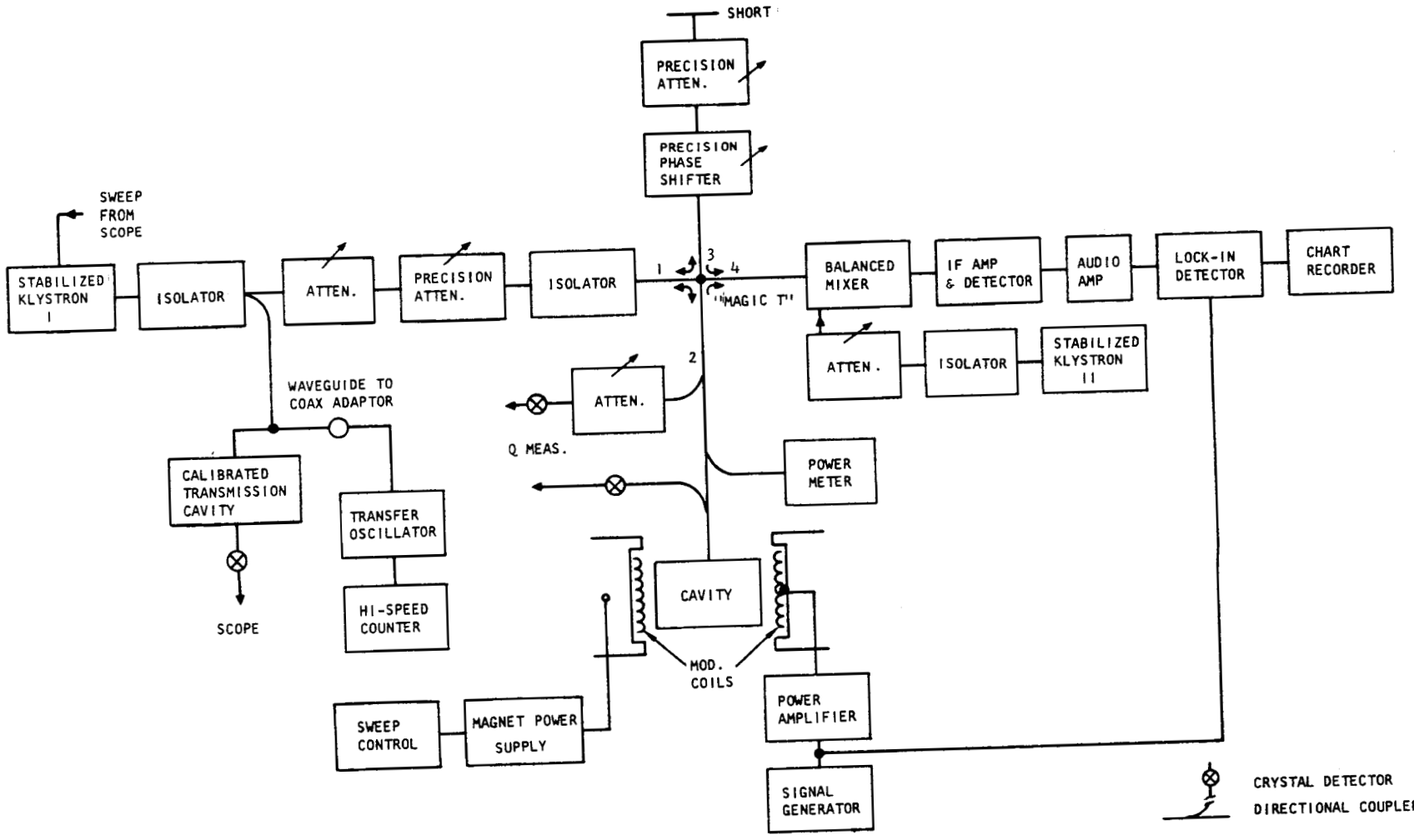

Fig. 5--Block diagram of ESR spectrometer

Teflon tubing to hold the assembly together. For measurements made thus far, samples were mounted in this manner after irradiation. The samples were placed in the center of the cavity on axis. The microwave magnetic field is polarized vertically along the cavity axis at this location and the dc magnetic field is horizontal and normal to the microwave field. Rotation of the sample about the axis of the cavity around a $[110]$ direction permits measurement of the resonance as a function of crystal orientation.

The cryostat used in the ESR studies is shown schematically in Fig. 6. It is designed to be used with a Varian 6-in. or 12-in. electromagnet. Provision is made for the addition of a liquid nitrogen heat shield with the large vacuum spaces at top and bottom being used for storage tanks.

An irradiation station two inches from the bottom of the inner dewar is provided with 0.001-in. stainless steel windows to allow passage of an irradiating electron beam. After irradiation, the sample is raised to a position in the microwave cavity approximately 6 in. above the irradiation station. Since the cavity is pressurized with helium to prevent entrance of liquid, the sample and sample rod pass through seals at the bottom of the cavity and the top of the cryostat.

Provision for continuous pump-out of the vacuum space is made for use with Viton O-rings or the space may be sealed off and indium O-rings used. The temperature of the liquid in the cryostat may also be lowered by pumping on the exhaust. The cavity was immersed in coolant contained in a metal dewar for measurements at low temperatures and was pressurized with helium to exclude the coolant from the interior of the cavity and thus prevent bubbles from introducing noise. Sample insertion was made by means of a Veeco vacuum quick coupling at the top of the dewar, thus permitting the sample to be changed at any time.

A powdered phosphorus-doped silicon marker was used that contained 10^{14} spins at 78°K with a line width of two gauss.* Its g-value was far enough removed from the A centers so that they could be easily distinguished.

3.8 DATA ANALYSIS

In the course of the experimental work described, there were two primary types of data, characterized by slow and fast time resolution. Measurements of such characteristics as the steady-state current and the average voltage across a sample, the thermocouple voltage, and the

*We are indebted to Prof. G. Feher, of the University of California, San Diego, California, for providing us with this sample.

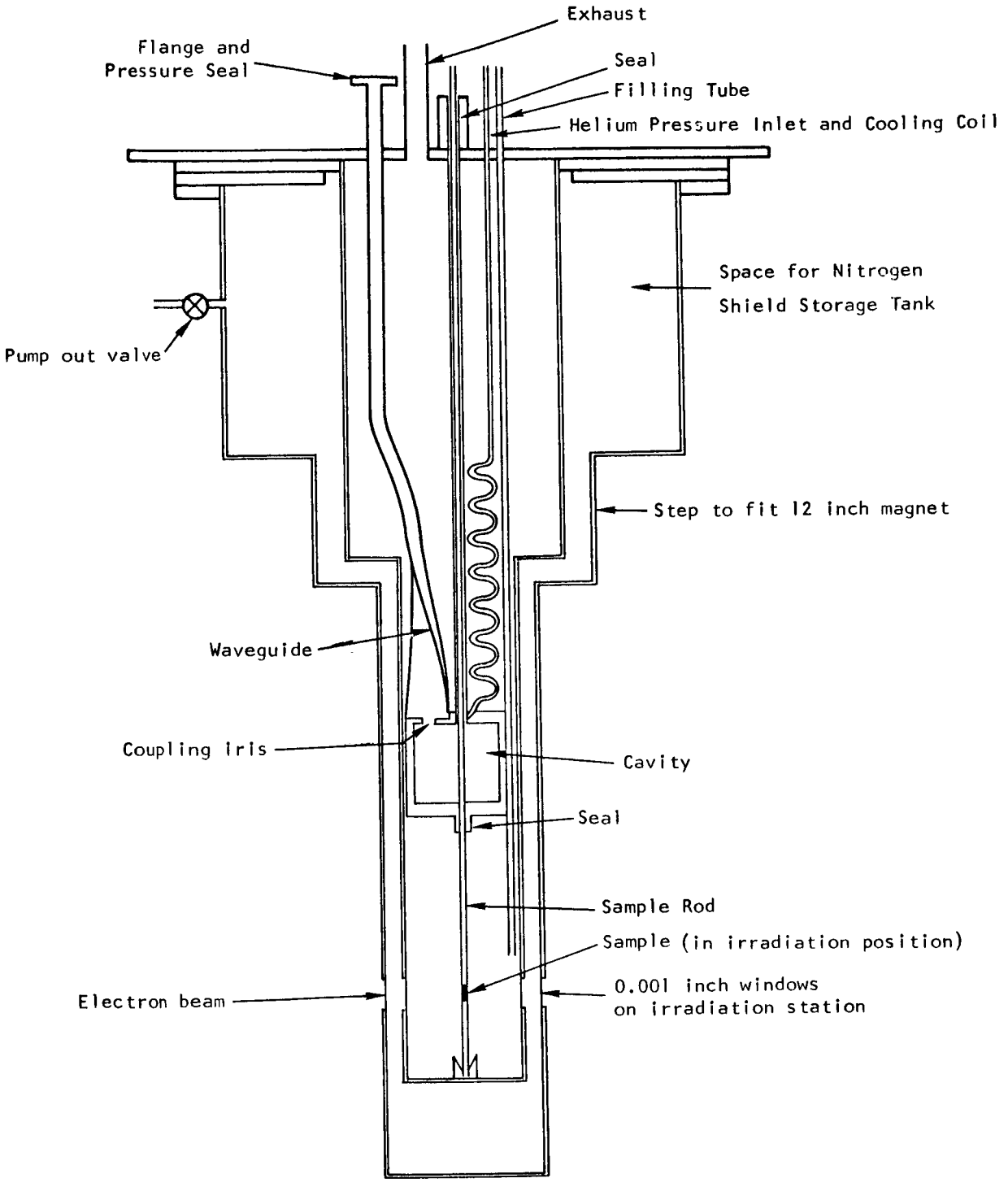

Fig. 6--Cryostat (dewar) used in ESR studies

voltage between the Hall probes, were performed with slow time resolution by a vacuum tube voltmeter and recorder system. These data were recorded on strip charts and subsequently read off manually for appropriate reduction and replotting in the form of conductivity, reciprocal Hall coefficient and Hall mobility vs temperature and irradiation flux. The fast time resolution data consisted of oscilloscope photographs of the change in voltage across the sample during and after a short accelerator irradiation pulse. These measurements were used to deduce the rate of recombination of excess carriers. A large number of data points were acquired by this method and the data reduction process could be very laborious. Therefore, a special system, developed in connection with other programs at General Atomic, was used to facilitate data reduction.

The primary information, as transmitted to the recording station by the special amplifier system at LINAC, was displayed on a Tektronix Type 551 dual-beam oscilloscope. The upper beam of the oscilloscope was reserved for displaying the signal from the amplifier observing the voltage across the sample; the lower beam always displayed a voltage proportional to the radiation monitor signal, usually in integrated form to be proportional to the integrated flux per pulse. These data were photographed by a special oscilloscope camera using Tri-X 70 mm film, resulting in transparent negatives of the oscilloscope trace. After development, each photograph was mounted against the face of another cathode-ray tube connected to a special film reading system. The beam of this cathode-ray tube was adjustable manually in the horizontal and vertical direction. It was first adjusted so that the light spot was superposed on the film at the point of the trace corresponding to the beginning of the accelerator beam pulse. Subsequently, it was stepped by equal increments along the horizontal (time) axis and repeatedly superposed under the photograph of the oscilloscope trace. The voltage necessary to deflect the cathode-ray tube beam onto this image was recorded each time by a digital voltmeter coupled to a Friden tape punch. In this fashion, a set of voltmeter readings were punched onto the tape which were proportional to the deflection of the oscilloscope beam at equal time increments along the oscilloscope trace. Voltages corresponding to a set of auxiliary data were also punched onto this same tape. These voltages corresponded to such items as photograph identification, the gain of the amplifier and oscilloscope, sweep speed, dc current through the sample, dc bias voltage across the sample before the radiation pulse, and accelerator monitor signal. The resulting information encoded in the tape was sufficient for the calculation of a quantity proportional to the conductivity of the sample as a function of time. The tape, containing information from a large number of oscilloscope photographs, was then processed by a Friden Flexowriter which

printed out the numbers on a sheet of paper for checking and also punched IBM cards with these numbers. The IBM cards were then processed with a specially encoded computer program by the IBM 7090 computer at General Atomic. The output from the computer consisted of the following items:

1. A listing of the pertinent auxiliary input information
2. A tabular listing of the voltage changes across the sample as a function of time, the conductivity of the sample, and the change in conductivity from its quiescent value
3. A calculation of the mean lifetime corresponding to a least-squares adjusted exponential fit to the change in conductivity as a function of time
4. A quantity measuring the accuracy of the least-squares exponential fit to the data
5. A series of quantities representing areas under the curves of various functions which are useful for comparison
6. A quantity proportional to the mobility of the excess carriers in the semiconductor sample deduced from the change of conductivity per unit radiation flux.

In cases where the fit to an exponential was very good, the lifetime of excess carriers could be assumed to be the least-squares adjusted value. In other cases the excess conductivity as a function of time was plotted on semilog paper, and appropriate regions of this plot were fitted by eye to a slope. In some cases, the excess conductivity decay corresponding to two or three different initial excess carrier densities was measured by changing the intensity of the accelerator radiation pulse. In those cases, the conductivity decay for all the intensities was plotted together on a single semilogarithmic graph to verify the independence of the decay rate, at a particular excess conductivity, from the earlier decay history. In these cases it was noted that, in the measurements for which the small residual noise induced by the linear accelerator power supply in the measurement system was negligible, the accuracy and reproducibility of this measuring system corresponded to a deflection on the original recording oscilloscope of approximately 0.1 to 0.2 mm. This uncertainty was primarily manifested as a shift in the slope of the base line for the oscilloscope photograph.

IV. GALVANOMAGNETIC STUDIES

4.1 THEORY OF GALVANOMAGNETIC MEASUREMENTS

The galvanomagnetic measurements performed for this program included conductivity and Hall coefficient measurements. The magnetoresistance was measured on occasion, but the interpretation of these data is difficult since they are particularly sensitive to uncontrolled quantities such as inhomogeneities in the sample and, hence, these data have not been analyzed.

In considering conductivity and Hall coefficient measurements, we must emphasize the relation between these quantities and the basic parameters of the semiconductor materials and the defects introduced into them. For example, the conductivity, σ, is related to the density of electrons, n, density of holes, p, the charge on the electrons, e_o, and the mobility of electrons and holes, μ_n and μ_p respectively, by the equation

$$\sigma = e_o (n\mu_n + p\mu_p).$$

In extrinsic n-type materials the thermal-equilibrium electron density, n_o, exceeds by far the thermal equilibrium minority hole density, p_o, and hence the thermal-equilibrium conductivity is given by

$$\sigma_o = e_o n_o \mu_n.$$

A corresponding equation applies to a p-type semiconductor. When excess carriers are generated within the material by radiation, they are generated as equal concentrations of electrons and holes, and hence the conductivity in the presence of excess carriers is generally given by

$$\sigma = e_o n_o \mu_n + e_o \Delta n(\mu_n + \mu_p).$$

The Hall coefficient of a sample has been shown to measure primarily the excess carrier density. Hence, in n-type material $1/R_H = r/n\, e_o$, where $r = \mu_H/\mu_c$, the ratio of Hall and conductivity mobilities.

The carrier removal rates quoted in this report among the experimental results are actually $\Delta(1/R_H e_o)/\Delta\Phi$ and not $\Delta n/\Delta\Phi$. The two terms differ by the ratio of the Hall mobility to the drift mobility with $\Delta n/\Delta\Phi$ being approximately 25 percent greater than $\Delta(1/R_H e_o)/\Delta\Phi$. This also holds true for the reciprocal mobilities, with $\Delta(1/\mu)/\Delta\Phi$ being approximately 25 percent greater than $\Delta(1/\mu_H)\Delta\Phi$. The reason for this is that a semiconductor such as silicon has a number of carrier bands, some of which are not spherically symmetrical.[23] For example, the conduction band in silicon has six minima at points along the [100] axis in momentum space. The lower constant energy surfaces are spheroids of revolution centered about the minima, characterized by longitudinal and transverse effective masses, m_e and m_t. $m_e = 0.90\ m_o$, and $m_t = 0.192\ m_o$,[24] where m_o is the electron mass. The valence band is centered about the origin of the Brillouin zone, but consists of three overlapping almost spherical bands, the first two being coincident at the origin. Hence, the top of the valence band contains two types of holes having effective masses; that is, $m_1 = 0.5\ m_o$, and $m_2 = 0.16\ m_o$ respectively. The third band may be very close to the other two ($\Delta E < .05$ ev), and hence may contribute holes even below room temperature.

Even for a single spherically symmetrical energy band the ratio, r, depends on the carrier scattering mode via the velocity dependence of the mean scattering time. The ratio, r, is related to the mean scattering time $\langle\tau\rangle$ and the mean square scattering time $\langle\tau^2\rangle$ by $r = \langle\tau^2\rangle/\langle\tau\rangle^2$. For scattering by acoustic lattice modes, it takes on the value $r = 3\pi/8 = 1.18$. For Coulomb scattering by ionized impurity centers, $r = 315\pi/512 = 1.93$. Furthermore, at temperatures above 50°K, the optical lattice modes significantly limit the mobility and further corrections to r are needed. For example, Long[25] has, in a very pure n-type silicon sample, shown an increase in r from 0.97 to 1.20 over the temperature range 100°K to 400°K. These data were fitted accurately to an appropriate theoretical superposition of acoustic and optical lattice modes with a small contribution from ionized impurity scattering. Moreover, for samples in which ionized impurity scattering is large, r depends on the relative magnitudes of lattice and impurity scattering. A study of ionized impurity scattering in silicon[26] again showed reasonable agreement with theory. Even the temperature dependence of the mobility agreed reasonably well with a calculation by Brooks[27] and Herring, based on various idealizations.

As a result of these considerations, one can, by choosing an average value of ~1.25, deduce the required carrier densities from Hall coefficient data within an accuracy of ± 30 percent. Detailed analysis of the scattering mechanisms in a particular sample and the use of available theoretical and experimental information probably allow the accuracy to be improved to better than 10 percent.

4.1.1 Analysis of Temperature Dependence of Hall Coefficients

It is possible to deduce information about the position of the energy levels responsible for the removal of carriers from the conduction band in n-type silicon, or from the valence band in p-type silicon, by observing the temperature dependence of the Hall coefficient. Consider n-type material as an example. To obtain the acceptor energy levels from Hall coefficient versus temperature measurements, use is made of the two following equations

$$n = N_c T^{3/2} \exp\left[-\frac{(E_c - E_F)}{kT}\right] \tag{1}$$

$$n_A = N_A \frac{1}{1 + \alpha\left\{\exp\left[-\frac{(E_A - E_F)}{kT}\right]\right\}} \tag{2}$$

where

$n \equiv$ density of electrons in the conduction band,

$N_c \equiv$ density of states in the conduction band,

$T \equiv$ absolute temperature,

$E_c \equiv$ energy of edge of the conduction band as measured from the top of the valence band (all energies used based on $E_v = 0$),

$E_v \equiv$ Energy of top of valence band,

$E_A \equiv$ Energy of acceptor level introduced by irradiation,

$E_F \equiv$ Fermi level energy,

$n_A \equiv$ density of ionized acceptor levels,

$N_A \equiv$ density of total acceptor levels,

$\alpha \equiv$ degeneracy factor, and

$k \equiv$ Boltzmann's constant

With the assumption that all other levels beside the one being considered are either full or empty, (i.e., the donor and acceptor levels are widely enough spaced in the gap so that, when the Fermi level is near one, it is more than a few kT away from all the others), the following manipulations may be made:

From Eq. (2)

$$\exp\left[-\frac{(E_A - E_F)}{kT}\right] = \alpha^{-1}\left(\frac{N_A}{n_A} - 1\right)$$

Substituting this into Eq. (1) to eliminate E_F

$$n = N_c T^{3/2}\, \alpha^{-1}\left(\frac{N_A}{n_A} - 1\right) \exp\left[-\frac{(E_c - E_A)}{kT}\right].$$

Taking the natural logarithm of both sides and re-arranging

$$\ln (nT^{-3/2}) + \ln \frac{\alpha}{N_c} - \ln\left(\frac{N_A}{n_A} - 1\right) = -\frac{E_c - E_A}{kT}$$

When $n_A \gtrsim 0.2N_A$, the term containing these quantities becomes negligible compared with the term containing n, thus

$$\ln (nT^{-3/2}) + \ln \frac{\alpha}{N_c} \approx -\frac{E_c - E_A}{kT}.$$

Taking the derivative with respect to $1/T$,

$$k \frac{d}{d(1/T)} \ln (nT^{-3/2}) \approx -(E_c - E_A).$$

Thus from the slope of a plot of $\ln (nT^{-3/2})$ versus $1/T$ the energy level of the acceptor may be found.

Figure 7 is a calculation of the temperature dependence of the electron concentration in n-type Si for various acceptor concentrations. For acceptor concentrations less than the initial donor concentrations, the temperature dependence of the Hall coefficient tends to reveal the energy level of the donor, although the freezing out of carriers onto the donor center is achieved at higher temperatures when the compensation is almost complete. When more acceptors are introduced than the original donor concentration, the acceptor energy level is seen in the temperature dependence of the Hall coefficient. The data in Fig. 7 were calculated from assumed energy levels of the donor at 0.044 ev, and of the acceptor at 0.16 ev, below the conduction band. The density of states in the conduction band, N_c, was assumed to be $5.55 \times 10^{15}\ T^{3/2}\ cm^{-3}$. Figure 7 illustrates quite dramatically the shift of the 0.044 ev slope to higher temperatures, as the compensation is increased, and the eventual transition to the 0.16 ev slope. This calculation can be summarized by saying that the temperature dependence of the Hall coefficient is most effective at revealing that defect center which would be partially occupied by electrons at a temperature of absolute zero. It does not give useful information about deeper levels, because these levels are filled at a higher temperature. It usually reveals these deeper levels at all only if their concentration is almost sufficient to use up the available electrons at very low temperatures.

As a result of these calculations, it should be borne in mind, therefore, that the observed carrier removal rate is due to all the deep lying acceptor states, but that the temperature dependence of the Hall coefficient reveals mostly the highest acceptor state which is being filled by the irradiation. Hence, in case there is more than one acceptor state introduced, it is not necessarily true that the observed carrier removal rate should be associated only with that level revealed by the temperature dependence measurements.

4.1.2 Analysis of Carrier Removal Rate as Function of Initial Resistivity

We will now compute the relation between the rate of radiation-induced carrier removal in a nondegenerate semiconductor and the initial carrier concentration. An n-type semiconductor is assumed for illustration purposes.

The electron density n is related to the position of the Fermi level, E_f, the bottom of the conduction band, E_c, the effective density of states in the conduction band, N_c, and the temperature, T, by

$$n = N_c \exp\left[-(E_c - E_f)/kT\right], \qquad (3)$$

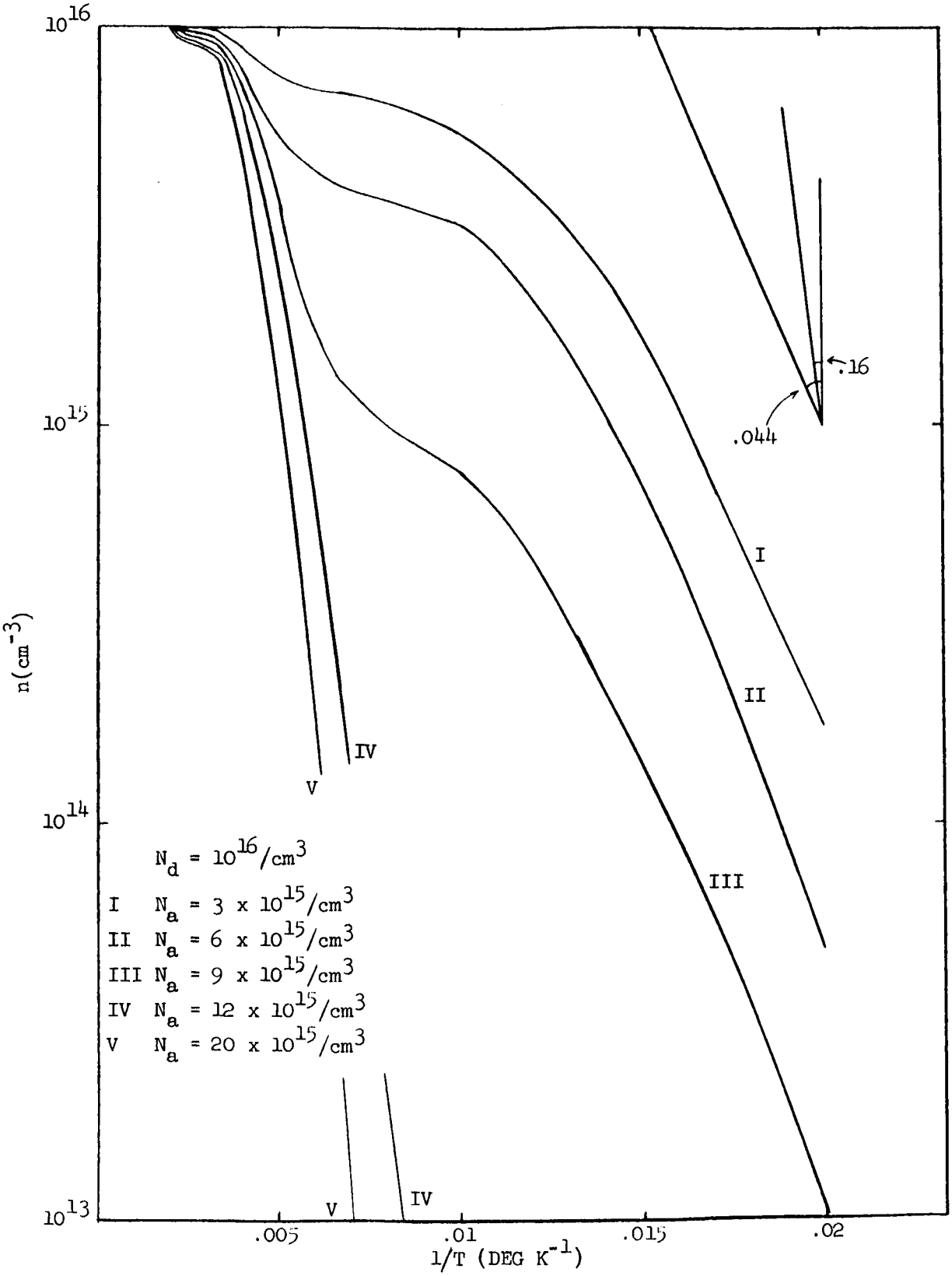

Fig. 7--Electron concentration in n-type silicon as a function of temperature

where $N_c = 5.55 \times 10^{15} T^{3/2}$ using $m^* = 1.1 m_o$. The fraction of acceptor-like trapping centers occupied by electrons, f_T, is given by the Fermi function:

$$f_T = \frac{1}{1 + \alpha_T \exp\left[(E_T - E_F)/kT\right]}, \tag{4}$$

where E_T is the energy of the trapping centers and α_T is a degeneracy factor for the trapping centers. In a similar manner, the fraction of the donor centers occupied by electrons, f_D, is given by

$$f_D = \frac{1}{1 + \alpha_D \exp\left[(E_D - E_F)/kT\right]}. \tag{5}$$

Charge neutrality requires that the change in density of electrons in the conduction band Δn, due to the radiation must be equal to the number of trapping centers introduced, N_T, times the fraction of the centers occupied by electrons, f_T, plus the number of donor centers originally present, N_D multiplied by the change in occupancy fraction, Δf_D,

$$-\Delta n = N_T f_T + N_D \Delta f_D. \tag{6}$$

The foregoing equations can be solved simultaneously for the number of trapping centers introduced,

$$N_T = -\Delta n \left\{ 1 + \frac{\alpha_D N_C N_D \exp\left[-(E_C - E_D)/kT\right]}{\left\{(n_o + \Delta n) + \alpha_D N_C \exp\left[-(E_C - E_D)/kT\right]\right\}\left\{n_o + \alpha_D N_C \exp\left[-(E_C - E_C)/kT\right]\right\}} \right\}$$

$$\times \left\{ 1 + \alpha_T \frac{N_C}{(n_o + \Delta n)} \exp\left[-(E_C - E_T)/kT\right] \right\}. \tag{7}$$

From the observed change in electron density, Δn, and the initial electron density, n_o, the total number of traps, N_T, can be calculated. If the Fermi level is not near the donor center, terms like $(n_o + \Delta n)$ can be neglected by comparison with $\alpha_D N_C \exp\left[-(E_C - E_D)/kT\right]$ and the expression simplifies to

$$N_T \approx -\Delta n\left\{1 + \frac{N_D}{\alpha_D N_C}\exp\left[-(E_C-E_D)/kT\right]\right\}\left\{1 + \alpha_T\left(\frac{N_C}{n_o+\Delta n}\right)\exp\left[-(E_C-E_T)/kT\right]\right\} \qquad (8)$$

Typical values indicate that, for room-temperature irradiations and the donor concentrations used in these experiments, the correction term in the first brackets of Eq. (8) is not significant and one can usually neglect the effect of the change in occupancy of the donor centers. For data taken at lower temperatures, this correction term will be significant.

Utilizing these formulas, the defect introduction rate can now be evaluated from the initial and final carrier densities, taking into account the exact value of the experimentally observed Δn. Alternately, it can be evaluated from the initial rate of change of carriers, in which the Δn term in the brackets can be neglected by comparison with n_o.

A discussion of the degeneracy factors, α_D and α_T is in order. The need for these degeneracy factions in the Fermi function can be derived from the following argument. Consider a metal which can accept an electron in any of g states, but having once accepted a single electron the other g-1 states are no longer available. An example of this is an acceptor center which can accept an electron in either of two equivalent spin orientations but, having accepted one electron, the energy state for the other electron would be very much higher due to Coulomb repulsion. In this case, we can calculate the Fermi function by the following argument. The Fermi function is equivalent to the statement that the ratio of the number of states which are full and available to be emptied, to the number of states which are empty and available to be filled is equal to $\exp\left[E-E_F/kT\right]$. In our model, if the Fermi function for the state is f, the number of states which are full and available to be emptied is equal to fN. The number of states which are empty and available to be filled is equal to $g(1-f)N$. Hence,

$$\frac{fN}{(1-f)gN} = \exp\left[-(E-E_F)/kT\right], \text{ and} \qquad (9)$$

$$f = \frac{1}{1 + \alpha\exp\left[+(E-E_F)/kT\right]},$$

where $\alpha = 1/g$.

The degeneracy factor $\alpha = 1/g$ is usually due to spin degeneracy of the electron. For example, a simple hydrogenic donor like phosphorus can have one electron in the un-ionized state. When it is ionized, it is

capable of accepting an electron in either of two spin states. Hence, the factor g is expected to be 2, and $\alpha = 1/2$ for such a center. The A center represents a similar situation in which an electron can be accepted in either of two spin states. The E center is expected to be different, because in the neutral state the E center already contains an unpaired electron, namely that electron associated with the phosphorus atom. Hence, in accepting another electron, this electron can only be accepted in the spin state opposite to the spin of the electron already present. However, once the E center is negatively charged, it can release an electron equivalently from either of the two spin states; therefore, for the E center, α is expected to be 2.

4.1.3 Analysis of Rate of Change of Hall Mobility with Irradiation

Further information about the defect centers can be deduced from the changes in the Hall mobility, μ_H. Long and Myers[26] give a formula for ionized impurity drift mobility based on the Brooks-Herring formula. This equation may be used to determine the rate at which ionized impurities are introduced by irradiation. This equation is

$$\mu_I = \frac{\eta T^{3/2}}{N_I(\ln b_1 - 1)} \tag{10}$$

where $$\eta = \frac{2^{7/2} k^{3/2} K^2}{\pi^{3/2} q^3 (m^*)^{\frac{1}{2}}}$$

and $$b_1 = \frac{6Km^*(kT)^2}{\pi\hbar^2 q^2 n'}$$

Here $\mu_I \equiv$ drift mobility due to ionized impurity scattering
$T \equiv$ absolute temperature
$N_I \equiv$ density of ionized impurity scatterers
$k \equiv$ Boltzmann's constant
$K \equiv$ dielectric constant
$q \equiv$ electronic charge
$m^* \equiv$ electron effectiveness
$n' \equiv n + (n+N_A)\left[1-(n+N_A)/N_D\right] \approx n$ (for extrinsic material, since $n = N_D - N_A$)
$n \equiv$ density of conduction electrons
$N_A \equiv$ density of ionized acceptors
$N_D \equiv$ density of ionized donors .

By proper manipulation of the equation and by substituting values appropriate to silicon and our experimental conditions, the result becomes

$$\frac{\Delta N_I}{\Delta \Phi} = \frac{5.3 \times 10^{21} \frac{\Delta \left(1/\mu_H\right)}{\Delta \Phi} + 1.25 \Delta \frac{\left(1/R_H e\right)}{\Delta \Phi}}{43.9 - \ln \left(1/R_H e\right)_o}$$

where the values used were

$K = 12$
$m^* = 0.3\ m_o$ (Note: Long and Myers[26] determined experimentally that this is best value for B-H approximation)
$m_o = 9.1 \times 10^{-28}$ gm
$k = 1.38 \times 10^{-16}$ erg/°K
$q = 1.6 \times 10^{-19}$ coul
$T = 290°K$
$\hbar^2 = 1.11 \times 10^{-54}$ erg^2 sec^2
$n = \mu_H/\mu\ (1/R_H e)$
$\mu_H/\mu = 1.25.$

The values of $\Delta N_I/\Delta\Phi$ thus obtained will be the initial rate of introduction of ionized impurities, since initial carrier concentrations and initial carrier removal rates are used.

The assumptions used in this analysis are as follows:

1. The change in mobility is caused entirely be the change in the ionized scattering mobility; i.e., $\Delta(1/\mu)/\Delta\Phi = \Delta(1/\mu_I)/\Delta\Phi$.
2. Only singly charged ionized scatterers are introduced.
3. Positively and negatively charged centers scatter equally.

The use of the Brooks-Herring formula further assumes that:

1. The Born approximation holds; i.e., $\frac{2Km^* kT\epsilon}{\pi\hbar q^2 n'} >> 1$. (Here ϵ is the energy of the carrier)
2. Scattering is describable by a (scalar) relaxation time.
3. Current carriers occupy states on spherical surfaces of constant energy in k-space.
4. Electron-electron interaction can be neglected.
5. Special scattering effects originating in the impurity cell or immediate vicinity can be ignored.

4.2 EXPERIMENTAL RESULTS

For n- and p-type silicon, the conductivity, carrier concentration, and carrier mobility all decrease with irradiation. Evidently the defects formed are of the acceptor type which remove electrons from the conduction band, leading to a decrease in the conductivity and carrier concentration. Also, the defects must form new ionized scattering centers which cause a decrease in the carrier mobility. The Hall and conductivity data will be discussed first.

Various types of samples provided by the Czochralski process, i.e, pulling from a melt in a quartz crucible (QC), or by floating zone refining (FZ), were irradiated at room temperature with electrons of various energies. During the bombardment, a continuous record was kept of the conductivity and, at intervals, the irradiations were interrupted to permit Hall effect measurements to be made. From these data, the reciprocal Hall mobility (proportional to the total carrier-scattering cross section) was calculated and also plotted as a function of electron flux.

After irradiation, the samples were cooled to 78°K and the Hall and conductivity data were taken as a function of temperature. As discussed in Section 4.1, a plot of $\ln(nT^{-3/2})$ versus $1/T$ yields the energy level of the acceptor which is partially filled by electrons. Energy levels obtained in this way are presented below with the other data.

Figure 8 presents the change of conductivity, reciprocal Hall coefficient, and reciprocal Hall mobility during irradiation for a 7 ohm-cm P-doped, n-type QC silicon sample irradiated at 300°K with 30-Mev electrons. Figure 9 is a plot of $\ln(1/R_H e_o T^{-3/2})$ versus $1000/T$ for this same sample. For this sample, cool-downs were performed at various levels of electron flux, with acceptor energy levels being deduced from the linear portions of the curves representing higher flux levels.

A set of curves corresponding to Figs. 8 and 9, but for an 0.5 ohm-cm P-doped QC silicon sample is shown in Figs. 10 and 11. Another similar set for 0.1 ohm-cm, P-doped FZ silicon is shown in Figs. 12 and 13. Another set for 0.4 ohm-cm, P-doped FZ silicon is shown in Figs. 14 and 15.

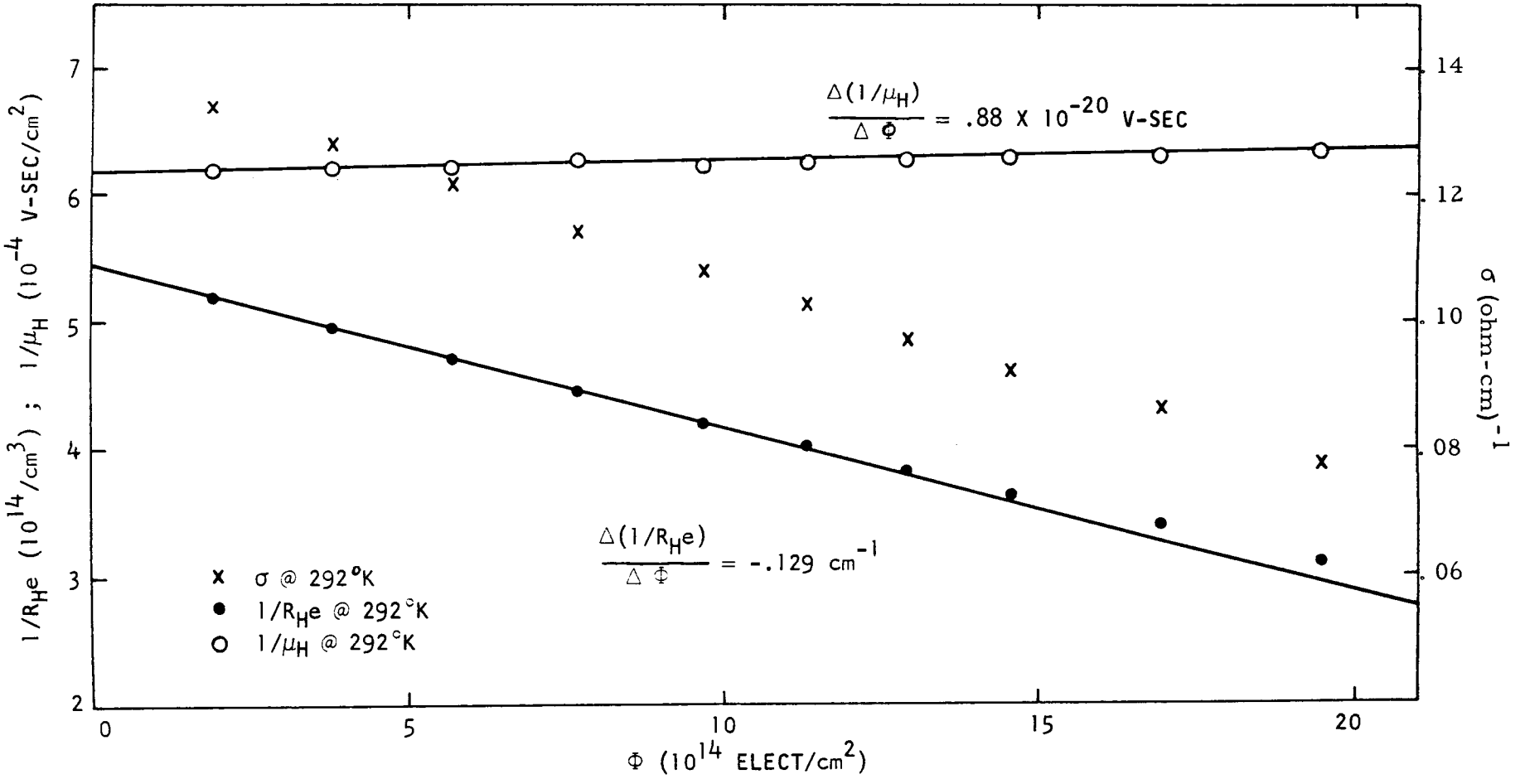

Fig. 8--Galvanomagnetic measurements during irradiation - 7 ohm-cm QC silicon

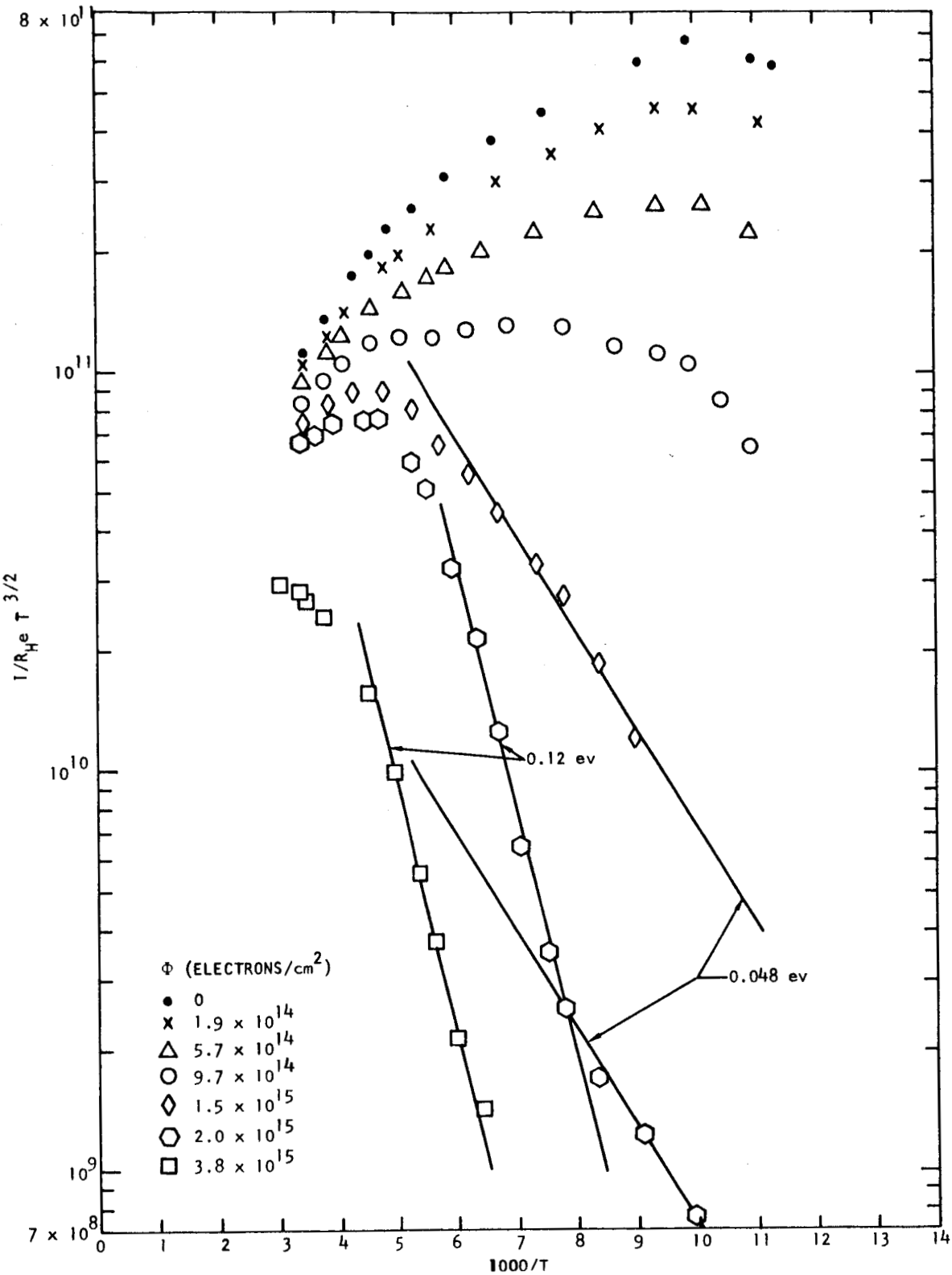

Fig. 9-- Temperature dependence of Hall coefficient - 7 ohm-cm QC silicon

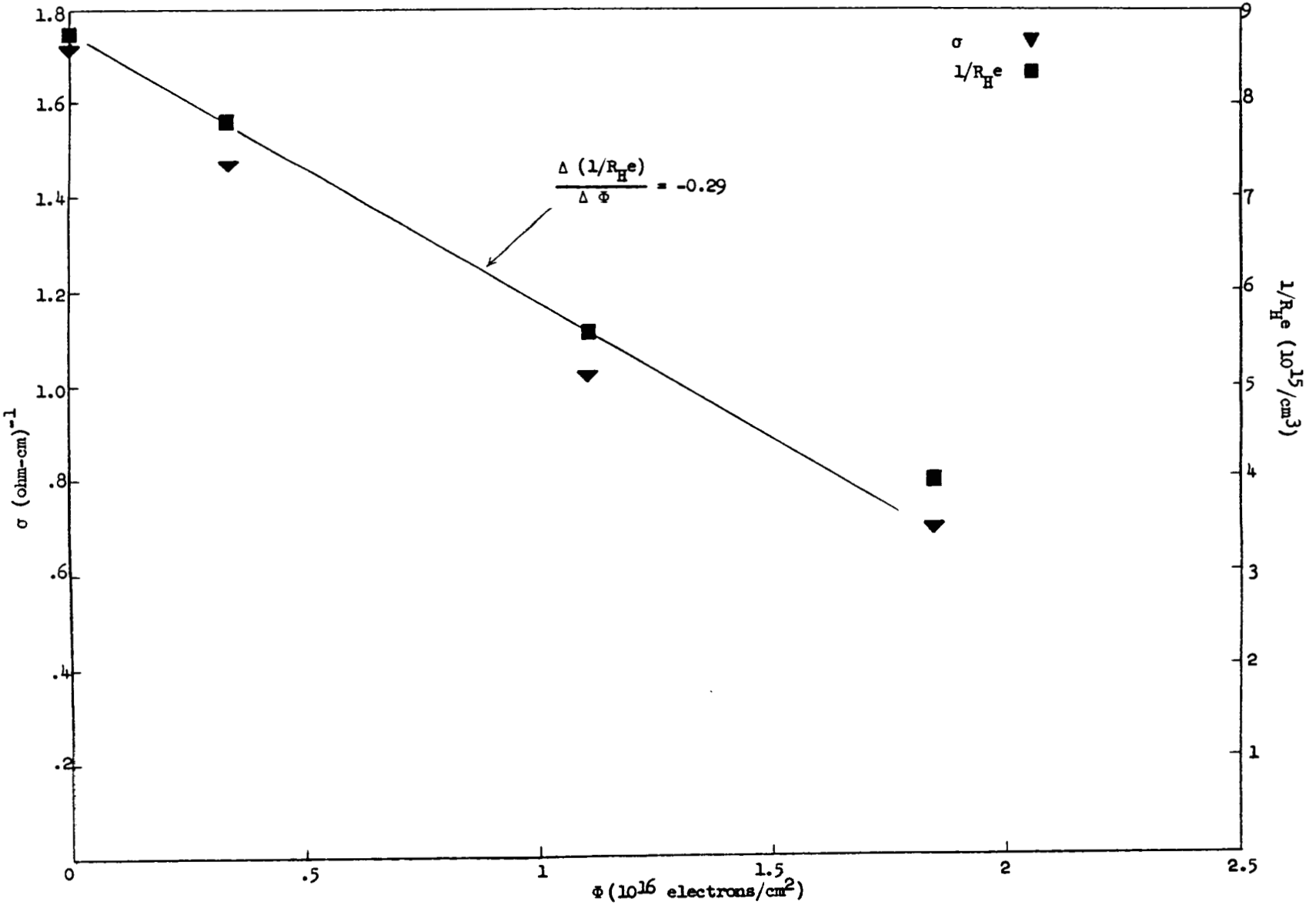

Fig. 10--Galvanomagnetic measurements during irradiation - 0.5 ohm-cm QC silicon

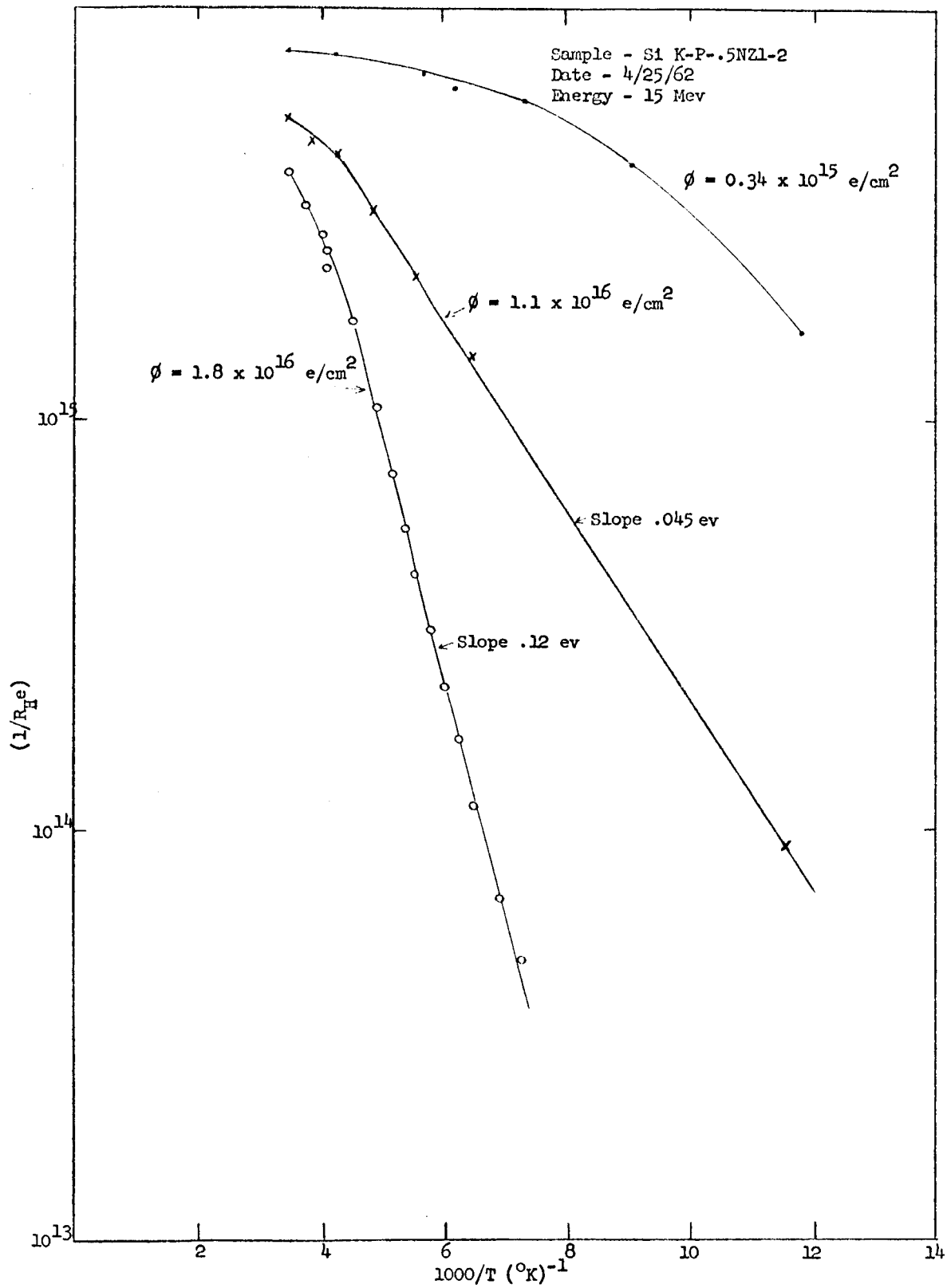

Fig. 11--Temperature dependence of Hall coefficient - 0.5 ohm-cm QC silicon

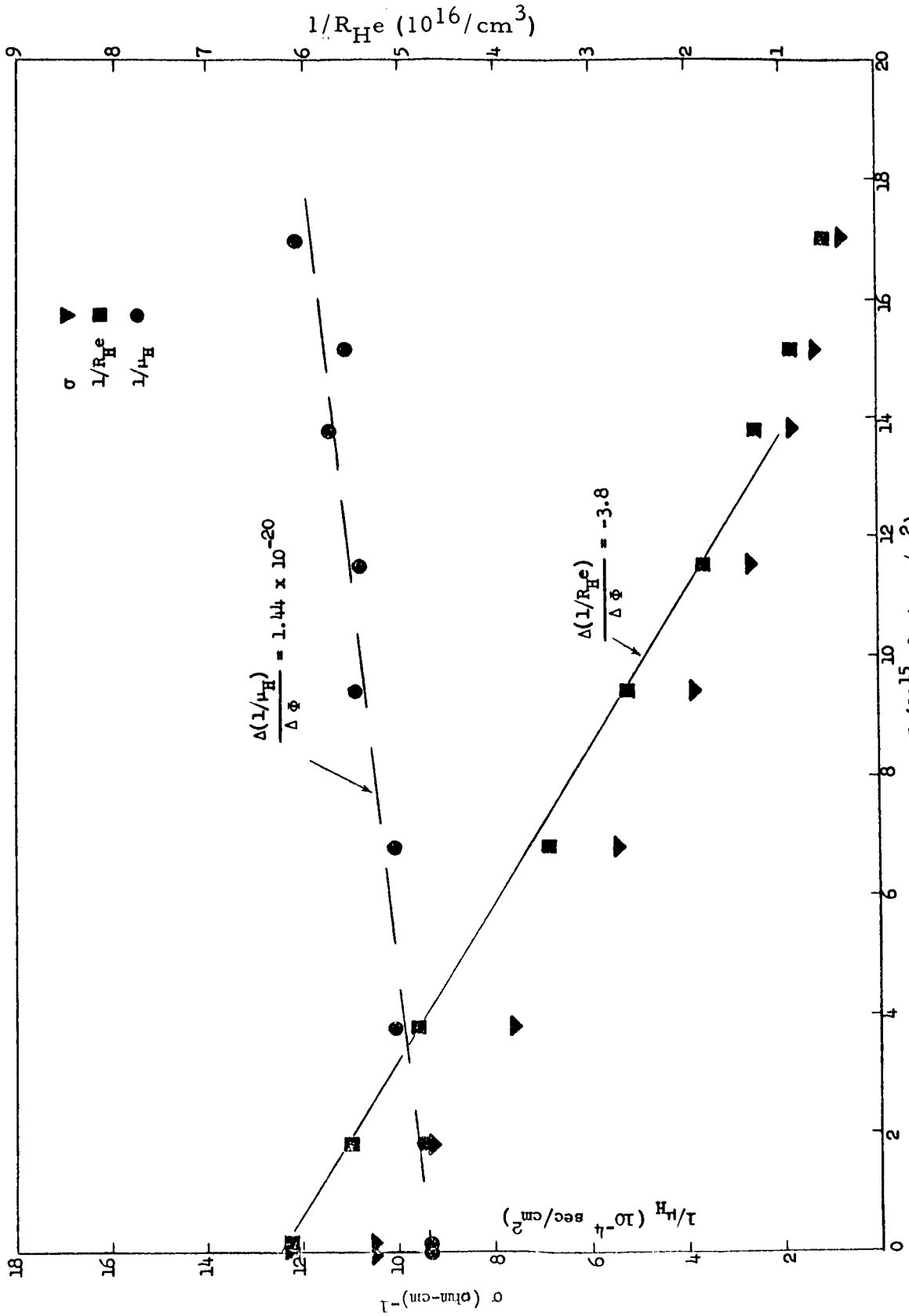

Fig. 12--Galvanomagnetic measurements during irradiation - 0.1 ohm-cm FZ silicon

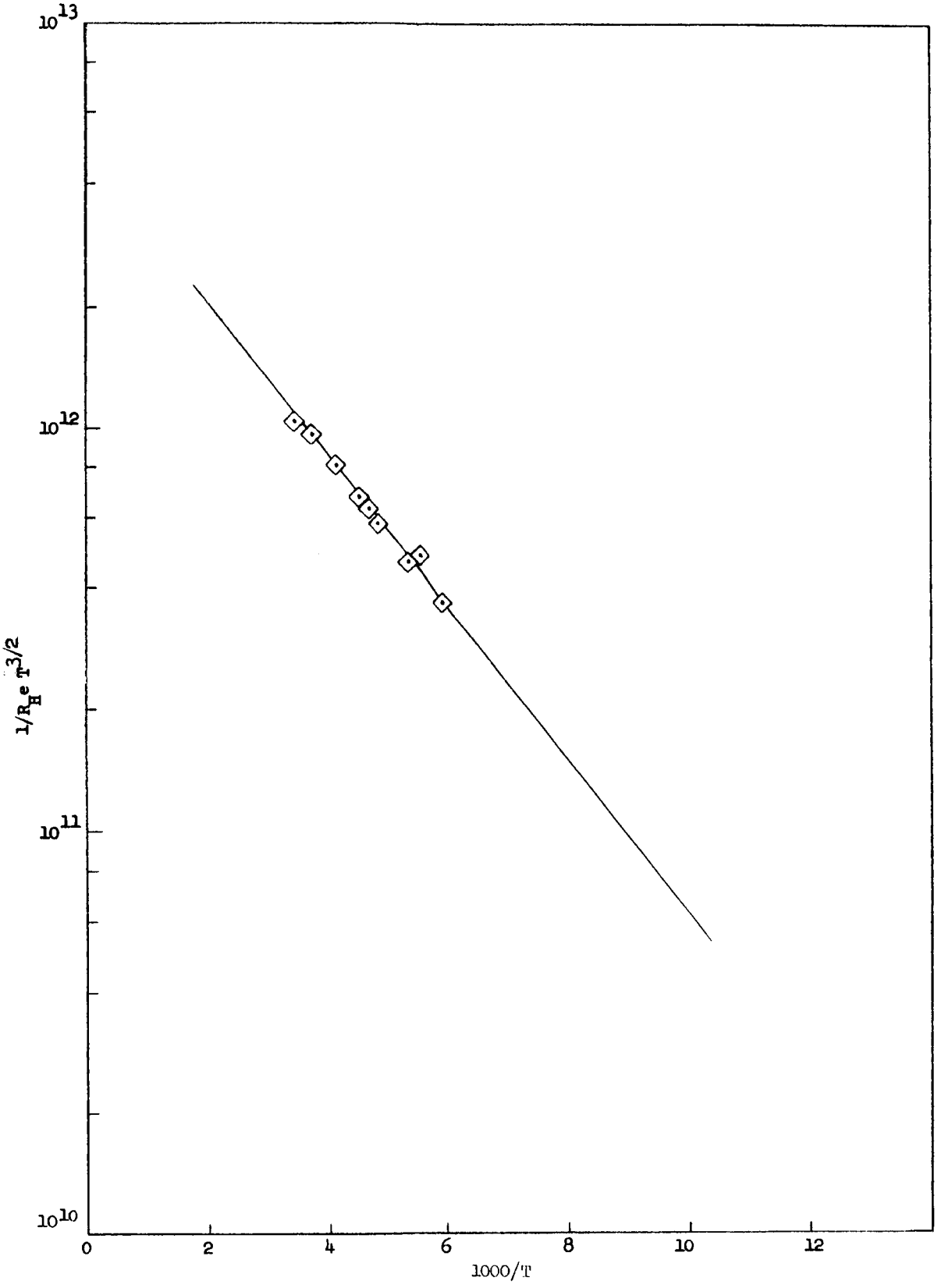

Fig. 13--Temperature dependence of Hall coefficient - 0.1 ohm-cm FZ silicon

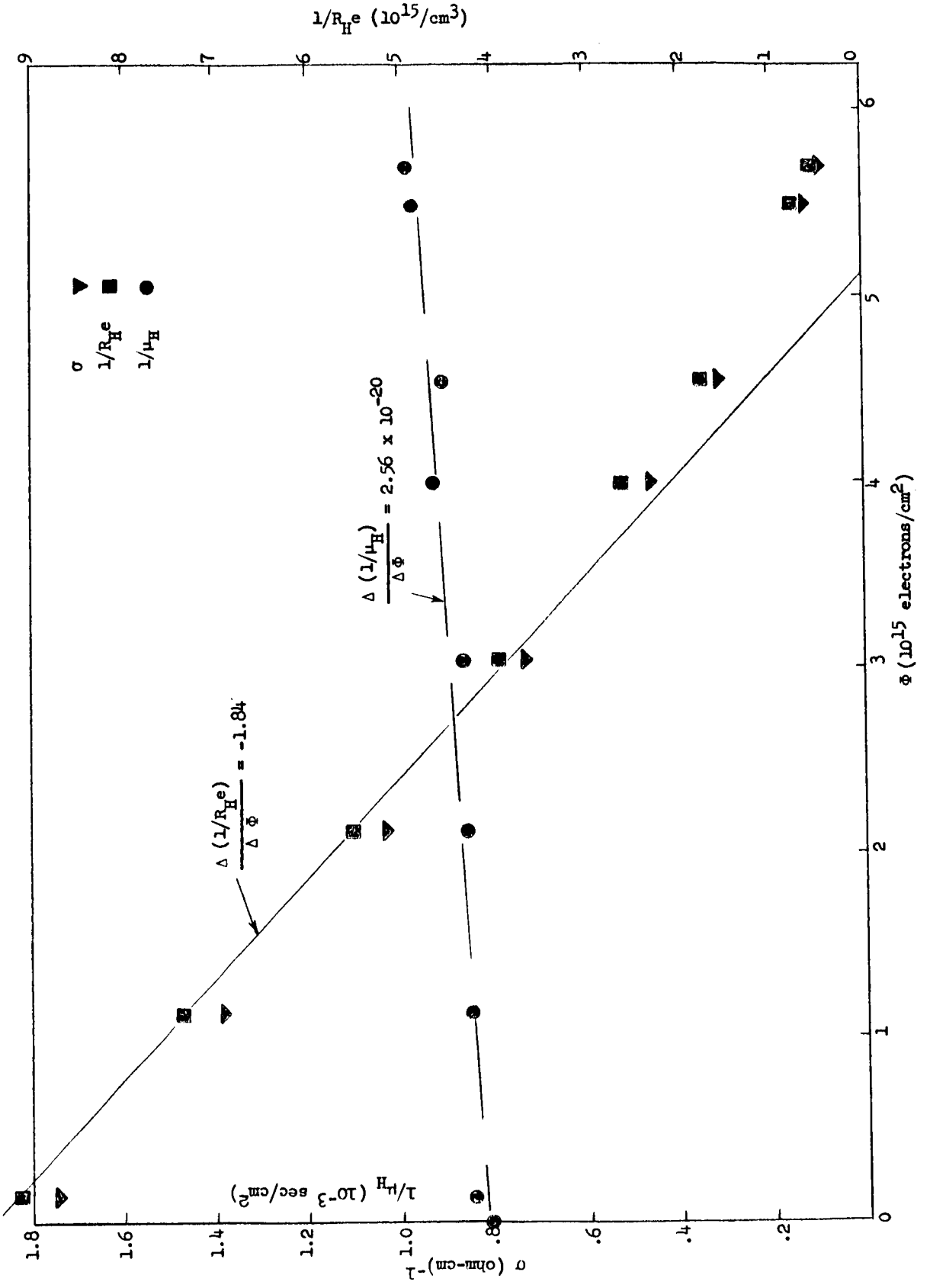

Fig. 14--Galvanomagnetic measurements during irradiation - 0.4 ohm-cm FZ silicon

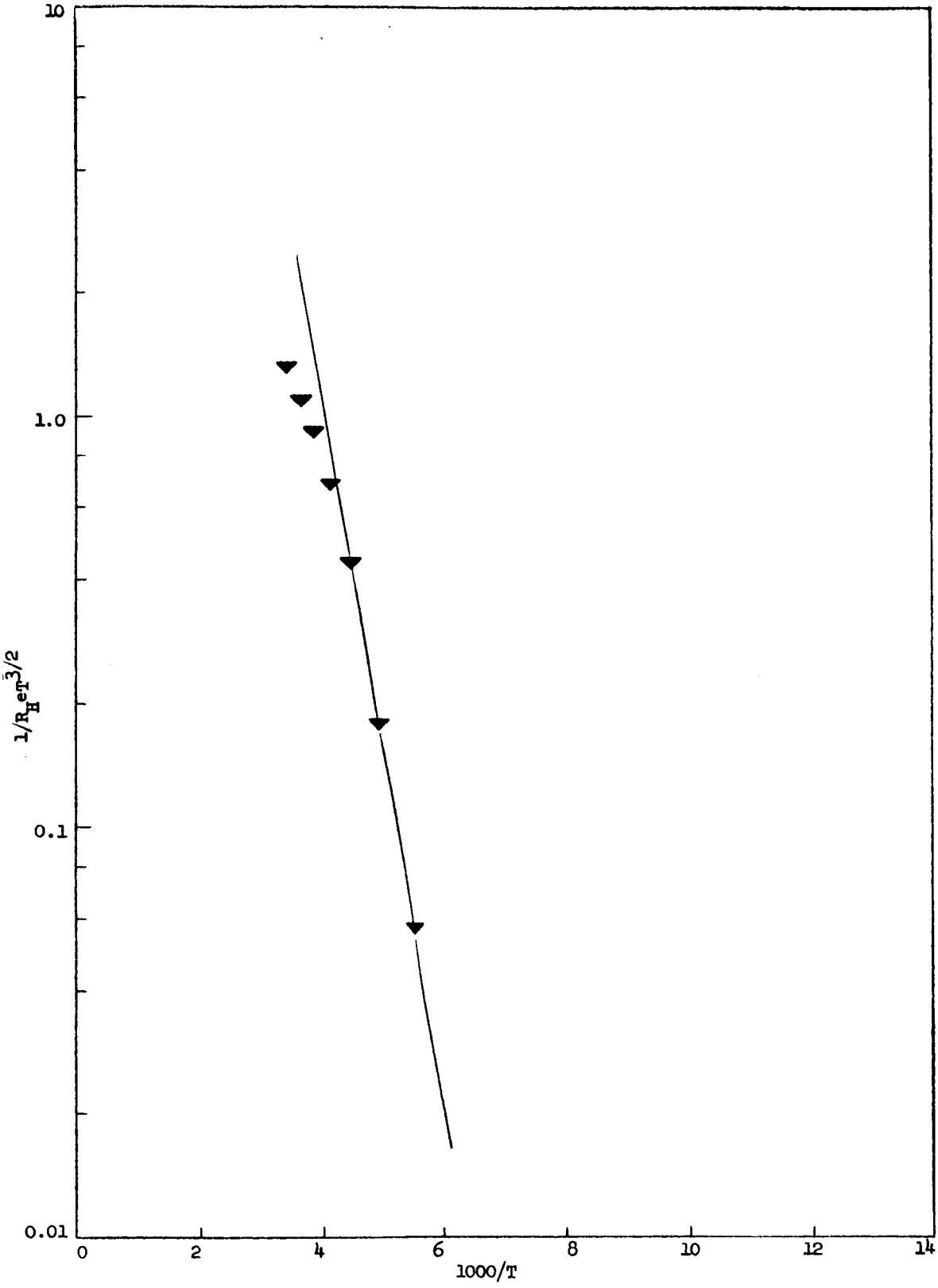

Fig. 15--Temperature dependence of Hall coefficient - 0.4 ohm-cm FZ silicon

Samples of As-doped, floating-zone (FZ) grown silicon irradiated at 292°K with 30-Mev electrons yielded the results shown in Table 2.

Table 2

As-DOPED FZ SILICON IRRADIATED WITH 30-MEV ELECTRONS

Resistivity (ohm-cm)	$\Delta(1/R_H e)/\Delta\Phi$ (cm^{-1})	$\Delta(1/\mu_H)/\Delta\Phi$ (v-sec) ($\times 10^{-20}$)	$E_C - E_A$ (ev)	Φ(elect/cm^2) ($\times 10^{15}$)
0.5	.85	.3	.17 .03	24.0 9.1
1.5	.45	.1	.03 .08	11.0 3.9
15.0	.15	<.64	.26 .17	2.4 1.2

Samples of P-doped FZ silicon were also irradiated with 30-Mev electrons. These results are listed in Table 3.

Table 3

P-DOPED FZ SILICON IRRADIATED WITH 30-MEV ELECTRONS

Resistivity (ohm-cm)	$\Delta(1R_H e)/\Delta\Phi$ (cm^{-1})	$\Delta(1/\mu_H)/\Delta\Phi$ (v-sec) ($\times 10^{-20}$)	$E_C - E_A$ (ev)	Φ(elect/cm^2) ($\times 10^{15}$)
0.1	3.8	1.4	.04	17.0
0.4	1.8	2.6	.17	5.7
5.0	0.94	7.2	.08	0.77
50.0	1.1	20.0	.36	0.08

Phosphorus-doped silicon crystals grown by the Czochralski technique (i. e., pulling from a melt in a quartz crucible) were irradiated with electrons of various energies. These results appear in Table 4.

Table 4

P-DOPED QC SILICON IRRADIATED WITH ELECTRONS AT VARIOUS ENERGIES

Bombarding Electron Energy (Mev)	Resistivity (ohm-cm)	$\Delta(1/R_H e)/\Delta\Phi$ (cm^{-1})	$\Delta(1/\mu_H)/\Delta\Phi$(v-sec) ($\times 10^{-20}$)	$E_C - E_A$(ev)	$\Phi \frac{\text{electron}}{cm^2}$ ($\times 10^{15}$)
5	7.0	.05	1.1	.06	1.1
5	10.0	.05	0.75	.22	3.8
5	50.0	.04	15.0	--	0.1
10	0.5	.23	0.39	--	9.4
15	0.1	.97	0.07	--	57.0
15	0.5	.29	0.59	.10	18.0
15	50.0	.05	15.0	--	1.0
30	0.1	.88	0.32	.10	97.0
30	0.5	.60	0.95	.22	38.0
				.25	14.0
30	7.0	.15	1.2	.17	6.5
				.12	3.8
30	10.0	.17	0.64	.21	1.4
30	50.0	.09	60.0	--	0.1

A 10 ohm-cm B-doped (p-type) FZ sample was irradiated with 8×10^{15} 30-Mev electrons/cm^2. The bombardment results were $\Delta(1/R_H e)/\Delta\Phi = -.3$/cm, and $(1/\mu_H)/\Delta\Phi = 5.3 \times 10^{-20}$ v-sec; a donor level at 0.27 ev above the valence band edge was deduced from the temperature run.

The carrier removal rates quoted are initial removal rates; the removal rate toward the end of a prolonged irradiation experiment may well be considerably smaller. $\Delta(1/\mu_H)/\Delta\Phi$ data given also represent initial rates, although these are constant to higher flux levels than the removal rates.

Figures 16 and 17 present the carrier removal rate and rate of change of reciprocal Hall mobility data given in Tables 2, 3, and 4 plotted versus the initial carrier concentration. Especially noteworthy is the significantly higher carrier removal rate in FZ silicon compared to QC silicon.

4.3 ANALYSIS AND DISCUSSION

4.3.1 Temperature Dependence of Hall Coefficient

Using the formulas from Section 4.1.1, the following results were obtained from our irradiation experiments. For a number of defects smaller than the original donor or acceptor concentrations, the energy levels obtained are essentially those of the original donor or acceptor level which is being compensated. In our data, these levels range from 0.03 to 0.06 ev. After these levels are compensated, a series of deeper levels is found, as will now be discussed in more detail. First, consider the FZ AS- and P-doped crystals. For both donors, a level of 0.17 ev is found. The question arises as to whether this is the A-center, for it occurs irrespective of the original donor. It is conceivable that there is enough oxygen in these crystals so that an appreciable number of A centers are formed. For larger irradiations, deeper levels are seen; for example, a 0.26 ev level in 15 ohm-cm As-doped material. Also, in P-doped material, the E center, vacancy-phosphorous combination giving rise to the 0.36-ev level, is observed.

For QC crystals, essentially the same results are obtained. In one crystal, a level at 0.17 ev is seen and, for longer irradiations, a level at about 0.22 ev appears. Deep lying levels in p-type material are also observed.

The great similarity in the results for both FZ grown and pulled crystals might signify that both materials contain about the same amount

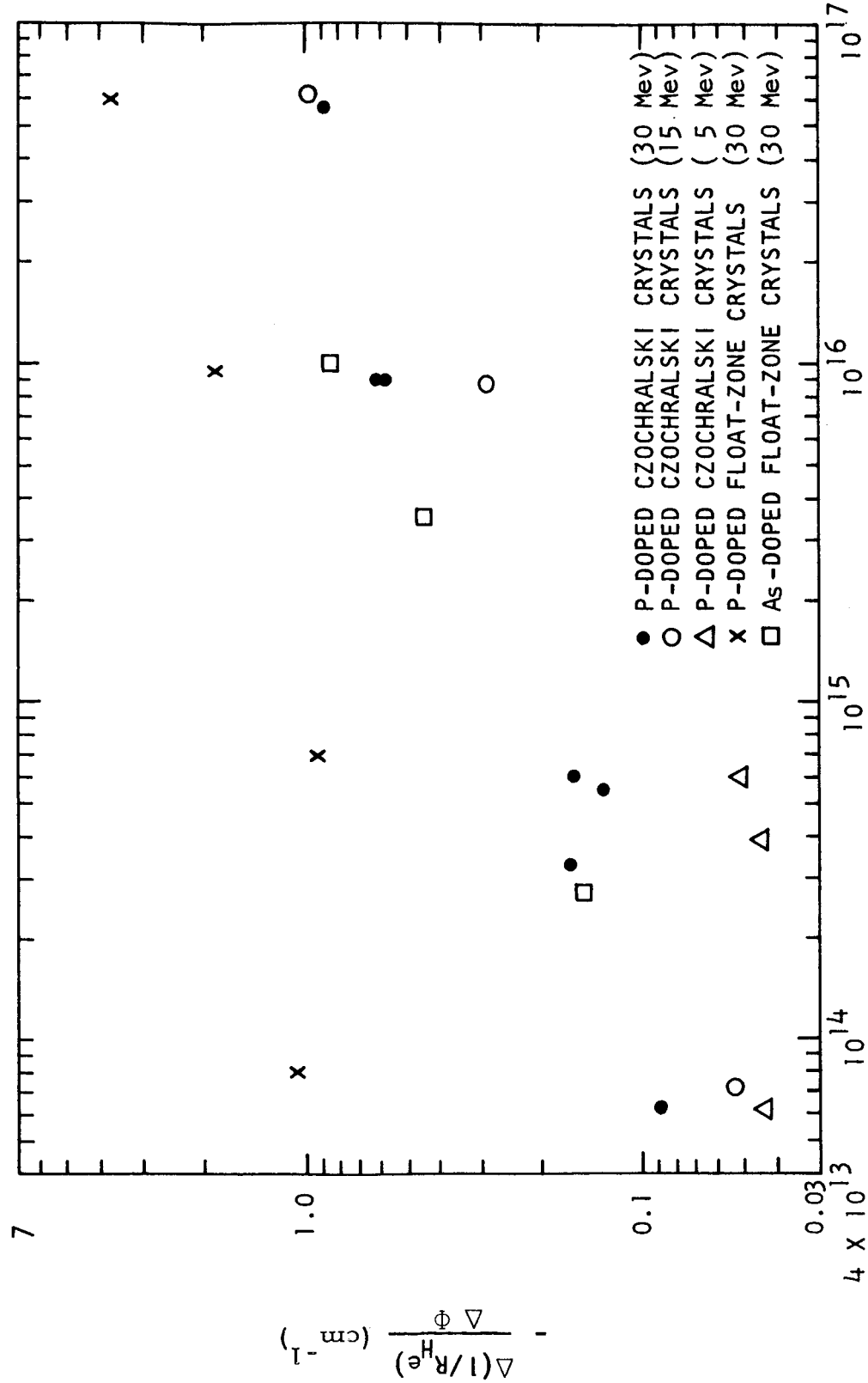

Fig. 16--Dependence of carrier removal rate on initial carrier concentration

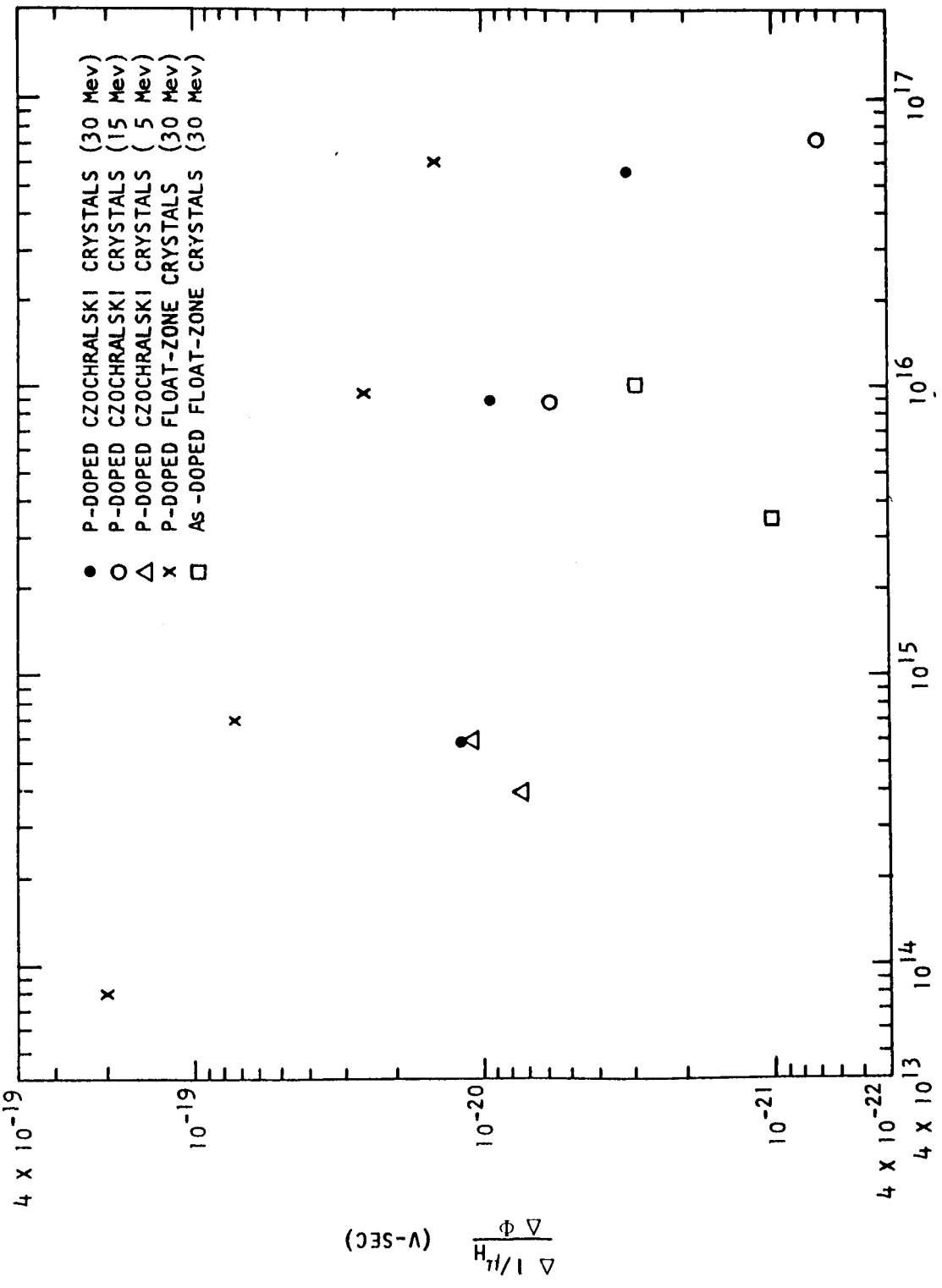

Fig. 17--Dependence of mobility change on initial carrier concentration.

of oxygen. However, the optical absorption measurements indicate large differences in oxygen concentration. The spin resonance studies must elucidate these points. The deep levels being formed (besides the E center), are not seen for irradiating electron energies around 1 Mev. Whether the material; i. e, initially present impurities, is responsible for this observation is not clear.

4.3.2 Carrier Density as a Function of Electron Flux

Extensive analyses were performed on the data from the 50 ohm-cm P-doped sample. As the temperature dependence following irradiation indicated the deepest lying level of all the data to be 0.37 ev, it was felt that this sample was the only one which could be expected to compare favorably with models based on a single defect level.

A. The first method of calculating the trap formation rate was a direct calculation of N_T, the number of traps introduced by the total irradiation, based on the conduction-electron population before and after irradiation and an assumed trap level at 0.37 ev below the conduction band as indicated by the $1/R_He$ versus $1/T$ curve.

For sample SiM-P-50N1-2 considered here,

$$\frac{n_o}{n} = \frac{(1/R_H)_o}{(1/R_H)} = \frac{1.3 \times 10^{-5}}{4.6 \times 10^{-7}} \approx 28 \text{ at } T = 290^oK,$$

$$N_C = 5.55 \times 10^{15}\ T^{3/2} = 2.66 \times 10^{19}, \text{ at } T = 290^oK,$$

$$\alpha = 2,$$

$$kT = 0.025,$$

$$E_C - E_T = 0.37,$$

$$n = \frac{\mu_H}{\mu}\left(\frac{1}{R_He}\right) = 3.6 \times 10^{12},$$

and $N_T = 6.3 \times 10^{14}\ cm^{-3}$.

As the total electron flux received by this sample was 8.1×10^{13} 30-Mev electrons/cm^2, the formation rate of these acceptor sites is

$$\frac{dN_T}{d\Phi} = \frac{6.3 \times 10^{14}}{8.1 \times 10^{13}} = 7.8\ \frac{0.37 \text{ ev acceptors/cm}^3}{\text{30-Mev electrons/cm}^2}.$$

In summary, the assumptions that went into this calculation were:

1. $\alpha = 2$
2. $\frac{\mu_H}{\mu} = 1.25$
3. No acceptor levels more than 0.37 ev below the conduction band introduced by irradiation
4. No donor levels closer than 0.37 ev to the conduction band introduced by the irradiation.

B. Another method of calculating the trap formation rate depends on the initial rate of carrier removal. From the equation in Section 2.2,

$$\frac{dN_T}{d\Phi} = \frac{dn}{d\Phi}\left\{1 + \frac{N_D}{\alpha_D N_C}\exp\left[-(E_C-E_D)/kT\right]\right\}\left\{1 + \alpha_T \frac{N_C}{n_o}\exp\left[-(E_C-E_T)/kT\right]\right\}$$

$$= 1.6\ \frac{0.37\text{ ev acceptors/cm}^3}{30\text{-Mev electrons/cm}^2}\ .$$

C. This great disparity in the two preceding results indicates that a false premise has been made. The fact that initially the Fermi level lies rather high above the 0.37 ev trap level makes it reasonable to assume that each trap formed would be immediately filled, and the trap formation rate would then be equal to the initial carrier removal rate. This argument favors the solution in (B). However, if all the acceptor levels formed are at 0.37 ev below the conduction band, the analysis of (A) should yield the correct number of defects of this type formed. A look at the assumptions made in this analysis shows that the results might be quite different if there were other trap levels introduced below the 0.37 ev level.

Further contemplation of the type of defect assumed (the E center) discloses that a deeper trap must also be postulated. As the E center is known to be the association of a vacancy with a phosphorous donor and is known to be neutral with the Fermi level below it, there must be a deep level associated with the recapture of an electron by the defect to neutralize the charge of the originally ionized phosphorous donor.

Figure 18 shows the results of three different calculations. Plotted in this same figure are experimental data for sample SiM-P-50N1-2, in which n has been calculated from Hall coefficient data using a mobility ratio ($r = \mu_H/\mu$) of 1.25. Curve I is a calculation of n versus

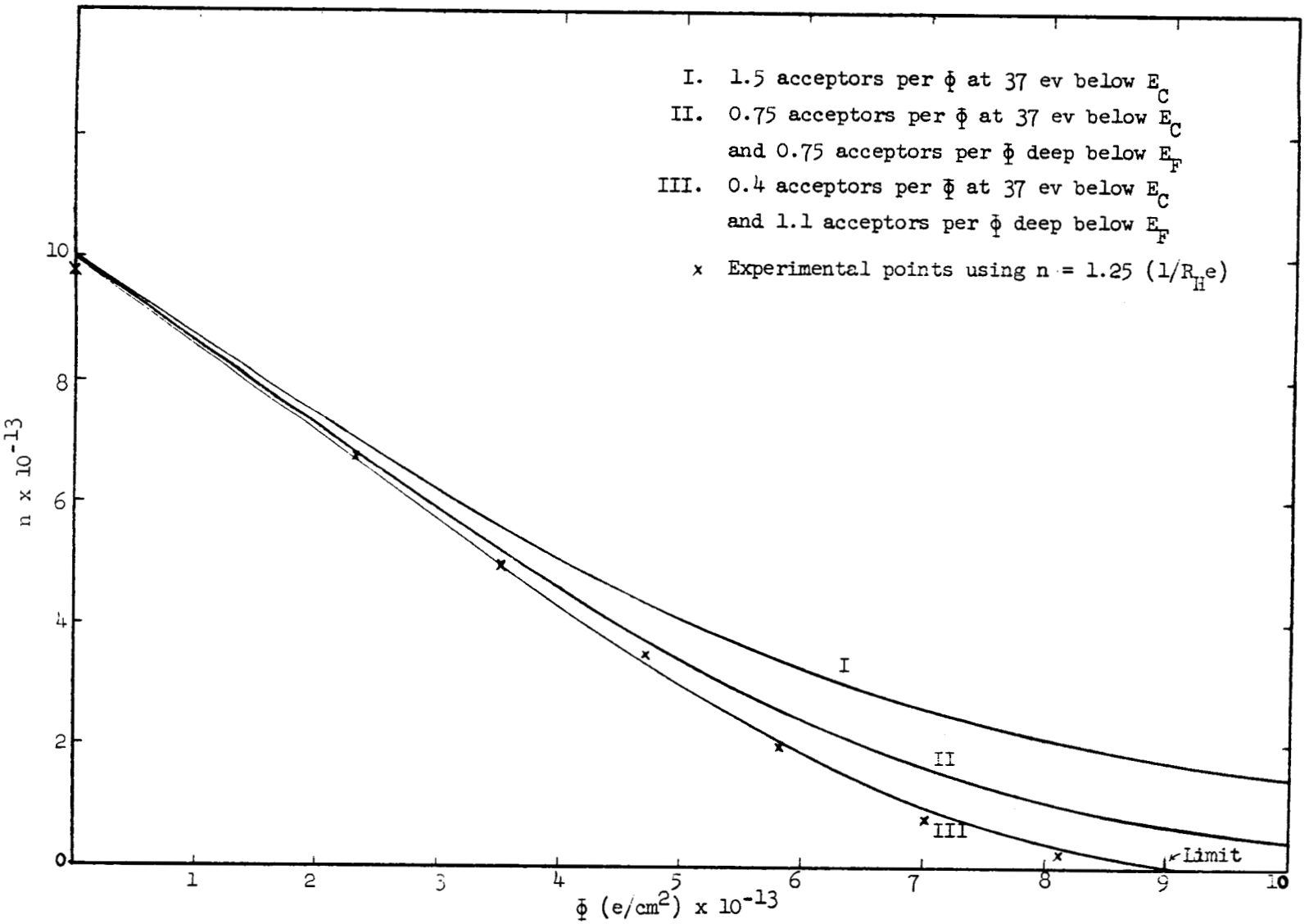

Fig. 18--Comparison of theoretical and experimental carrier concentration - 50 ohm-cm FZ silicon

Φ assuming only traps at 0.37 ev below the conduction band introduced at a rate of 1.5/cm per incident electron. Curve II is the same calculation with the assumption now of equal numbers of traps at the 0.37 ev level and at another level deep below the Fermi level, so that it is always full. The total trap formation rate is still 1.5/cm per incident electron. This model represents what might be expected if only the E-center type of defect were being formed. However, it may be seen that a good fit to the data is not achieved until a model is assumed in which three times as many deep traps as 0.37 ev traps are formed. This result is shown in Curve III.

This analysis indicates the formation of deep lying acceptor states introduced at a rate comparable with the E-center production. Possibly these are acceptor states of the J-C center.

4.3.3 Hall Mobiity and Carrier Removal Rates as a Function of Carrier Concentration

The data on carrier removal rates as a function of initial resistivity have been summarized in Fig. 16. Similarly, the mobility changes are summarized in Fig. 17 and Table 5. If we compare the rate at which scattering centers are introduced, $\Delta N_I/\Delta\Phi$, with the rate at which carriers are removed, $-\Delta(1/R_H e)/\Delta\Phi$, the former seems to be consistently larger by as much as an order of magnitude. It must be remembered that the observed mobility changes were very small, so that the rate $\Delta N_I/\Delta\Phi$ is probably uncertain to a factor of two. Within this error, the data suggest that the introduction rate of ionized impurity center in QC silicon is approximately 5/cm per 30-Mev electron, roughly independent of resistivity. This rate does not change rapidly with decreasing electron energy. The datum for 0.1 ohm-cm QC silicon irradiated at 15 Mev must be assumed to be suspect, since it differs so greatly from the results for the same resistivity at 30 Mev, and from a nearby resistivity at 10 Mev.

The picture for FZ silicon is even less clear. There appears to be a strong dependence on both the doping material (As or P) and resistivity. However, the results of the P-doped samples are almost inconsistent with our model of defect production. The rates of defect production appear to exceed the rate at which atoms are displaced, even without annealing.

Table 5

ANALYSIS OF HALL MEASUREMENTS

Resistivity (ohm-cm)	Dopant	Silicon Type	Bombarding Electron Energy (Mev)	$(E_C-E_F)_o$ (ev)	$(1/R_He)_o$ ($\times 10^{15}$) (m^{-3})	$-\Delta(1/R_He)/\Delta\Phi$ (cm^{-1})	$\Delta(1/\mu_H)/\Delta\Phi$ ($\times 10^{-20}$) (v-sec)	$\Delta N_I/\Delta\Phi$ (cm^{-1})
0.5	As	FZ	30	.20	10.0	0.85	0.3	2.1
1.5	As	FZ	30	.23	3.5	0.45	0.1	0.58
0.1	P	FZ	30	.16	61.0	3.8	1.4	13.0
0.4	P	FZ	30	.20	9.1	1.8	2.6	19.0
5.0	P	FZ	30	.27	0.7	0.94	7.2	36.0
50.0	P	FZ	30	.33	0.072	1.1	20.0	83.0
7.0	P	QC	5	.27	0.6	0.05	1.1	5.9
10.0	P	QC	5	.29	0.39	0.05	0.75	3.8
0.5	P	QC	10	.20	8.5	0.23	0.39	2.8
0.1	P	QC	15	.16	72.0	0.97	0.07	0.49
0.5	P	QC	15	.20	8.7	0.29	0.59	4.3
0.1	P	QC	30	.16	56.0	0.88	0.32	3.0
0.5	P	QC	30	.20	8.9	0.60	0.95	6.9
7.0	P	QC	30	.27	0.6	0.15	1.2	6.4
10.0	P	QC	30	.29	0.33	0.17	0.64	3.2

V. CARRIER LIFETIME MEASUREMENTS

5.1 THEORY OF RECOMBINATION OF EXCESS CARRIERS

The purpose of this section is to analyze the rates of recombination of excess carriers in a semiconductor. We emphasize those phenomena observed during experiments on carrier generation in semiconductor samples caused by the passage through them of pulses of penetrating, ionizing relativistic electrons. These experiments usually involved the following features:

1. Carriers were generated uniformly throughout a specimen.
2. The density of carriers generated could be predicted from a measurement of the radiation intensity.
3. The conductivity was measured as a function of time by a standard 4-point current-voltage measurement on a rod specimen.
4. The duration of the ionizing pulse was shorter than, or comparable to, the pertinent carrier decay times.
5. Recombination rates were measured as a function of temperature.
6. Recombination rates were measured as a function of the density of recombination centers introduced by prolonged irradiation.

The purpose of these experiments was to deduce the properties of the recombination centers, including:

1. Density, N_t
2. Position in the energy gap, E_t, relative to the top of the valence band
3. Capture cross section for electrons, σ_n, and for holes, σ_p.

We shall use the simplest model - a single recombination center with only two possible states, in which it does or does not contain an electron.

This discussion will be an adaptation of the analyses of Shockley and Read[28] and of Nomura and Blakemore.[29, 30] In particular, we will assume an extrinsic semiconductor, n-type for definiteness. The results can be easily applied to p-type material by exchanging symbols.

The following notation, after Nomura and Blakemore, will be adopted:

n_o = thermal equilibrium electron (majority carrier) density

Δn = excess equilibrium electron (majority carrier) density

p_o = thermal equilibrium hole (minority carrier) density

Δp = excess equilibrium hole (minority carrier) density

N_t = recombination center (trap) density

f_t = the fraction of traps occupied by electrons

f_o = the fraction of traps occupied by electrons in thermal equilibrium

c_n = capture rate of electrons per recombination center not already occupied by an electron

c_p = capture rate of holes per recombination center already occupied by an electron

E_g = electron energy difference between bottom of conduction band and top of valence band

E_i = electron energy difference between trap and bottom of conduction band

n_1 = thermal equilibrium conduction-band electron density if the Fermi level were at the trap energy level

p_1 = thermal equilibrium valence-band hole density if the Fermi level were at the trap energy level

γ = c_n/c_p

The ratio of capture cross sections, γ, is usually either much less than, or much greater, than unity. The assumption of a single-level trap center assures that in one of its two states (with or without electron) the trap is charged. Hence, one of the capture rates, c_n or c_p, is usually characteristic of a neutral trap and the other of an attractive Coulomb interaction between trap and carrier. The cross section for the attractive potential is usually larger by more than a factor of 10 than the neutral interaction cross section. Multiply charged traps, which may lead to repulsive Coulomb interactions and different charged states of the same

center, usually have more than two significant states, and will not be analyzed here.

The quantities n_1 and p_1 have been introduced as a convenient representation of the position of the trap center in the energy gap. Since they represent thermal-equilibrium densities, the general relation must be satisfied:

$$n_1 p_1 = n_o p_o = n_i^2 ,$$

where n_i is the intrinsic carrier density.

Since we assume an extrinsic n-type semiconductor, n_o is essentially independent of temperature. Hence, the minority carrier density depends on the temperature in the fashion

$$p_o \propto \exp (-E_g/kT).$$

The factors describing the position of the trap level are also temperature dependent.

$$p_1 \propto \exp \left[-(E_g - E_i)/kT \right]$$

$$n_1 \propto \exp (-E_i/kT).$$

The thermal equilibrium-occupation fraction f_o is:

$$f_o = \frac{n_o}{n_o + n_1} = \frac{p_1}{p_o + p_1}$$

If the Fermi level is well above the trap level ($n_o >> n_1$) the thermal occupation fraction is essentially constant at unity, but $(1 - f_o)$ is small and proportional to $\exp (-E_i/kT)$. If the Fermi level is well below the trap level ($n_o << n_1$), f_o is small and proportional to $\exp (-E_i/kT)$, and $(1 - f_o)$ is essentially constant at unity. Of course, as the temperature is increased, the Fermi level moves down in extrinsic n-type material, possibly passing through the trap level if it is in the upper half of the energy gap.

The capture rates, c_n and c_p, are usually assumed to be, at most, weakly dependent on temperature unless a repulsive Coulomb interaction is involved. Since we have ruled out this case, we shall assume the c's to be constant.

The remainder of this section will discuss recombination rates under various conditions, with emphasis on understanding the physical processes. For detailed numerical analyses the reader is referred to the articles by Nomura and Blakemore[29, 30] which present detailed computed solutions to the recombination problems.

5.1.1 Derivation of Recombination Rates

The rates of capture and re-emission of electrons and holes from a trap have been derived by Shockley and Read.[28] For nondegenerate semiconductors, the energy states in the conduction band and valence band can be averaged and all rates can be expressed in terms of average coefficients.

The rate of capture of electrons by the traps is:

$$U_{cn} = c_n N_t (1 - f_t) (n_o + \Delta n).$$

where

c_n = capture coefficient per trap,

$N_t (1 - f_t)$ = number of traps available for electron capture,

and $(n_o + \Delta n)$ = number of electrons available to be captured.

The rate of re-emission of electrons from the trap is:

$$U_{en} = c_n N_t f_t n_1 .$$

Thus the rate at which the excess electron density charges is given by:

$$- \frac{d\Delta n}{dt} = U_{cn} - U_{en} = c_n N_t \left[(1-f_t)(n_o + \Delta n) - f_t n_1 \right] .$$

A similar analysis applied to the hole capture and emission gives:

$$U_{cp} = c_p N_t f_t (p_o + \Delta p),$$

$$U_{ep} = c_p N_t (1-f_t) p,$$

and

$$- \frac{d\Delta p}{dt} = c_p N_t \left[f_t (p_o + \Delta p) - (1-f_t) p_1 \right] .$$

Space charge neutrality, or the statement that carriers can be only created as electron-hole pairs, requires a relationship between the trapped and free carrier densities: the excess electrons in the traps plus the excess electrons in the conduction band must equal the excess holes in the valence bands

$$N_t (f_t - f_o) + \Delta n = \Delta p$$

or

$$f_t = f_o + \frac{1}{N_t} (\Delta p - \Delta n).$$

Hence, the general equations which describe the recombination rates are:

$$-\frac{d\Delta n}{dt} = c_n N_t \left[(1-f_t)(n_o + \Delta n) - f_t n_1 \right] = c_n N_t \left[\Delta n (1-f_o) - \Delta f (n_o + n_1 + \Delta n) \right],$$

$$-\frac{d\Delta p}{dt} = c_p N_t \left[f_t (p_o + \Delta p) - (1 - f_t) p_1 \right] = c_p N_t \left[\Delta p f_o + \Delta f (p_o + p_1 + \Delta p) \right],$$

and

$$f_t = f_o + \Delta f = f_o + \frac{1}{N_t} (\Delta p - \Delta n).$$

These equations can be reduced to second order differential equations in one variable each, as was done by Nomura and Blakemore.[29] However, we will use them in their present form to reveal the physical nature of the recombination processes.

5.1.2 General Carrier Trapping Behavior

If a very short pulse of radiation generates excess-carrier pairs in a semiconductor originally in thermal equilibrium, the initial rate of carrier removal is calculated by setting $\Delta n = \Delta p$ and $\Delta f = 0$. The rates of removal of electrons and holes will not in general be equal unless the quantity

$$\Gamma = \frac{c_n (1-f_o)}{c_p f_o} = \frac{c_n n_1}{c_p n_o} = \gamma \frac{n_1}{n_o}$$

is unity. For $\Gamma > 1$ the electrons are removed faster than the holes, forcing an increase in the electron density on the traps (Δf increases). For $\Gamma < 1$ the holes are removed faster and Δf decreases.

The separation point, $\Gamma = 1$, is determined by the relative position of the Fermi level and the trap level and the ratio of capture cross sections. For a donor-like trap, the two charge states are + and 0, leading to a value of $\gamma > 1$. For an acceptor-like trap, the charge states are 0 and -, leading to $\gamma < 1$.

Consider a trap in the upper half of the energy gap. At very low temperatures the Fermi level is near the conduction band and $\Gamma < 1$, leading to minority hole trapping. As the temperature is increased, the Fermi level moves away from the conduction band and may cross a point (E_i - kT log γ) below the conduction band. At this temperature $\Gamma = 1$ and the recombination process of both carriers is a simple exponential with a decay time

$$\tau = \tau_{no}(1 + p_1/p_o) = \tau_{po}(1 + p_o/p_1),$$

where $\tau_{no} = 1/c_n N_t$ and $\tau_{po} = 1/c_p N_t$ are the lifetimes which the free carriers would have if all traps were available for their capture. At higher temperatures the Fermi level falls below this cross-over point and $\Gamma > 1$, leading to majority electron trapping.

The transition to electron trapping occurs at a lower temperature for a donor-like trap in which $\gamma > 1$ and the transition level is above the trap level, than for an acceptor-like trap. The transition never occurs for a trap level in the lower half of the energy gap in n-type material.

Large Trap Density - If the trap density, N_t, is very large compared to the available excess electrons and holes, the change in trap occupancy, Δf, is negligible compared to f_o, and the electron-hole density decreases independently along the exponential curves with decay times

$$\tau_n = \frac{1}{c_n N_t (1-f_o)} = \tau_{no}\left(\frac{n_o + n_1}{n_1}\right) ,$$

and

$$\tau_p = \frac{1}{c_p N_t f_o} = \tau_{po}\left(\frac{n_o + n_1}{n_o}\right) .$$

In this case, the conductivity decays as the sum of two exponentials, with amplitudes proportional to the carrier mobilities.

At very low temperatures, $n_1 << n_o$ and τ_p is almost constant, with τ_n decreasing with increasing temperature as $\exp(E_i/kT)$. For a trap level in the upper half of the energy gap, a transition temperature will be

reached, above which $n_1 >> n_o$. At higher temperatures, τ_n is constant and τ_p increases with increasing temperature as $\exp(-E_i/kT)$. For the trap level in the lower half of the energy gap, $n_1 << n_o$ and the low temperature behavior holds throughout.

Small Trap Density - If the trap density is very small compared to the injected carrier density, the different decay rates for the electron and hole densities cannot be sustained for an appreciable time. In the limit of very small N_t, the occupancy of the trap shifts rapidly to a new value so that the rates of electron and hole decay are equal, this process consuming a negligible fraction of the carriers. The solution for the decay following this adjustment is:

$$-\frac{d\Delta n}{dt} = -\frac{d\Delta p}{dt} = \frac{N_t \, \Delta n \, (n_o + p_o + \Delta n)}{1/c_n \, (p_o + p_1 + n) + 1/c_p \, (n_o + n_1 + n)}$$

$$f_t = \frac{c_n \, (n_o + \Delta n) + c_p \, p_1}{c_p \, (p_o + p_1 + \Delta n) + c_n \, (n_o + n_1 + \Delta n)}$$

since $\Delta n = \Delta p$ at all times during the decay. The effective decay time (which varies with excess-carrier density for large excess-carrier densities) has the familiar Shockley-Read form:

$$\tau = \frac{\Delta n}{-\frac{dn}{dt}} = \frac{\tau_{no} \, (p_o + p_1 + \Delta n) + \tau_{po} \, (n_o + n_1 + \Delta n)}{n_o + p_o + \Delta n}$$

Under low generation conditions, in n-type material, we can neglect Δn and p_o compared to n_o and p_1,

$$\tau \approx \tau_{po} \, (1 + n_1/n_o) + \tau_{no} \, (p_1/n_o)$$

$$f_t = \frac{c_n \, n_o + c_p \, p_1}{c_p \, (p_1) + c_n \, (n_o + n_1)}$$

At very low temperatures, n_1 and p_1 are small enough that only the first term, τ_{po}, is significant and the lifetime is temperature-independent. In this case, the recombination is limited by the rate of capture of a minority carrier by the trap, which, once captured, is always promptly annihilated by a majority carrier.

For a trap level above the center of the gap, n_1/n_o will become larger than unity above a transition temperature, and the lifetime will then increase as exp $(-E_i/kT)$. For a trap level below the center of the gap the term $\tau_{no}(p_1/n_o)$ will become dominant at higher temperatures, leading to a similar increasing temperature dependence as exp $\left[-(E_g - E_i)/kT\right]$, where $(E_g - E_i)$ is clearly the energy for ionization of the trap from the valence band. In either case, the high temperature dependence of the lifetime yields the ionization energy of the trap, either to the conduction or valence band.

Under higher generation conditions, the change of decay rate as the carrier density decreases is also characteristic of the position of the trap level. If the level is near either band (high temperature) corresponding to $\Gamma > 1$ or $p_1/n_o > 1$, the decay becomes slower as it proceeds. For the trap level nearer the middle of the gap, so that $\Gamma < 1$ and $p_1/n_o < 1$, the decay becomes faster as it proceeds. For $\Gamma = 1$ or $p_1/n_o = 1$, the decay is exponential, with a decay time equal to the low-level generation decay time.

Intermediate Trap Density - The intermediate case, in which excess carrier densities and trap densities are comparable, is much more difficult to solve, because an appreciable fraction of one type of carrier is held on the traps, changing their occupancy so that decay rates of the two types of carriers tend to become equal. Numerical solutions have been performed by Nomura and Blakemore,[29, 30] and we will only discuss qualitative features of these solutions.

For a trap level close to the conduction band, $\Gamma > 1$, the electrons are trapped faster than the holes can recombine with them, and the occupancy of the trap states increases ($\Delta f > 0$). As a result, the free electron density remains less than the free hole density throughout the ensuing decay. However, the hole capture rate is increased drastically by the increase in f_t. Even for a trap density 10 times the initial generation level and $\Gamma = 5$, the decay soon follows fairly closely the Shockley-Read form applicable to small trap densities.

For a trap level close to the valence band, $\Gamma < 1$ and $p_1/n_o \gamma > 1$, the free hole density remains less than the free electron density throughout the decay. The hole trapping quickly forces the electron density decay to follow the rate τ_{po}. However, re-emission of holes from the traps slows down markedly, especially at the larger values of $p_1/n_o \gamma$ and N_t. When $p_1/n_o \gamma = 1$, and during the lower carrier-density portions of the decay, the trapped electron has an equal chance of being thermally re-excited or annihilated by a hole. During the earlier portion of the decay, when possibly

$$\frac{p_1}{n_o \gamma} \frac{p_o}{p_o + \Delta p} < 1,$$

the annihilation with a hole would have preference.

For a donor-like trap level ($\gamma>1$) not near either band ($\bar{\tau}<1$, and $p_1/n_o\gamma<1$), the decay is not prolonged by re-emission, and follows closely a straight exponential with decay time τ_{po}. There is a slight increase in decay time during latter portions of the decay.

For an acceptor-like trap-level ($\gamma<1$) not near either band, the decay is initially determined by electron capture, and is intermediate between τ_{po} and $\tau_{no}\,(1 + n_o/n_1)$.

5.1.3 Dependence of Excess Carrier Lifetime on Temperature and Excess Carrier Density

In the experiments performed on the change in carrier lifetime in silicon, the following are typical values of carrier and trap densities:

The majority carrier density, $n_o \sim 10^{14}$ to 10^{15},

Excess carriers, $\Delta n \sim 0.1$ to $0.2\ n_o$,

Recombination centers, $N_T \sim 10^{10}$ to 10^{12}.

Under these conditions, the analysis for the case of low trap density should be appropriate and the Shockley-Read formula applicable. The assumption of small excess carrier density is not necessarily applicable, particularly since the excess carrier density can be assumed to be large compared to the minority carrier concentration. The pertinent approximation to the Shockley-Read formula is then given by

$$\tau = \tau_{po}\left(1 + \frac{n_1}{n_o + \Delta n}\right) + \tau_{no}\left(\frac{p_1 + \Delta n}{n_o + \Delta n}\right). \qquad (11)$$

If the recombination center is above the center of the energy gap, the further approximation, $n_1 \gg p_1$, can be applied. Usually the ratio of these quantities is much larger than any differences between τ_{po} and τ_{no}.

It is particularly interesting to investigate this equation as a function of excess carrier density Δn. Let us consider first the case of a recombination center well above the center of the gap, so that $p_1 \tau_{no}$ is much smaller than $n_1\ \tau_{po}$. In this case, the dependence of the lifetime, τ, on injection level and temperature can be seen by the following expression:

$$\tau = (\tau_{po} + \tau_{no} \frac{\Delta n}{n_o + \Delta n}) + \tau_{po} \frac{n_1}{n_o + \Delta n}. \qquad (12)$$

$$= \frac{\tau_{po}(1 + n_1/n_o) + (\tau_{no} + \tau_{po})\,\Delta n/n_o}{1 + \Delta n/n_o}$$

The only appreciable temperature dependence is in the n_1 factor of the second term. At very low injection levels and low temperatures, the lifetime should be τ_{po}. At very high injection levels, $\Delta n >> n_o$, the low temperature lifetime approaches $\tau_{po} + \tau_{no}$. The higher temperature lifetime is dominated by the second term, $\tau_{po} n_1/(n_o + \Delta n)$.

Hence, if τ_{no} is not too small compared with τ_{po} a study of the dependence of the lifetime on injection level can reveal both the values of τ_{po} and τ_{no}. This type of analysis has previously been applied to interpretations of the lifetime in irradiated silicon by Galkin, et al.,[9] although in these experiments the lifetime measurements were performed on diode structures rather than homogeneous silicon samples.

In the other cases, where the recombination center is below the center of the gap in n-type material, the term $n_1 \tau_{po}$ is neglected by comparison with $p_1 \tau_{no}$, resulting in the expression

$$\tau = (\tau_{po} + \tau_{no} \frac{\Delta n}{n_o + \Delta n} + \tau_{no} \frac{p_1}{n_o + \Delta n}. \qquad (13)$$

$$= \frac{(\tau_{po} + \tau_{no} p_1/n_o) + (\tau_{no} + \tau_{po})\,\Delta n/n_o}{1 + \Delta n/n_o}$$

The only significant difference between this expression and the previous one is that the coefficient of the temperature-dependent term is now not determined by the low-injection lifetime at low temperatures. It should be noted that the absolute values of n_1 and p_1 are uniquely determined by the position of the defect center in the energy gap and the temperature, and do not depend upon the concentration of these centers. As a result, a study of the temperature dependence of the carrier lifetime is subject to internal consistency checks between the low temperature constant-lifetime, the slope of the temperature-dependent region and the position of the transition between the constant and temperature-dependent regions. Analysis of the measurements on carrier lifetime in a sample of QC silicon

in terms of this theory will be described in a later section of this report.

5.2 EXPERIMENTAL RESULTS

Preliminary measurements on carrier lifetime in silicon were performed during the development of the experimental technique for lifetime measurements and, hence, are not considered as reliable as the later results. A measurement of the excess carrier lifetime as a function of temperature performed on a 7 ohm-cm QC P-doped silicon sample is shown in Fig. 19. Due to contact rectification problems, only the temperature region in the vicinity of room temperature and above could be explored during these studies. Before irradiation, the activation energy deduced from the slope of the semilogarithmic plots of lifetime versus reciprocal temperature is 0.048 ev, suggesting that the donor center, which has an ionization energy of approximately this amount, is responsible for recombination. After irradiation, the slope in the vicinity of room temperature indicates an activation energy of 0.13 ev.

Another measurement on 50 ohm-cm FZ P-doped silicon gave serious contact rectification problems, especially below room temperature. In the temperature range between 300°K and 340°K, the slope of the semilogarithmic plot of lifetime versus reciprocal temperature indicated an activation energy of approximately 0.1 ev. Since the lifetime only changed by less than a factor of 2 over the measurement interval, this value cannot be considered reliable. Measurements with lower resistivity in silicon were less subject to contact rectification problems but, unfortunately, the initial carrier lifetime was also appreciable less. Figure 20 illustrates a set of lifetime measurements for 0.5 ohm-cm QC P-doped silicon. The initial lifetime at room temperature was approximately 2.2 μsec and was independent of temperature down to almost 100°K. Below that temperature the decay split into two components, the shorter one having a 2-μsec decay time. The longer lifetime increases rapidly as the temperature is lowered, reaching a value of 13 μsec at 86°K. This behavior is probably a manifestation of long-lived carrier trapping. The measurements made after irradiation by 2.7×10^{13} 30-Mev electrons/cm^2 are also shown in Fig. 20. The very short lifetime makes these measurements subject to large errors and measurements in the temperature range between 100°K and 160°K were not feasible. However, the pertinent features which can be considered reliable are that the lifetime decreases below room temperature and at least a portion of the carriers undergo a decay with a long lifetime in the vicinity of liquid nitrogen temperature.

The first extensive experiment on excess carrier lifetime was performed on a 7 ohm-cm QC silicon crystal on June 13, 1962. The techniques described in Section 3.5 were utilized. The lifetime was measured as a function of temperature between room temperature and liquid nitrogen

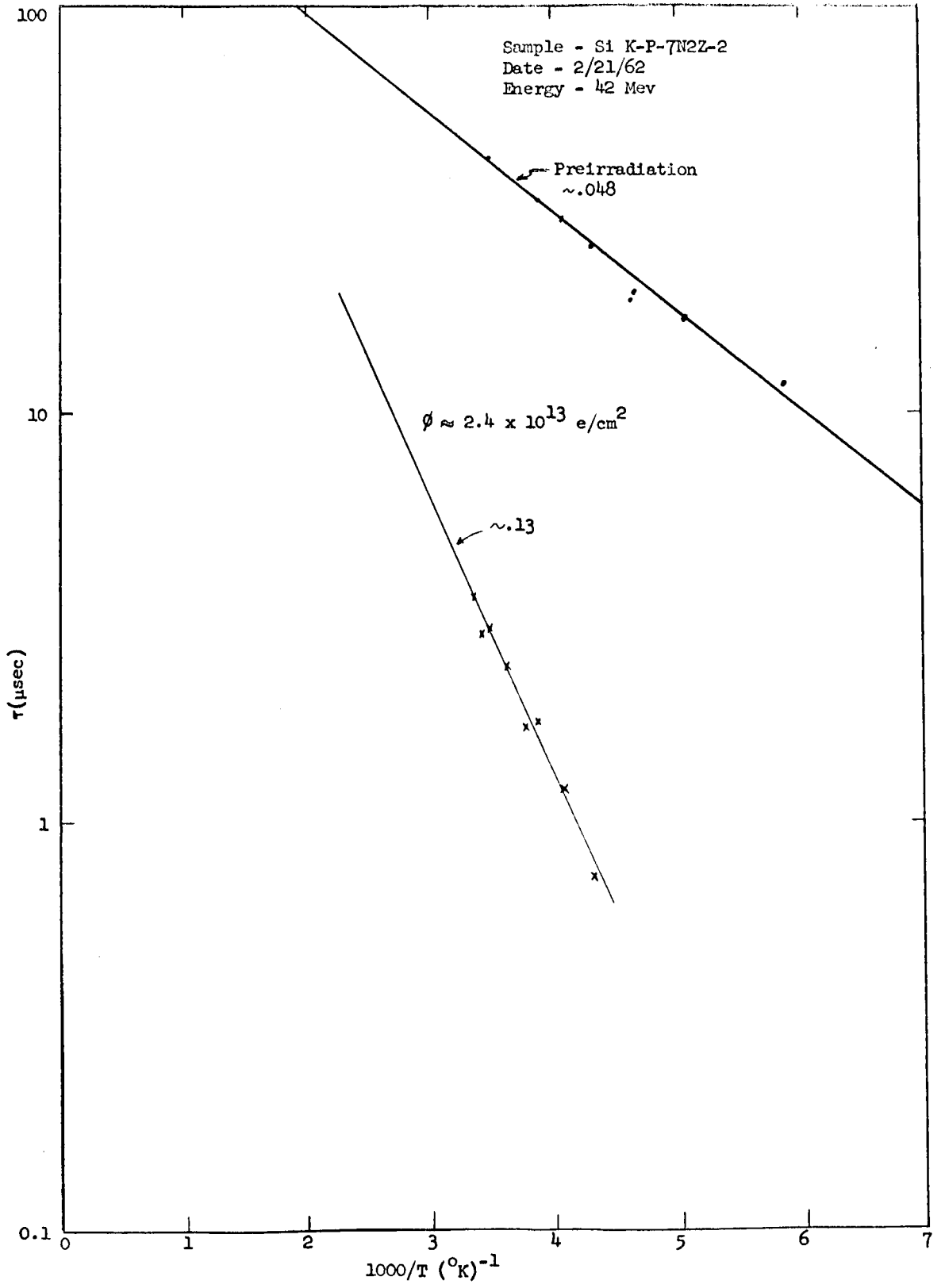

Fig. 19--Temperature dependence of carrier lifetime - 7 ohm-cm QC silicon

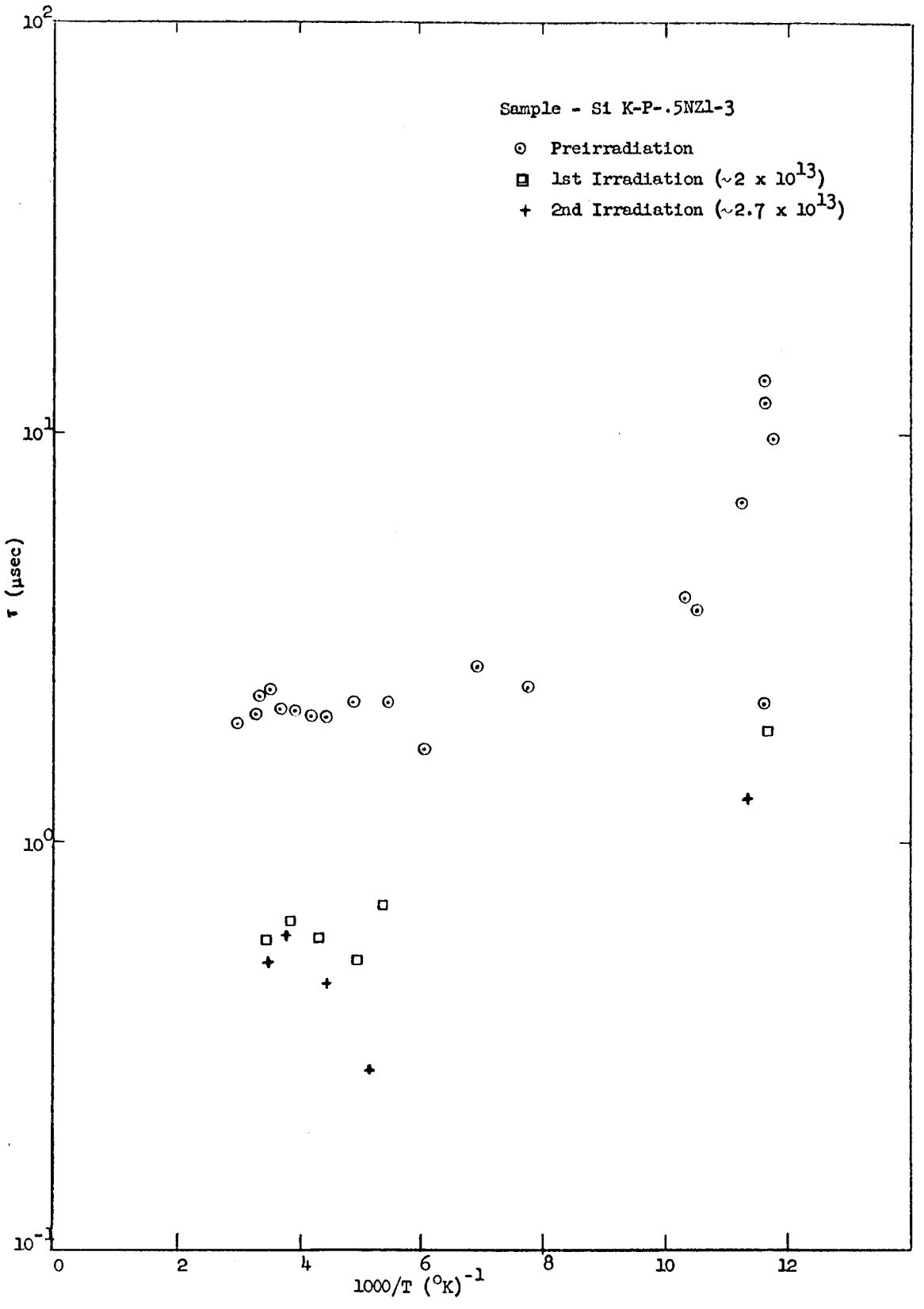

Fig. 20--Temperature dependence of carrier lifetime - 0.5 ohm-cm QC silicon

temperature before irradiation and after three successively increasing radiation exposures.

The results of this experiment are shown in Fig. 21. Most of the analysis has been performed on the data following the 7.9×10^{11} electrons/cm^2 irradiation because these represent a significant radiation-induced decrease in lifetime and at the same time yield lifetimes in the region where they are accurately measurable. Two important features appear in this curve. The lifetime is observed to decrease rapidly below room temperature and subsequently level off. However, somewhat surprisingly, the lifetime increases again drastically as the temperature is lowered to just above liquid nitrogen temperature. The decrease below room temperature can be understood in terms of the Shockley-Read model. However, the increase at lower temperature is not as easily interpreted.

It has been tempting to attribute such increases in lifetimes at low temperatures to carrier trapping. In other words, a minority carrier is trapped at a doubly-charged defect center and remains there for a long time due to the net repulsive Coulomb interaction between the center and the majority carrier. The lifetime of the majority carrier, in this case, is limited by thermal re-ionization of the minority carrier from the trapping center or by eventual recombination in the face of the repulsive interaction. However, in the present experiment we perform a check on this model. Those carriers which are trapped and those which recombine without trapping should either be observed as an early fast decay component in the conductivity, or else should fail to contribute to the conductivity at all if their lifetime is too short.

We have calculated a quantity, μ^*, proportional to the change in conductivity observed per excess carrier produced by the radiation. The number of excess carriers produced were deduced from the accelerator beam monitor. The change in conductivity was deduced from the change in voltage observed across the sample. If all of the carriers are observed at all of the measurement temperatures, then the temperature dependence of μ^* should be identical to the temperature dependence of the sum of the electron and hole mobilities. The data are plotted in Fig. 22 and indicate excellent agreement with the $T^{-2.5}$ dependence deduced from experiments on pure Si[25]

As a result of this analysis, it can be concluded that the conductivity associated with most of the carriers formed by the radiation was observed even at the earliest times after the ionization pulse. Unfortunately, the accuracy of the measurement of absolute conductivity at present is not adequate to rule out the possibility that the holes, which represent only 20 percent of the total conductivity, might be trapped at a doubly-charged center allowing the electrons to remain free for a long period of time.

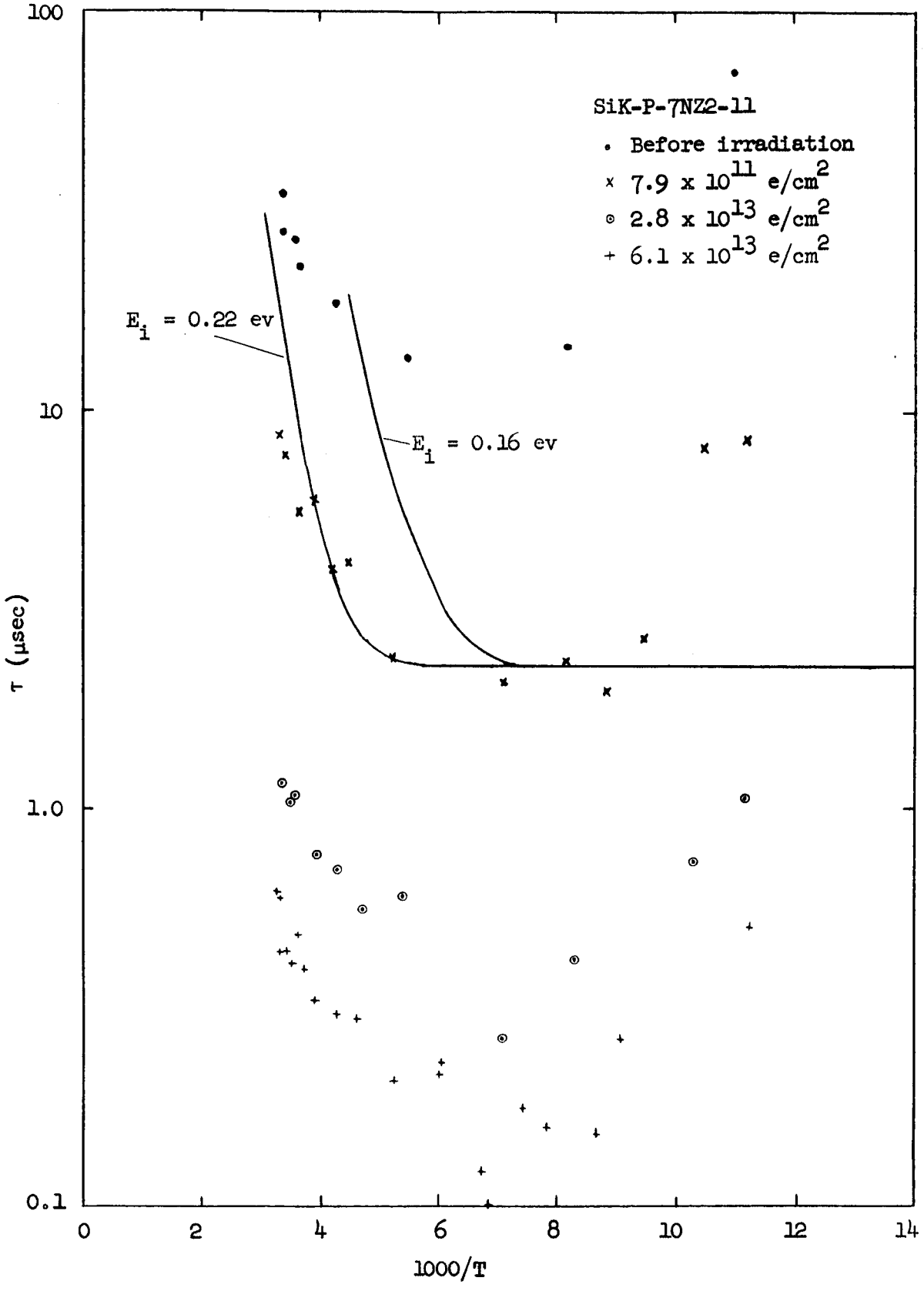

Fig. 21--Temperature dependence of carrier lifetime - 7 ohm-cm QC silicon

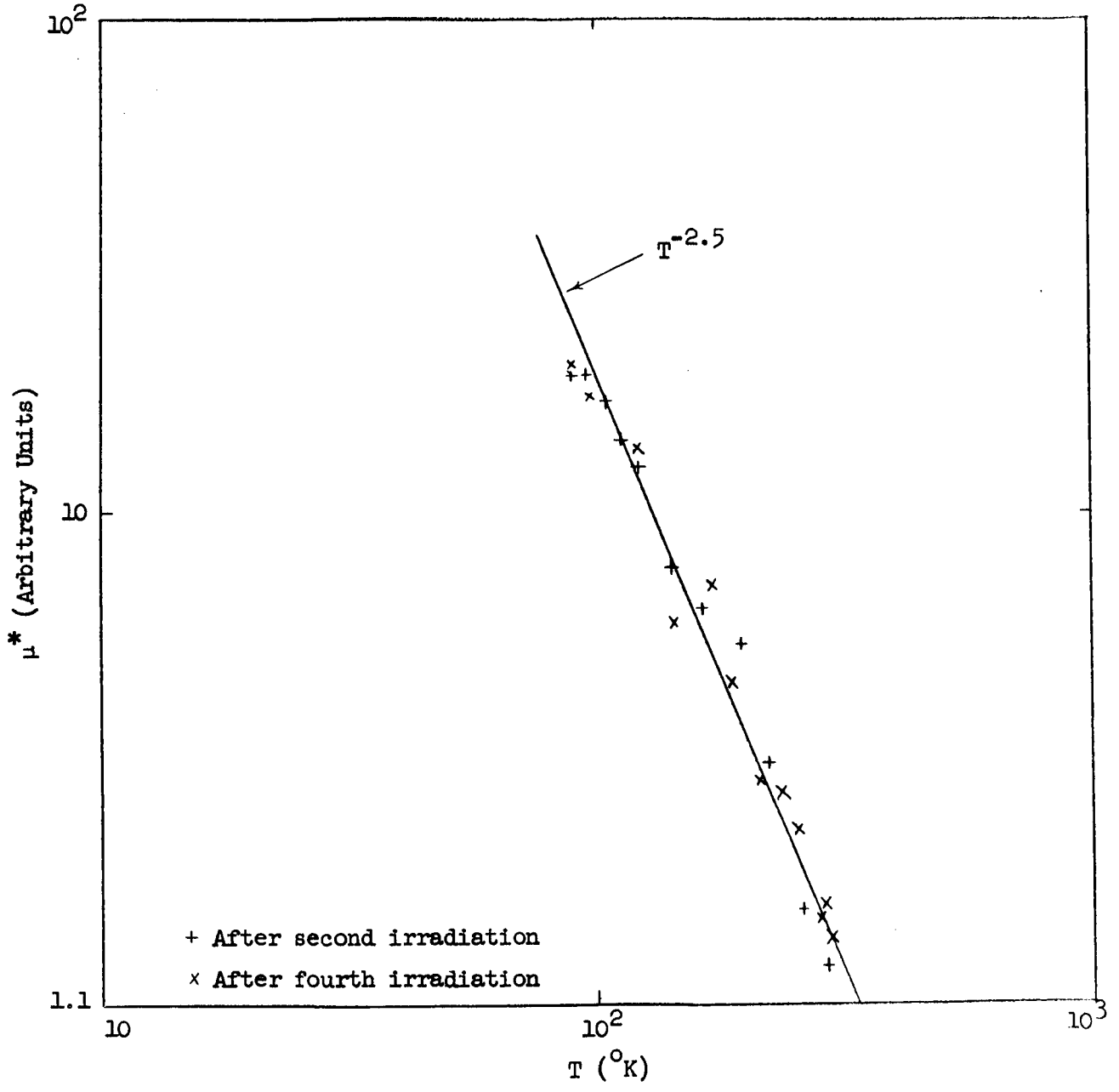

Fig. 22--Temperature dependence of μ^* - 7 ohm-cm QC silicon

This possibility would still be somewhat surprising for the following reasons:

1. If a trapping center appeared in competition with the observed recombination center, one would expect to see, at least in an intermediate temperature range, a combination of two exponential decays. This combination was not observed during this experiment.

2. The trapping centers responsible for this effect could probably not be the ones introduced by the radiation, because the total number of them in this experiment was less than $10^{12}/cm^3$ for the first irradiation curve in Fig. 21, and yet the excess carriers introduced during the pulsed excitation experiments numbered approximately $10^{14}/cm^3$. It is not likely that this many excess carriers could be trapped at so few trapping centers. However, the fact that the apparent trapping phenomenon appears in the pre-irradiation lifetime studies may indicate that defects originally present in the material, and presumably more numerous than those introduced by the radiation, might be responsible for trapping.

The high temperature behavior of the lifetime is in general agreement with the Shockley-Read theory. The excess carriers introduced, Δn, are somewhat less than the initial carrier concentration n_o and therefore, unless τ_{no} is larger than τ_{po}, these measurements may be considered to represent low injection conditions. In this case, assuming a relatively constant lifetime in the intermediate temperature region of about 2.2 μsec, the entire theoretical lifetime curve can be calculated from an assumed ionization energy for the recombination center. It can be seen from the two curves shown in Fig. 21 that an ionization energy of 0.16 ev, which corresponds to the A center, is inconsistent with the data. The slope of the temperature dependence seems to favor such an ionization energy or possibly a lower one, but the temperature at which the lifetime increases suggests a higher ionization energy such as 0.22 ev. Of course, one can assume that the center is actually in the lower half of the energy gap and, in this case, the position of the transition and slope do not need to correspond as accurately. However, in this case we are also not dealing with the A center.

The measurements taken after longer irradiations suggest a continuation of the trend seen after the first irradiation. In general, the lifetimes decrease significantly upon irradiation and they also achieve a minimum as a function of temperature at an intermediate point between room temperature and liquid nitrogen temperature. The last set of

measurements, in which lifetimes down to 0.1 μsec were observed, represents less accurate numbers than any of the others because of the extremely short decay times.

Another sample of 7 ohm-cm QC silicon was subsequently irradiated on September 18, 1962, and subjected to a thorough analysis. Among the experiments performed with this sample were measurements of the dependence of carrier recombination rates on the density of excess carriers generated within the sample. The data from this sample were reduced by the semi-automatic film-reading system and data-reduction computer programs. Hence, the decay curves were mapped out much more thoroughly and the detailed dependence of the decay curves on excess carrier density could be evaluated. The shape of the conductivity decay before irradiation deduced from photographs taken at three different accelerator radiation intensities is shown in Fig. 23. The conductivities from the three different accelerator intensities were superposed by translating in time so as to match the amplitude of the excess conductivity. It can be seen that the excess conductivity follows a single exponential decay except for the early portion of each decay curve, where the decay seems to be somewhat steeper. This effect can be ascribed to diffusion of the excess carriers and subsequent recombination at the surface. Before irradiation, the lifetime in the sample was rather long (about 55 μsec) and diffusion with surface recombination can contribute significantly. In the later portions of each decay we would expect a single exponential decay characterized by a combination of volume recombination plus normal mode diffusion to the surface with associated surface recombination. In the early portions of the decay, however, higher diffusion modes should appear and a faster decay of the excess carrier density should be exhibited as shown. After irradiation, on the other hand, when the recombination lifetime in the volume has been decreased significantly, this effect should disappear, in agreement with the experimental results shown in Fig. 24.

Figures 23 and 24 have also served to illustrate the degree of reproducibility between the data taken with different levels of excess carrier generation. Subsequent figures of this nature will not reproduce all of the data points as in these figures, but will only show a curve fitted to the individual calculated points.

The decay curve before irradiation of this same sample near liquid nitrogen temperature is shown in Fig. 25. An apparent increase in decay rate at the high injection level suggestive of higher-mode diffusion is seen. At the lower excess carrier levels another apparent increase is indicated. After irradiation the decay curve in Fig. 26 is seen. In this case the decay appears to follow a single exponential down to an excess conductivity of about 5 percent of the thermal equilibrium conductivity. Below that value the apparent decay rate increases.

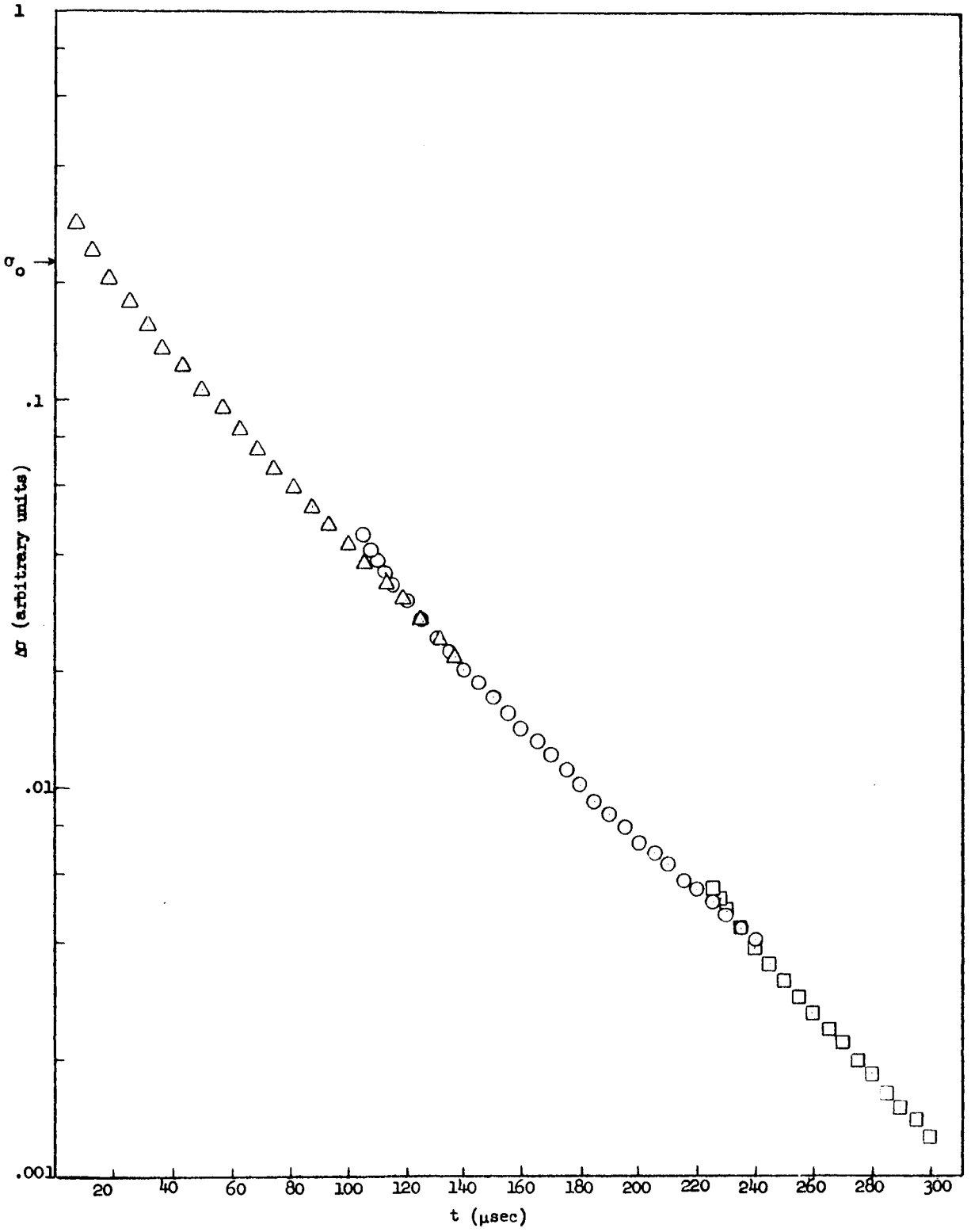

Fig. 23--Decay of excess conductivity - 7 ohm-cm QC silicon before irradiation, 380°K

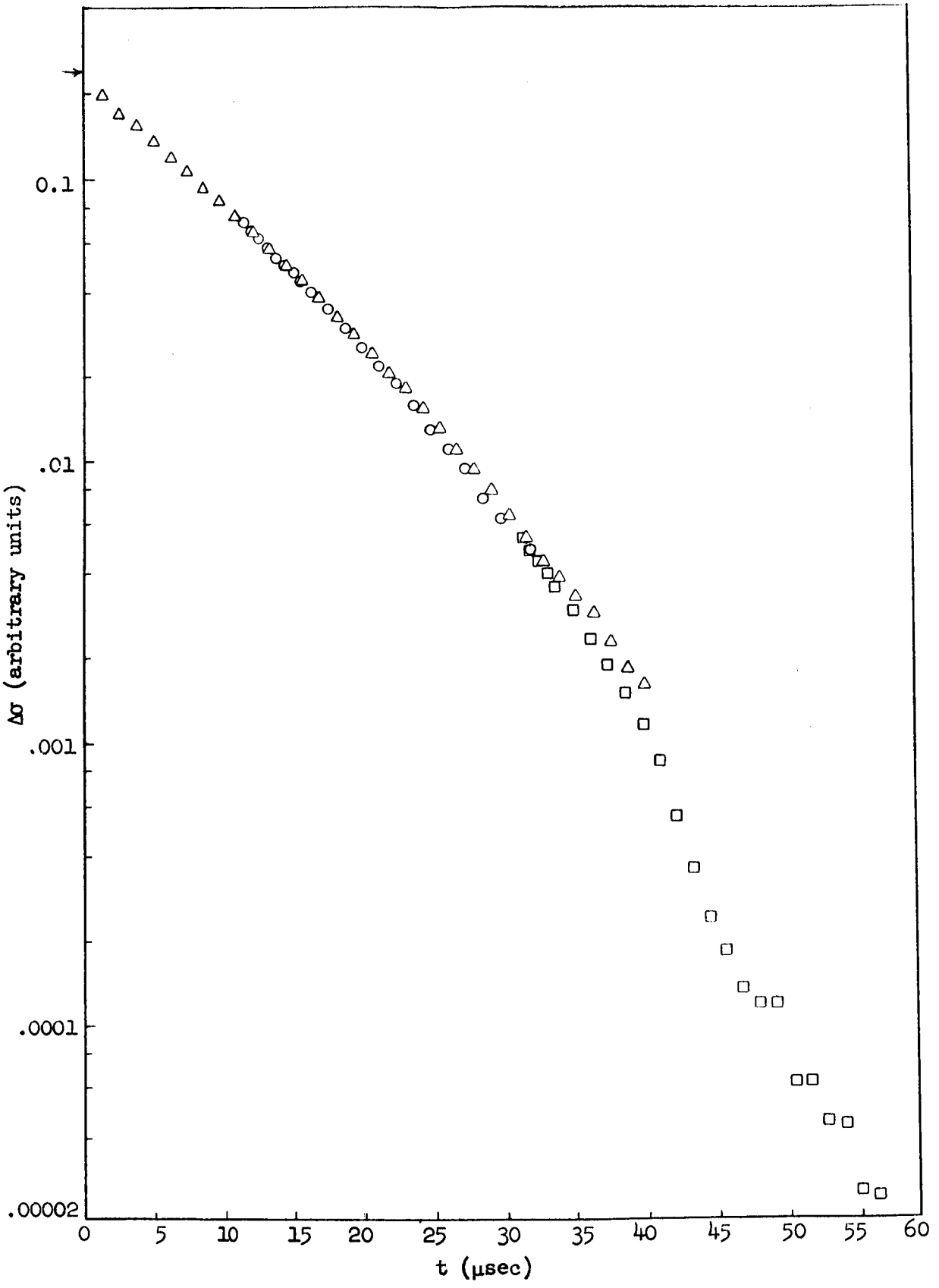

Fig. 24--Decay of excess conductivity - 7 ohm-cm QC silicon (5.2×10^{12} electrons/cm^2, 380°K)

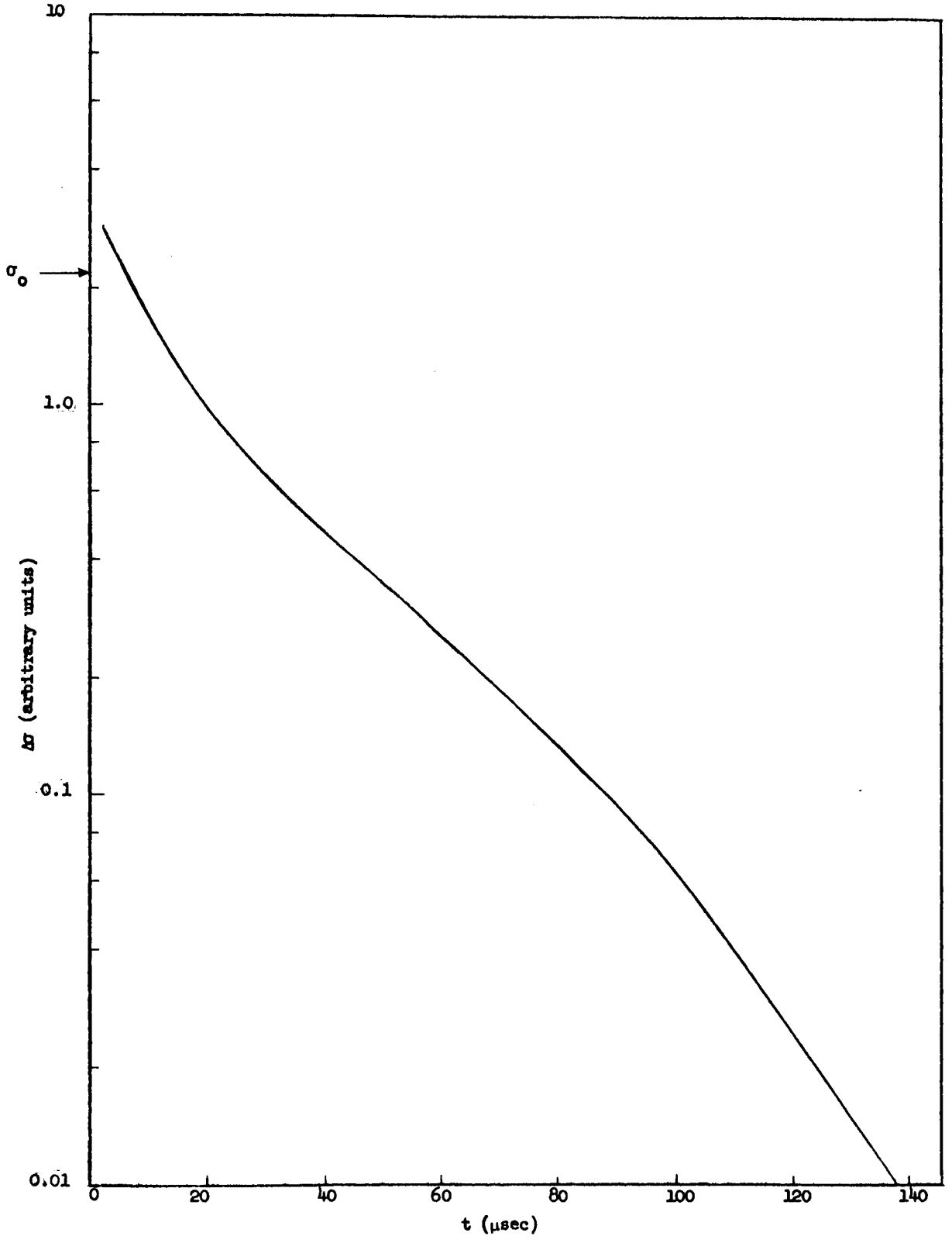

Fig. 25--Decay of excess conductivity - 7 ohm-cm QC silicon before irradiation, 100°K

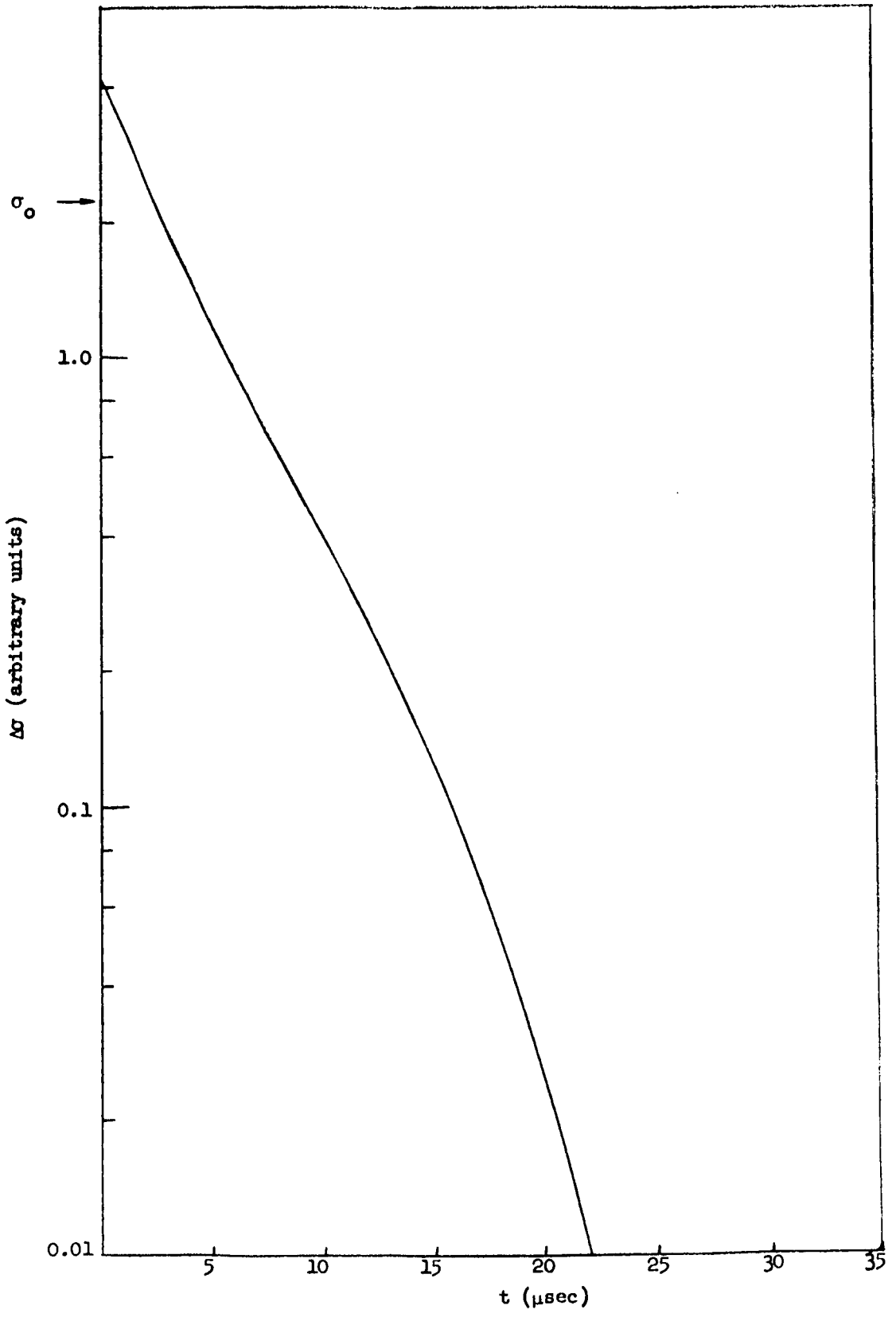

Fig. 26--Decay of excess conductivity - 7 ohm-cm QC silicon (5.2×10^{12} electrons/cm^2, 100°K)

Figures 27 and 28 show the decays after another irradiation amounting to a total flux of 1.7×10^{13} electrons/cm^2 at a temperature of 380°K and 100°K respectively. Again, an appreciable change in the decay rate as a function of excess carrier density is seen at the higher temperature. The decay rate at liquid nitrogen temperature appears to be a single exponential except for an increase in decay rate below 5 percent excess-carrier density. At 300°K, the shape of the decay curves was very similar to that observed at 380°K, although the lifetimes were somewhat different. The results of the measurement of the decay rate as a function of temperature are displayed in Fig. 29. The decay behavior previously observed in this type of material is seen again in the vicinity of room temperature. The slope of the decay curve indicates an activation energy of approximately 0.11 ev. In an intermediate region, between 110 and 200°K, the decay time is relatively constant; in the vicinity of liquid nitrogen temperature, the decay time increases rapidly with decreasing temperature.

In order to check that the excess electrons observed were, in fact, all of the electrons created, the ratio of excess conductivity at the end of the accelerator pulse, corrected for any decay during the accelerator pulse, to the integrated ionization flux was evaluated. This quantity, called μ^*, is proportional to the sum of the electron and hole mobilities. The temperature dependence of this quantity, as evaluated after the first and second irradiations, is shown in Fig. 30.

It is surprising that the slope of this curve is only 1.82 instead of the expected value near 2.5. The same slope was observed before irradiation and hence cannot be ascribed to defect impurities induced by the irradiation. It is possible that this particular sample contained a high enough concentration of ionized impurity centers before irradiation to significantly affect the temperature dependence of the mobility. On the other hand, it would be surprising if a small amount of carrier trapping at the lower temperatures would produce such a smooth temperature dependences as is observed. Hence, we will assume that the temperature dependence of the mobility as seen indicates that essentially all of the carriers produced by the radiation are actually observed, with the possible qualification that the holes could be trapped because their contribution to the over-all conductivity is less than the inaccuracies in the μ^* measurements.

After a last irradiation amounting to an integrated flux of 2.4×10^{14} electrons/cm^2, the lifetime was too short to be directly measurable. However, rough calculations of the lifetime were performed by electronically integrating the signals and, from this quantity, evaluating the equilibrium in the conductivity between rate of production and rate of decay of

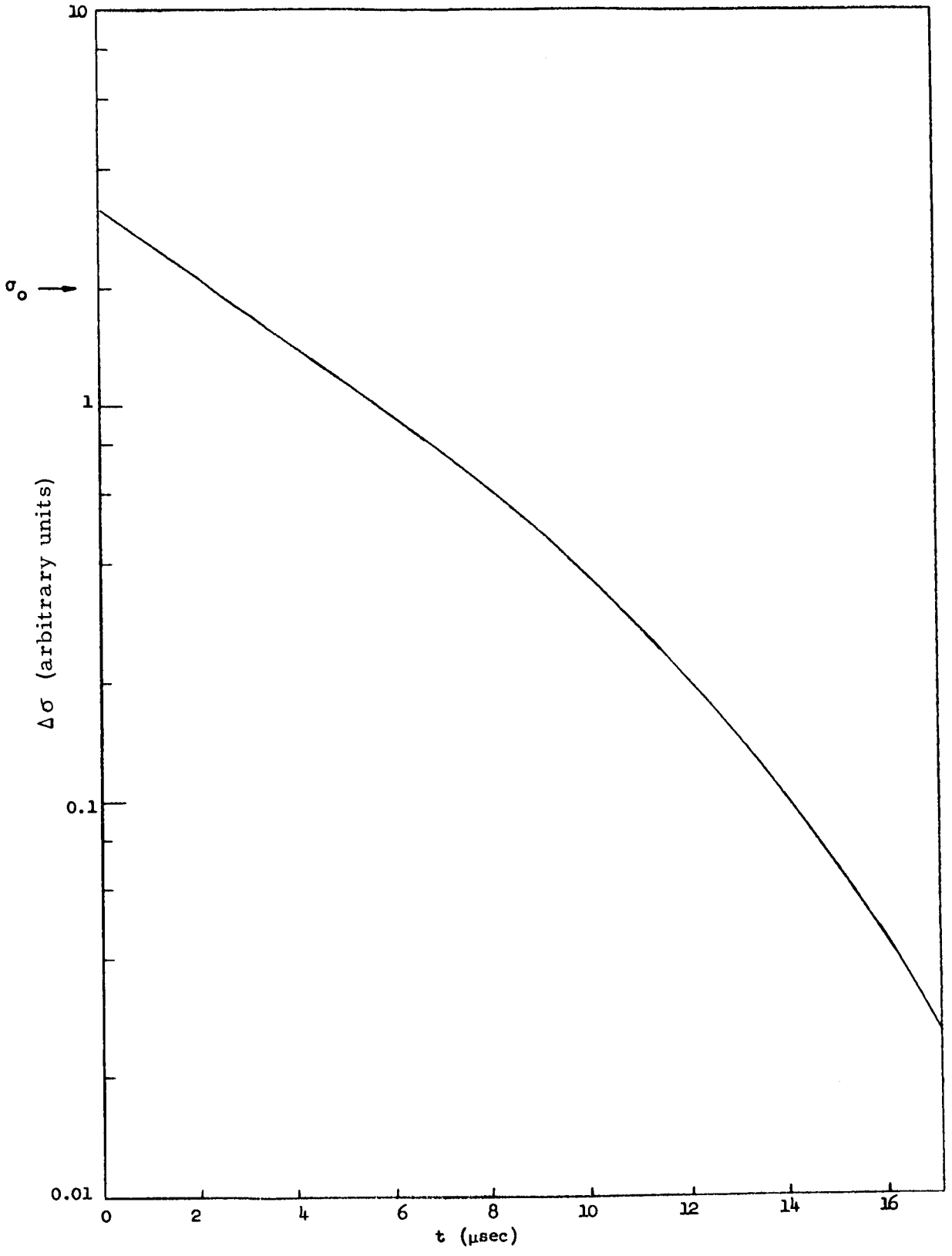

Fig. 27--Decay of excess conductivity - 7 ohm-cm QC silicon (1.7×10^{13} electrons/cm^2, $380^{\circ}K$)

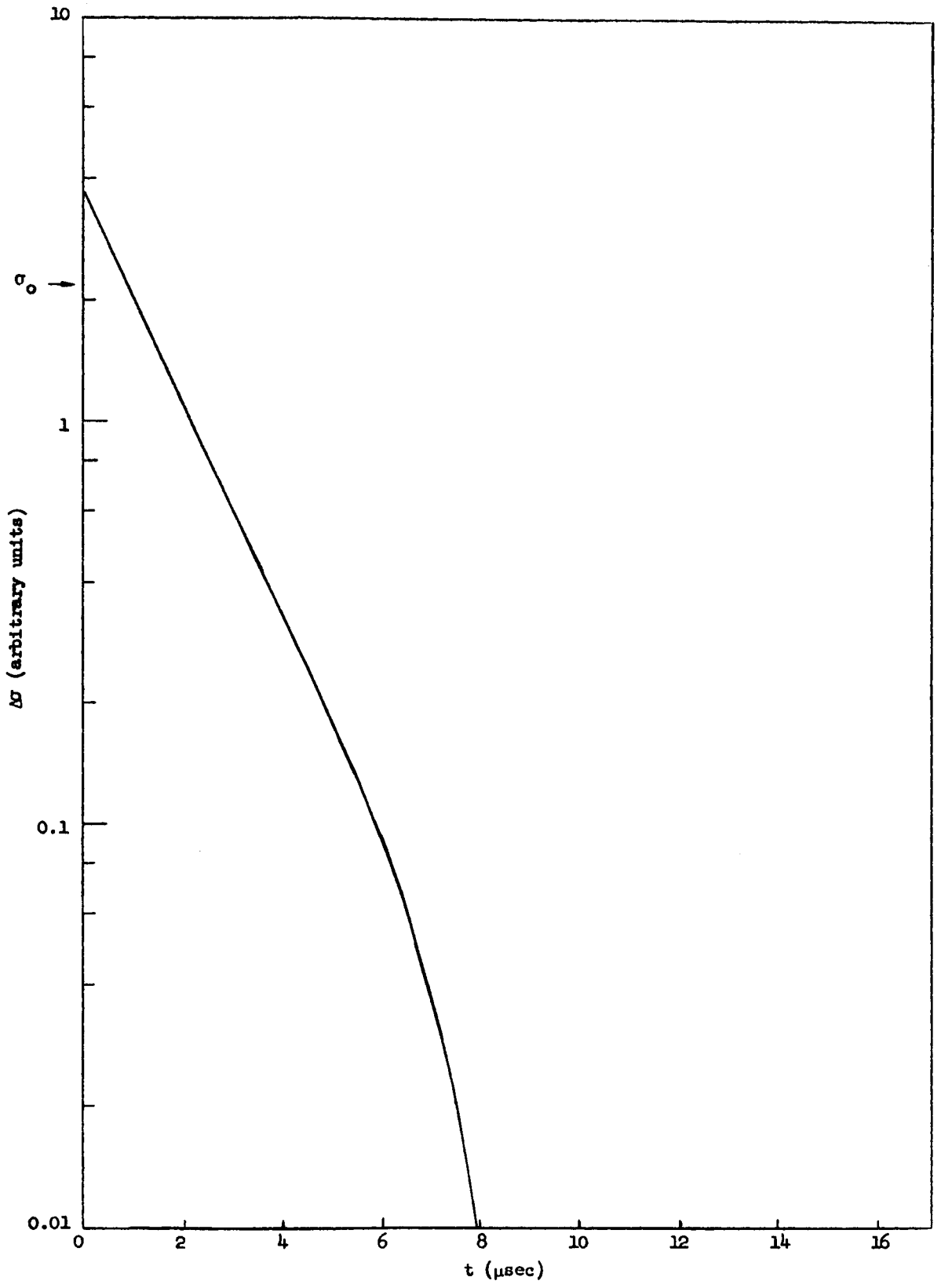

Fig. 28--Decay of excess conductivity - 7 ohm-cm QC silicon (1.7×10^{13} electrons/cm^2, 100°K)

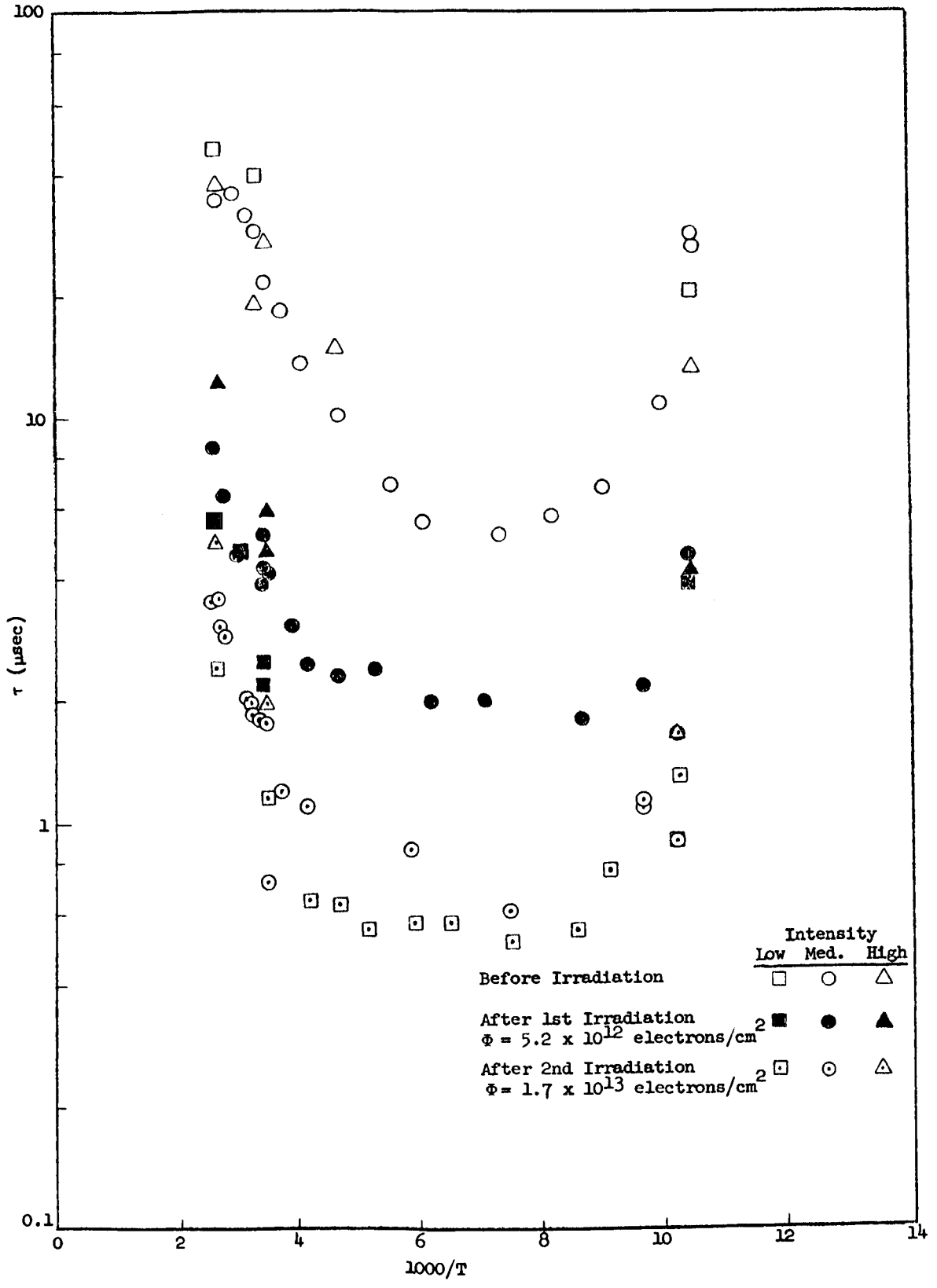

Fig. 29--Temperature dependence of carrier lifetime - 7 ohm-cm QC silicon

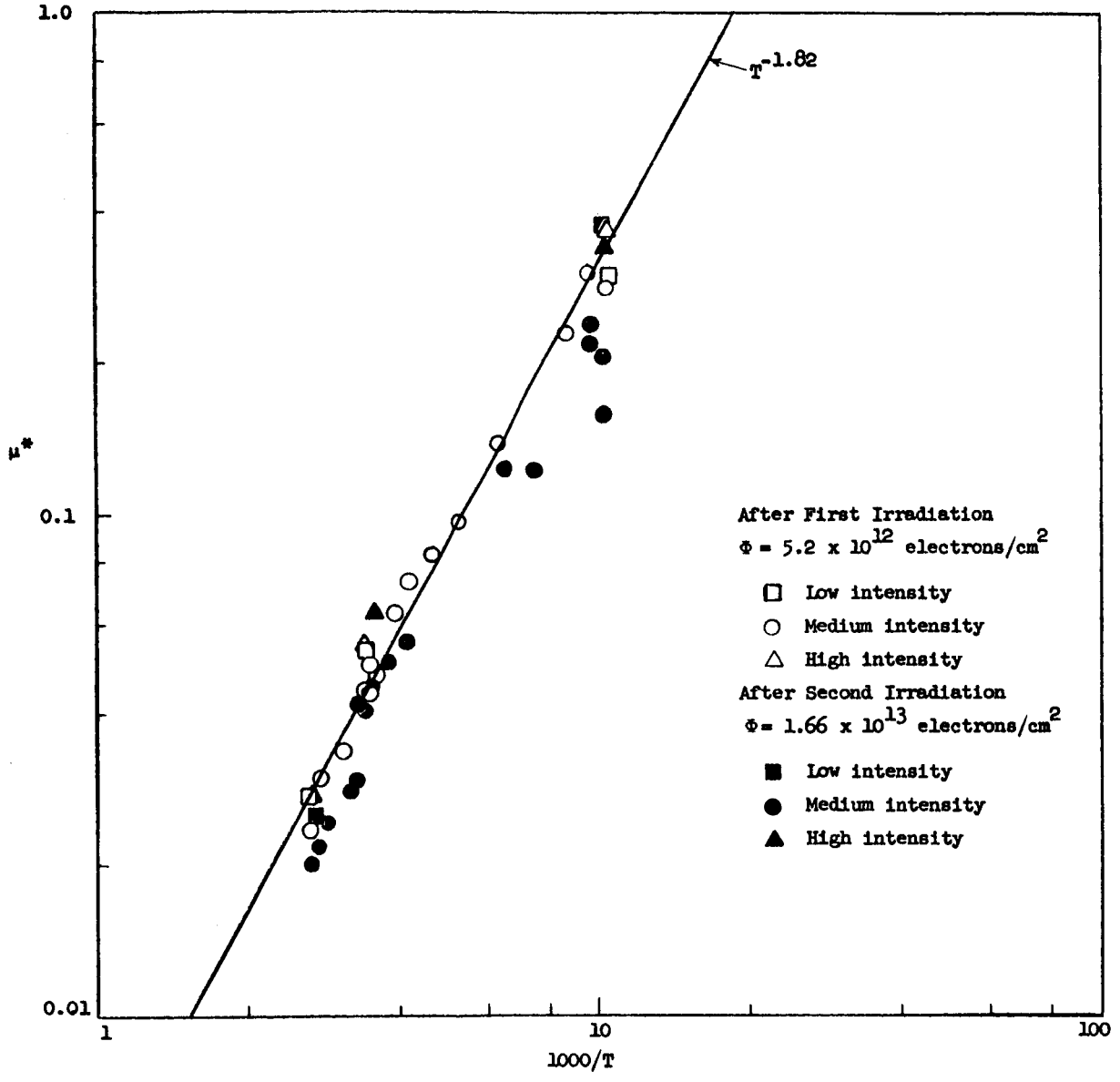

Fig. 30--Temperature dependence of μ^* - 7 ohm-cm QC silicon

the excess carriers. This calculation is based upon the equation

$$\int \Delta \sigma \, dt = \mu^* \tau M$$

where M is the integrated accelerator flux in the same units used for calculating μ^* from the excess conductivity data. This equality is valid for an exponential carrier relaxation process and independent of whether τ is short, comparable, or long compared to the ionization pulse width. The resultant values of the carrier lifetimes were in the vicinity of 0.25 μsec near room temperature, increasing by almost a factor of 2 up to 380°K. The region around liquid nitrogen temperature and up to room temperature was clouded by nonreproducibilities in the measurement, and the results cannot be trusted. It is possible that there were some contact rectification effects.

The Shockley-Read theory implies that the quantity $\tau (1+\Delta n/n_o)$ should be a linear function of the quantity $\Delta n/n_o$. From curves similar to those shown in Figs. 23 through 28, the slope as a function of $\Delta\sigma$ was used to calculate the data points in Fig. 31.

The rate of change of lifetime at room temperature deduced from these data is dependent upon the carrier injection level. It is seen that before irradiation there is essentially no dependence of the lifetime upon excess carrier density, apart from diffusion effects, but after irradiation there is a strong dependence of the lifetime on excess carrier density. To first order, it is expected that the reciprocal of the lifetime should be proportional to the number of defects introduced. The rate of change of lifetime with irradiation for the lowest excess carrier densities used (~1-percent of n_o) is given by the expression

$$\frac{d(1/\tau)}{d\Phi} = 5 \times 10^{-8} \text{ cm}^2/\text{sec}.$$

Another sample of QC material with almost the same carrier concentration was irradiated on November 2, 1962. The lifetime measurements were performed with only one carrier-generation intensity corresponding to the medium intensity used during the experiments of September 18, 1962. The temperature dependence of this sample was taken from a different boule, secured from a different manufacturer, to check the reproducibility of the results in different QC materials. The temperature dependence of the lifetime before irradiation and after irradiation is shown in Fig. 32. The decay curves observed during this run show the same general behavior seen for the September 18 sample. Before irradiation, the decays were accurately exponential; after irradiation, the slope of the decay increased in the latter portion, corresponding to the lower excess-carrier concentrations. The rate of change of reciprocal lifetime

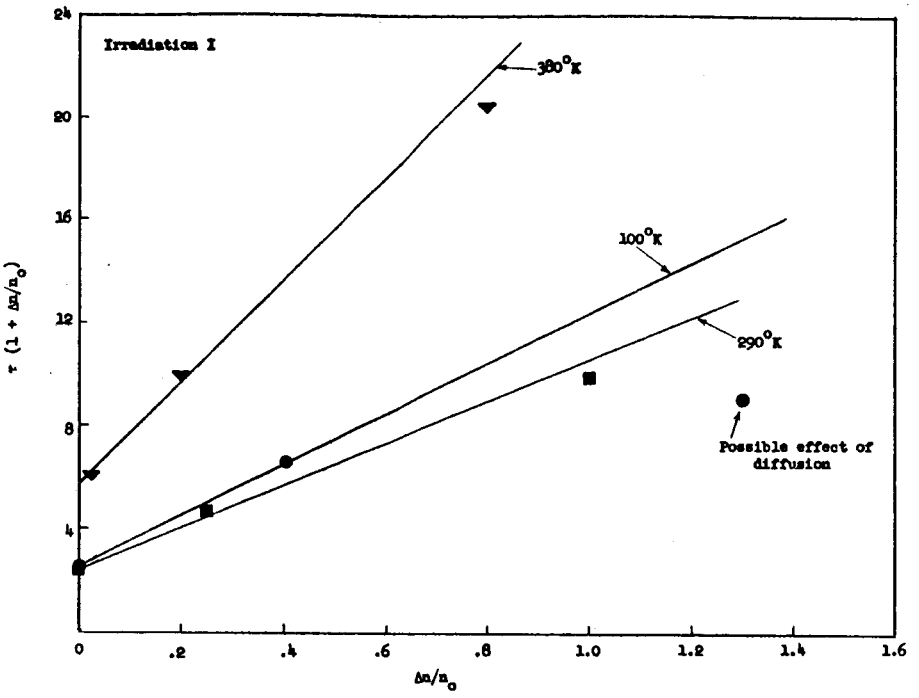

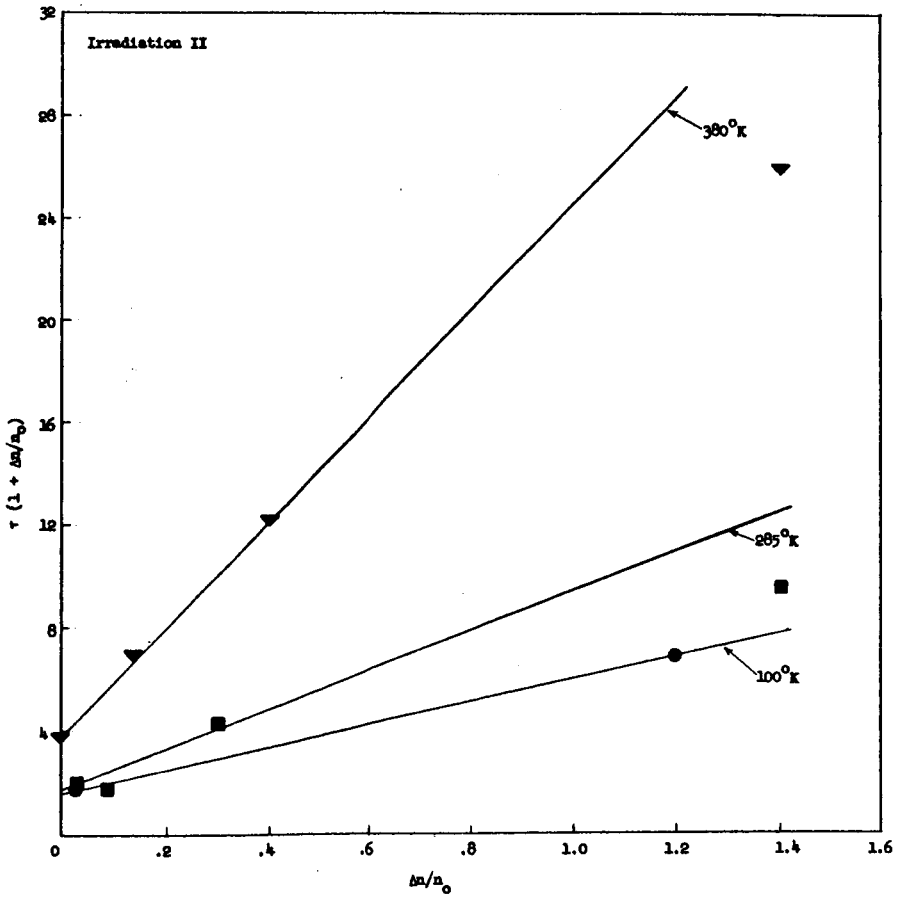

Fig. 31--Dependence of lifetime on excess carrier concentration - 7 ohm-cm QC silicon

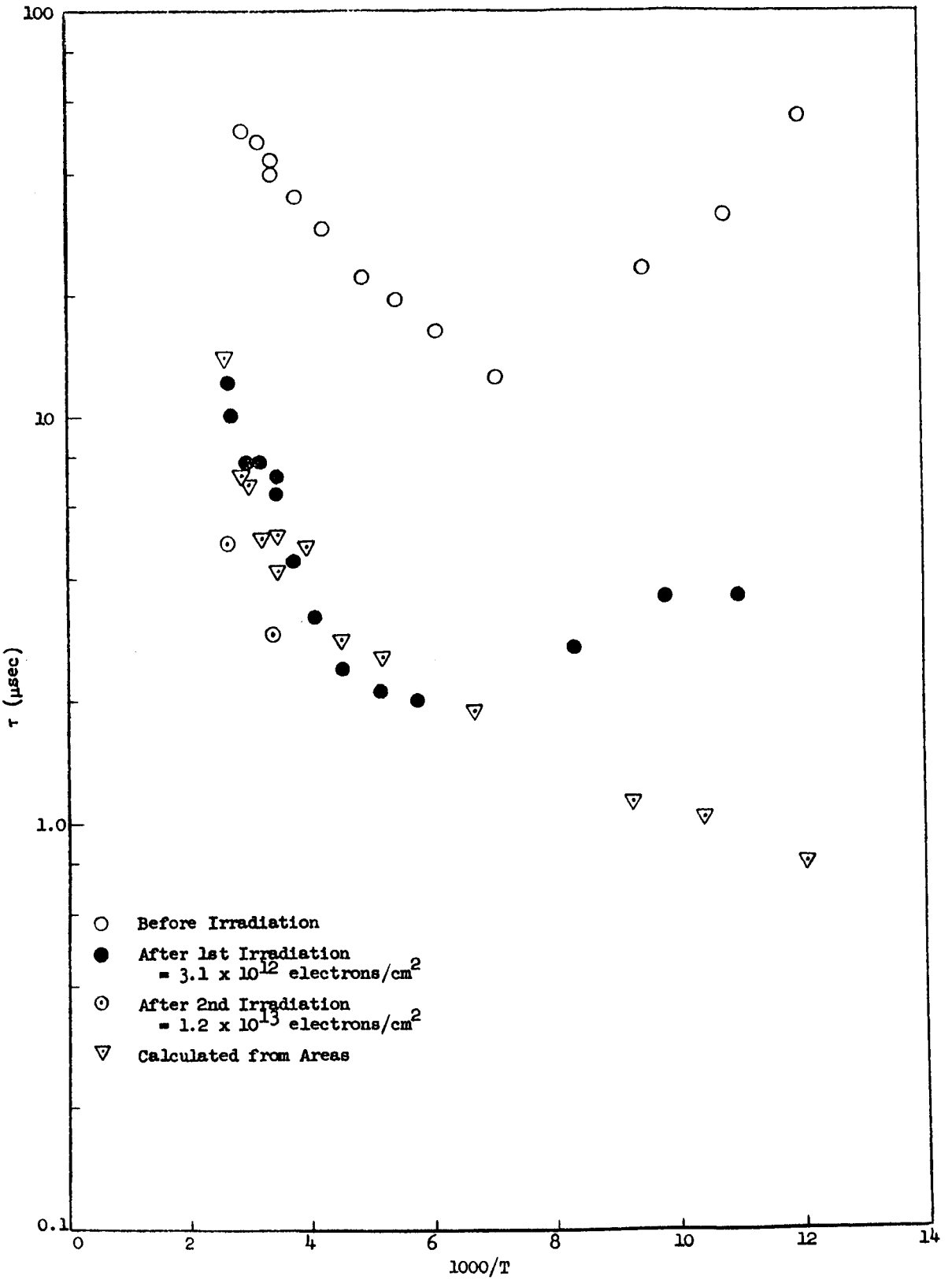

Fig. 32--Temperature dependence of carrier lifetime - 10 ohm-cm QC silicon

for this run is given by

$$\frac{d(1/\tau)}{d\Phi} = 4.2 \times 10^{-8} \text{ cm}^2/\text{sec},$$

a value consistent with the previous result, considering the high intensities used to measure τ. Similar to the previous sample, the lifetime was measured after the last irradiation by observing the magnitude of the excess conductivity and assuming a temperature dependence of μ^* to be the same as before irradiation. (See Fig. 33.) In this case, the slope of the μ^* versus temperature curve was an exponent of 2.33, which is more nearly in agreement with the published information for pure lattice phonon scattering. As seen in Fig. 32, the lifetimes calculated by this method did not exhibit the increase at low temperatures seen for direct lifetime measurements. It is not yet clear whether these measurements were sufficiently accurate to make this fact significant.

Another experiment was peformed with a 10 ohm-cm n-type FZ silicon crystal. In this material, the apparent increase in lifetime near liquid nitrogen temperature was never observed. The temperature dependence of the lifetime as a function of excess carrier density is shown in Fig. 34. The shape of the excess carrier decay curve before irradiation is shown in Figs. 35 and 36. In this case, the lifetime was somewhat shorter than in the previously irradiated QC samples, and the apparent higher-mode diffusion contribution at early times in the decays was not observed. Decays were exponential over the entire range of observation. After an irradiation by 6.5×10^{12} electrons/cm^2, the excess carrier decays were as shown in Figs. 37 and 38. Again, the increase of decay rate at lower excess carrier concentrations is observed. After a total irradiation by 3.8×10^{13} electrons/cm^2, the decay rate is shown in Fig. 39, corresponding to the 380°K temperature. This time, the decay rate at liquid nitrogen temperature was too fast to allow accurate measurements to be made at the low excess carrier concentrations.

The rate of change of lifetime for this sample was calculated to be

$$\frac{d(1/\tau)}{d\Phi} = 4.8 \times 10^{-8} \text{ cm}^2/\text{sec}.$$

The temperature dependence of μ^* was again used to calculate some of the lifetimes after the last irradiation, and again the slope of 2.37 as shown in Fig. 40 is consistent with published values. The dependence of lifetime on carrier concetration for this sample is summarized in Fig. 41.

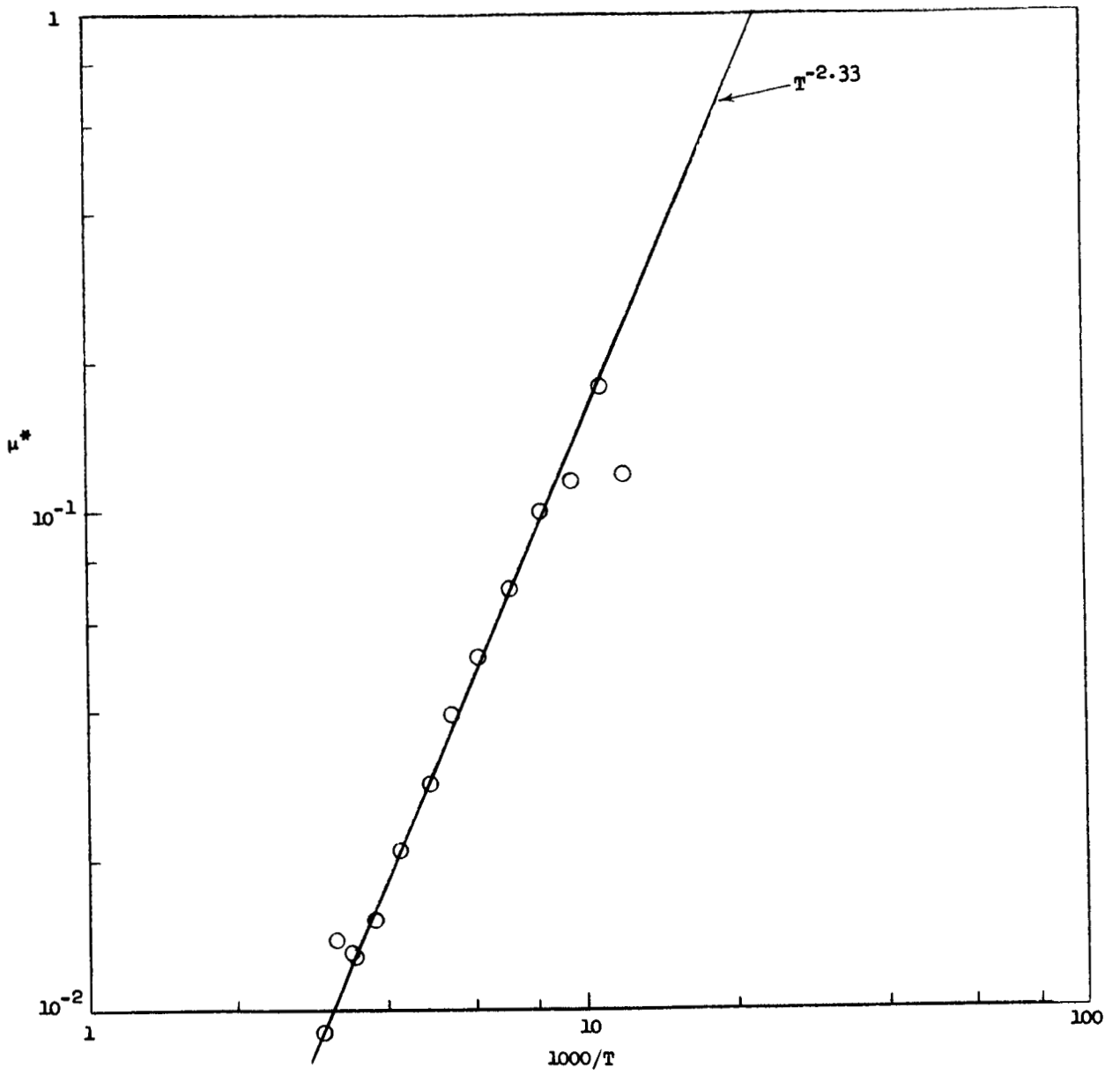

Fig. 33--Temperature dependence of μ^* - 10 ohm-cm QC silicon

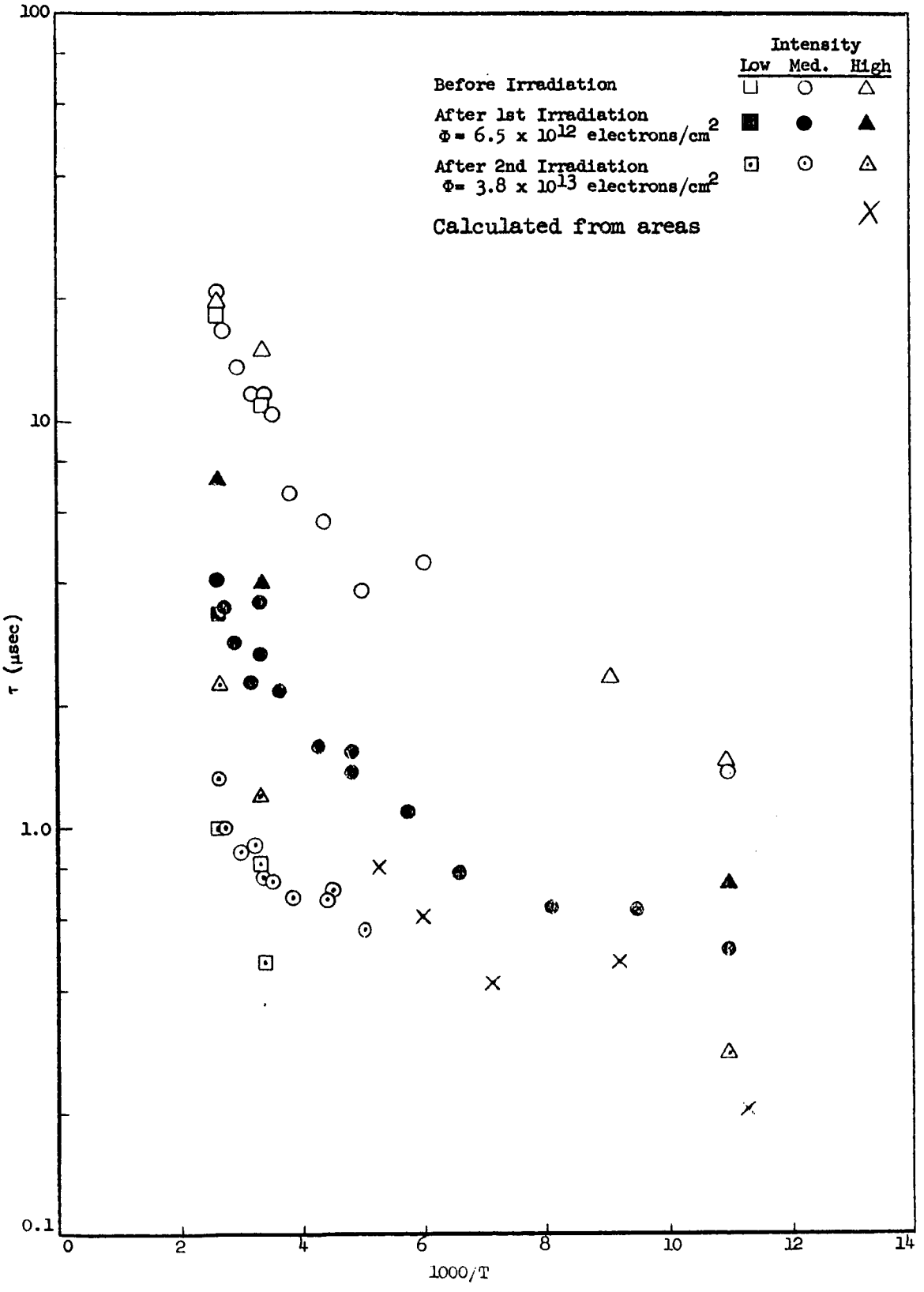

Fig. 34--Temperature dependence of carrier lifetime - 10 ohm-cm FZ silicon

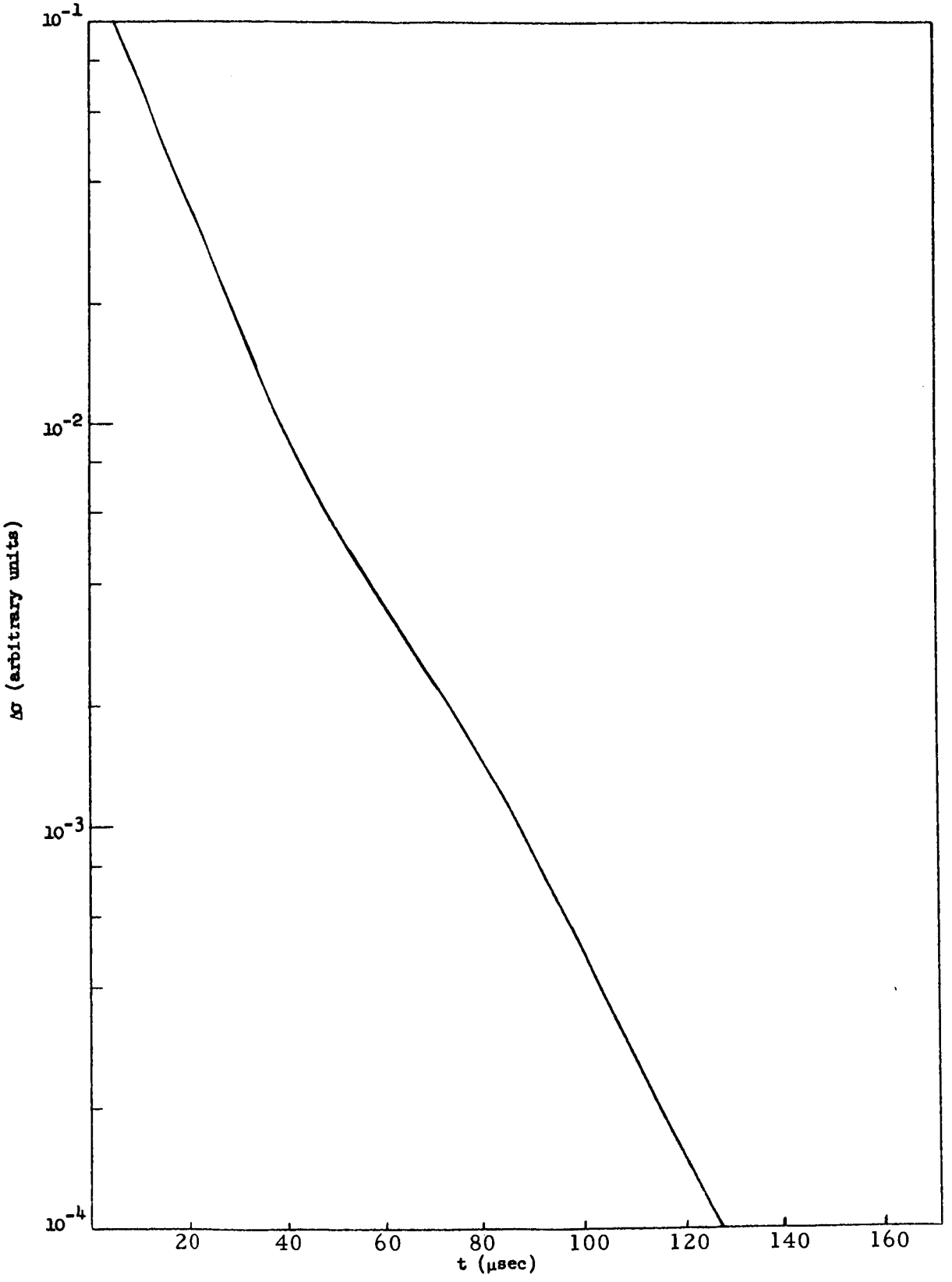

Fig. 35--Decay of excess conductivity - 10 ohm-cm FZ silicon before irradiation, 380°K

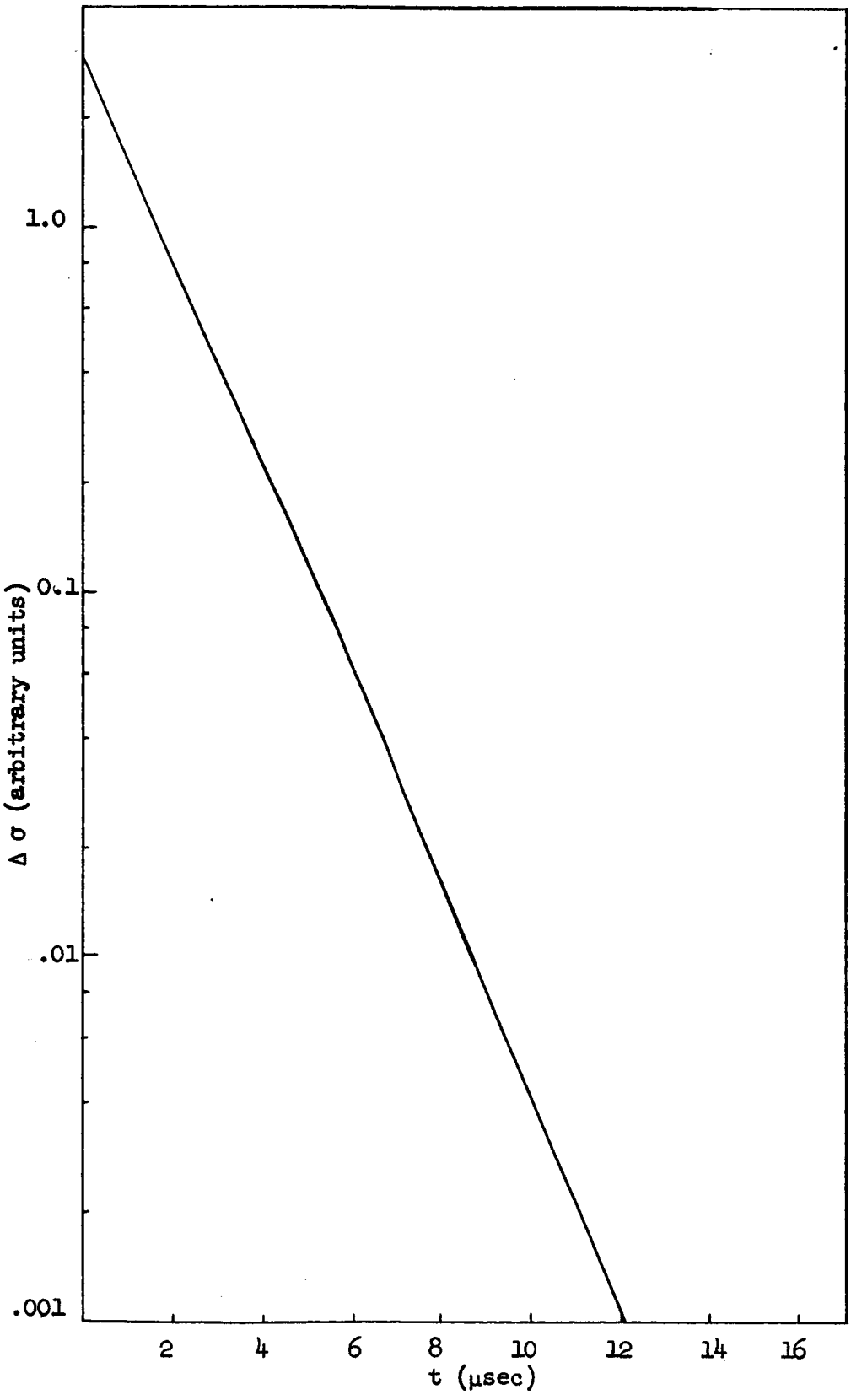

Fig. 36--Decay of excess conductivity - 10 ohm-cm FZ silicon before irradiation, 100°K

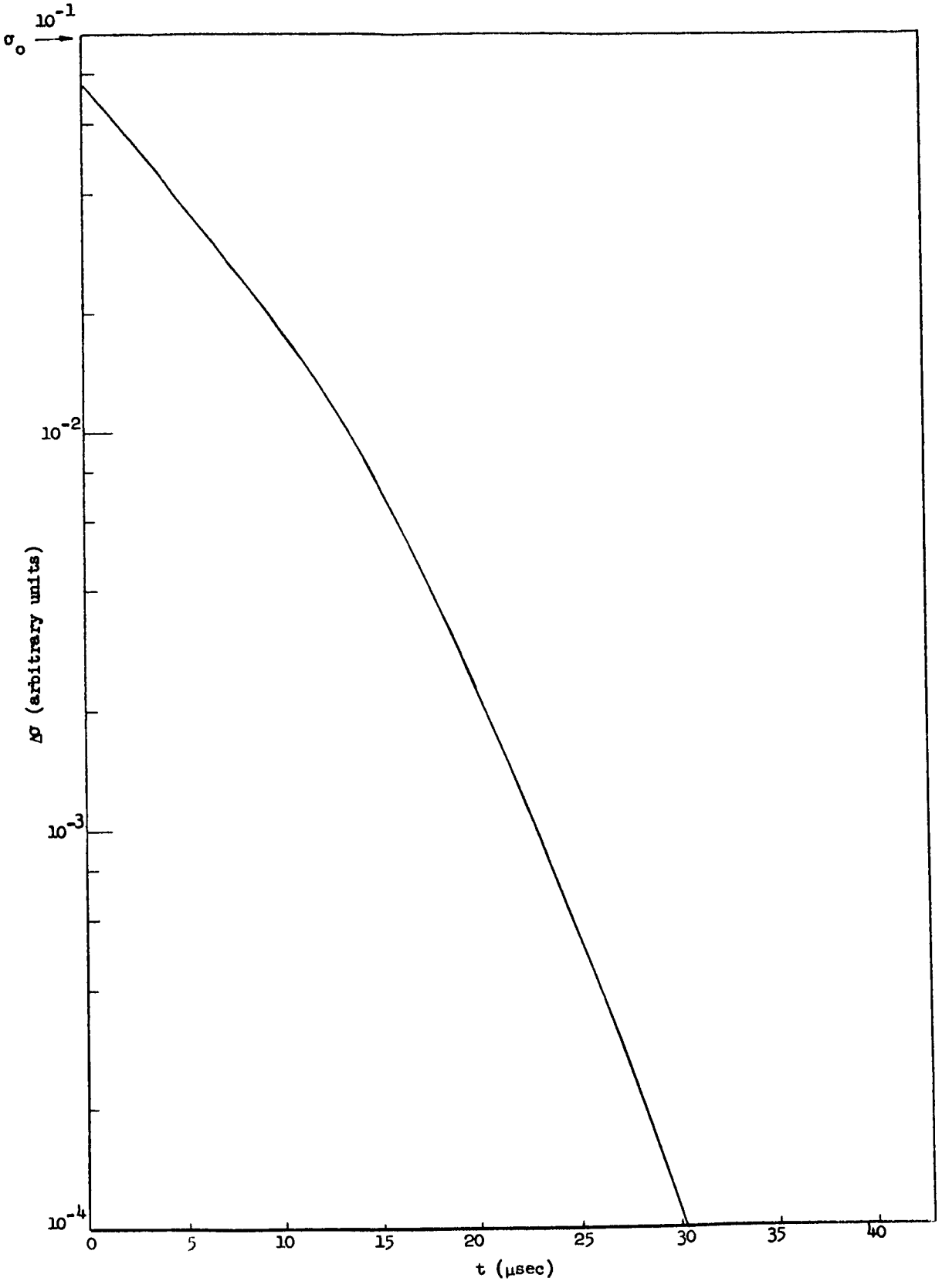

Fig. 37--Decay of excess conductivity - 10 ohm-cm FZ silicon (6.5×10^{12} electrons/cm^2, 380^oK)

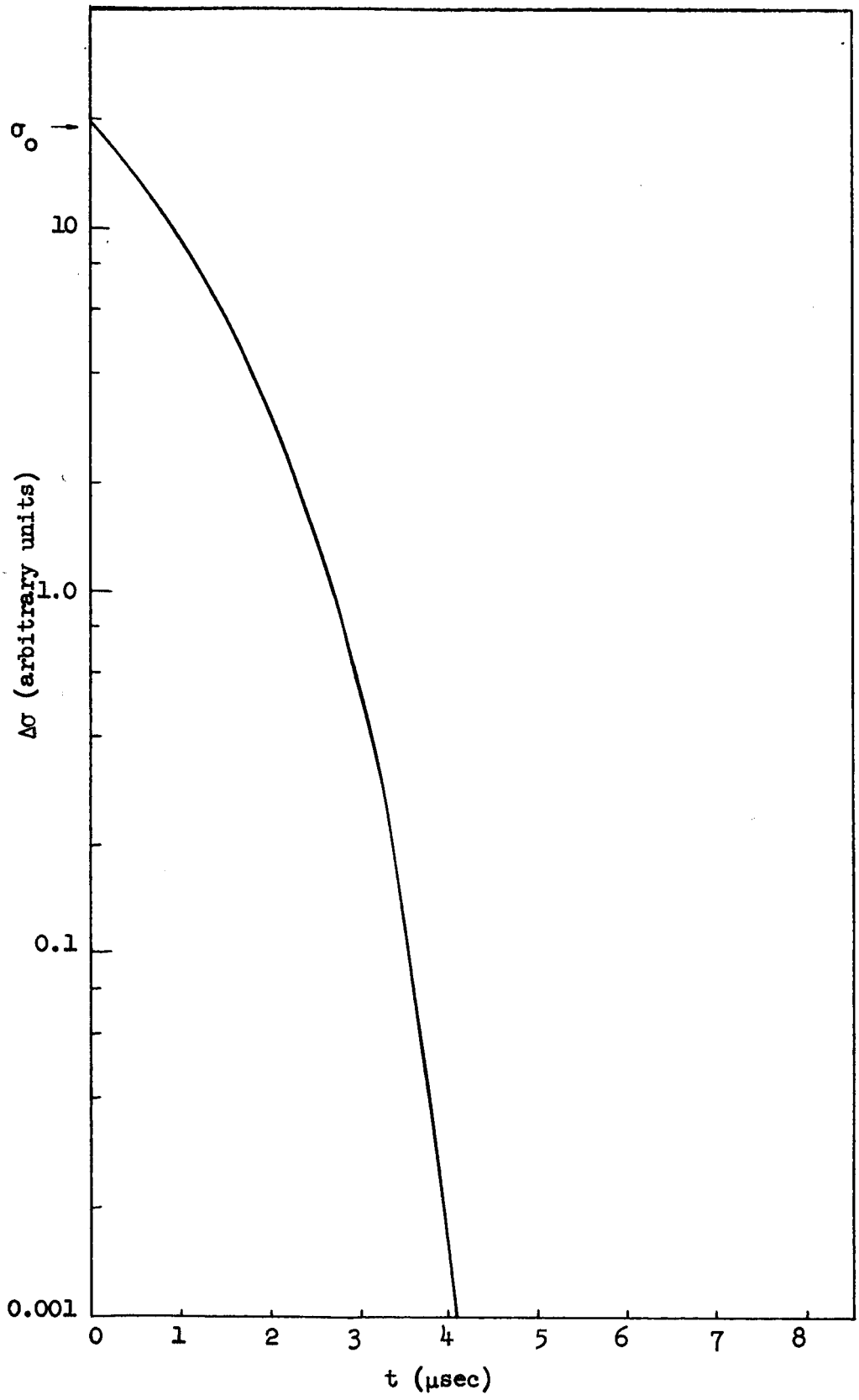

Fig. 38--Decay of excess conductivity - 10 ohm-cm FZ silicon (6.5×10^{12} electrons/cm^2, 100°K)

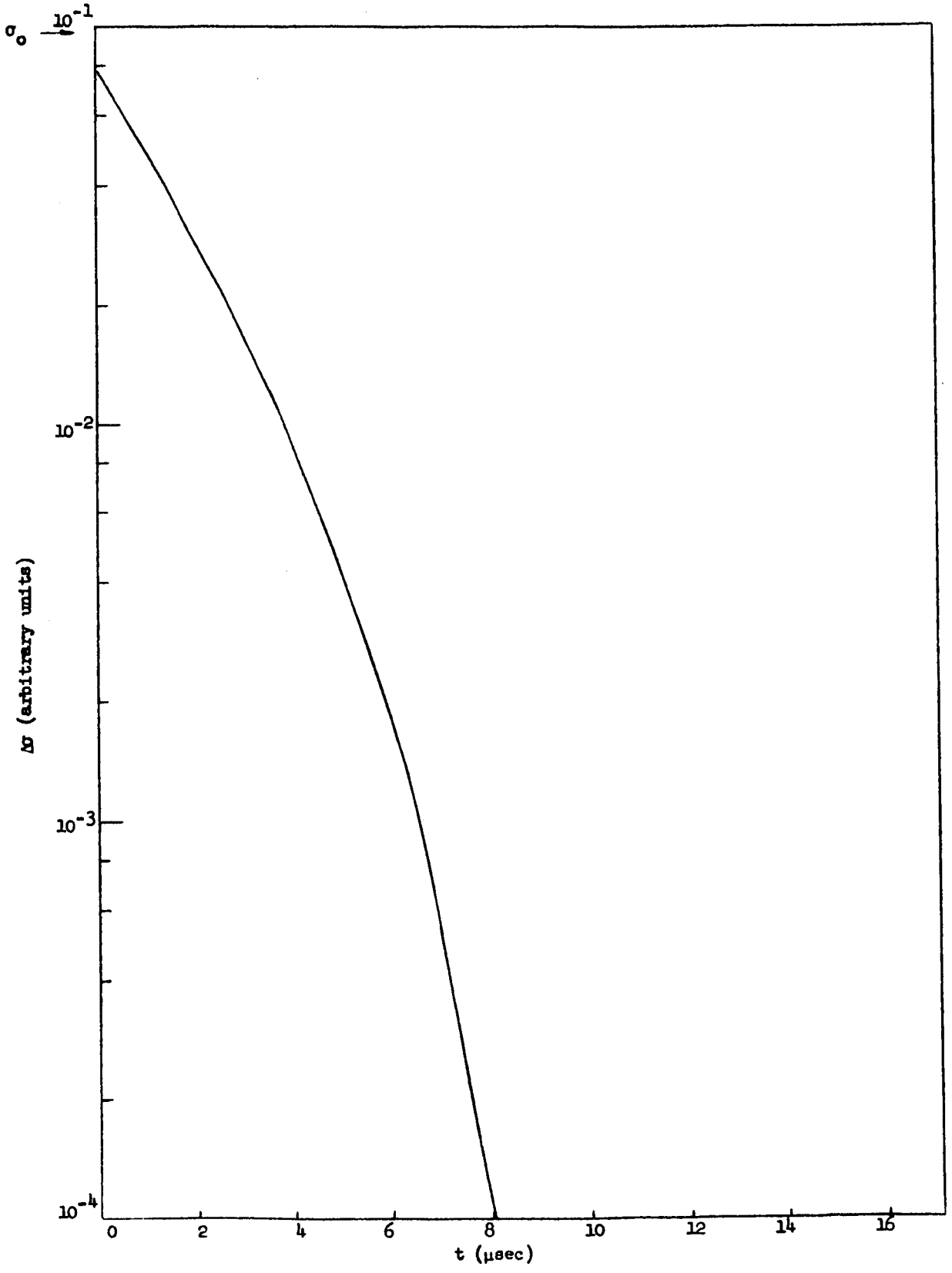

Fig. 39--Decay of excess conductivity - 10 ohm-cm FZ silicon (3.8×10^{13} electrons/cm^2, 380°K

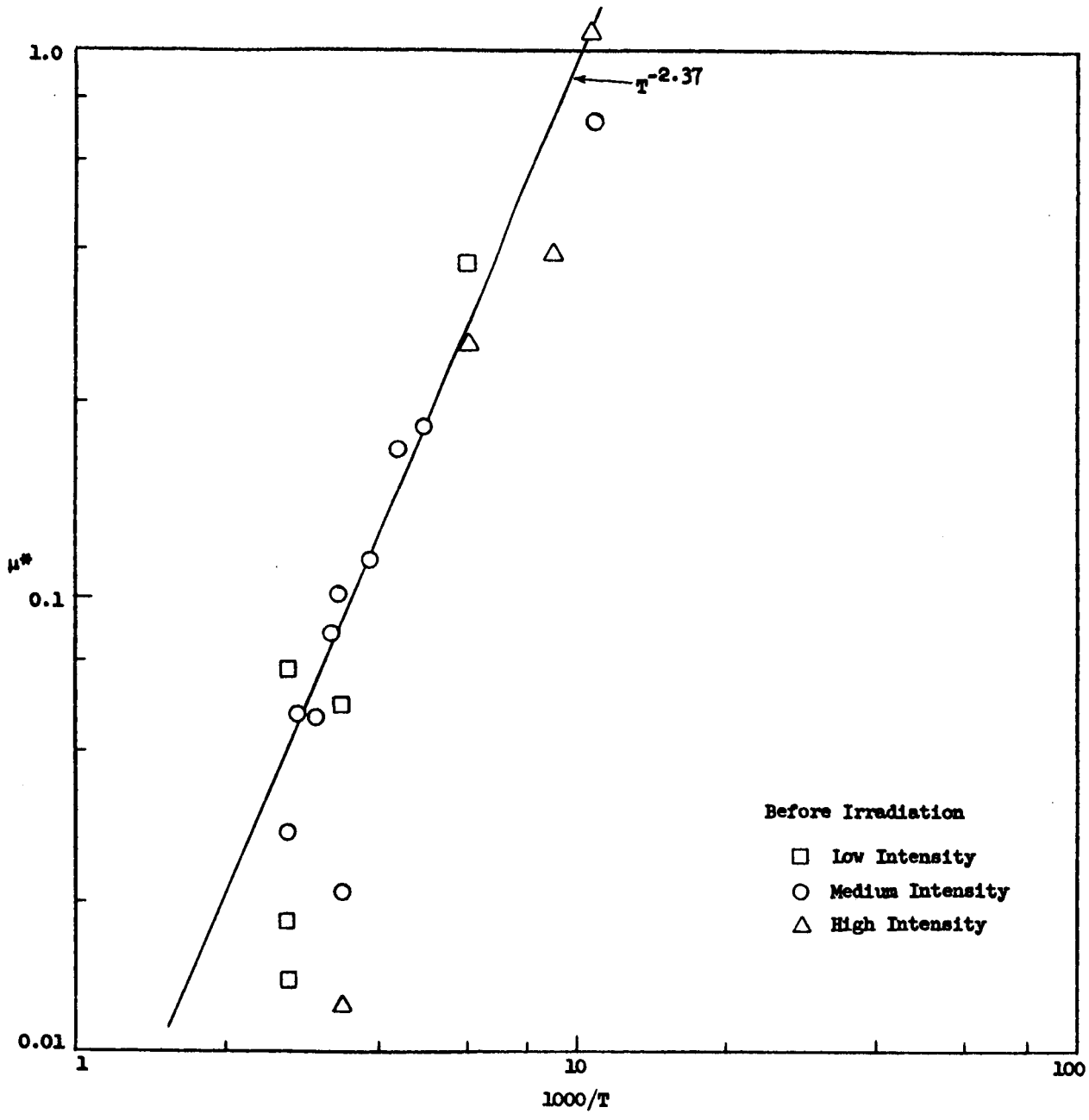

Fig. 40--Temperature dependence of μ^* - 10 ohm-cm FZ silicon

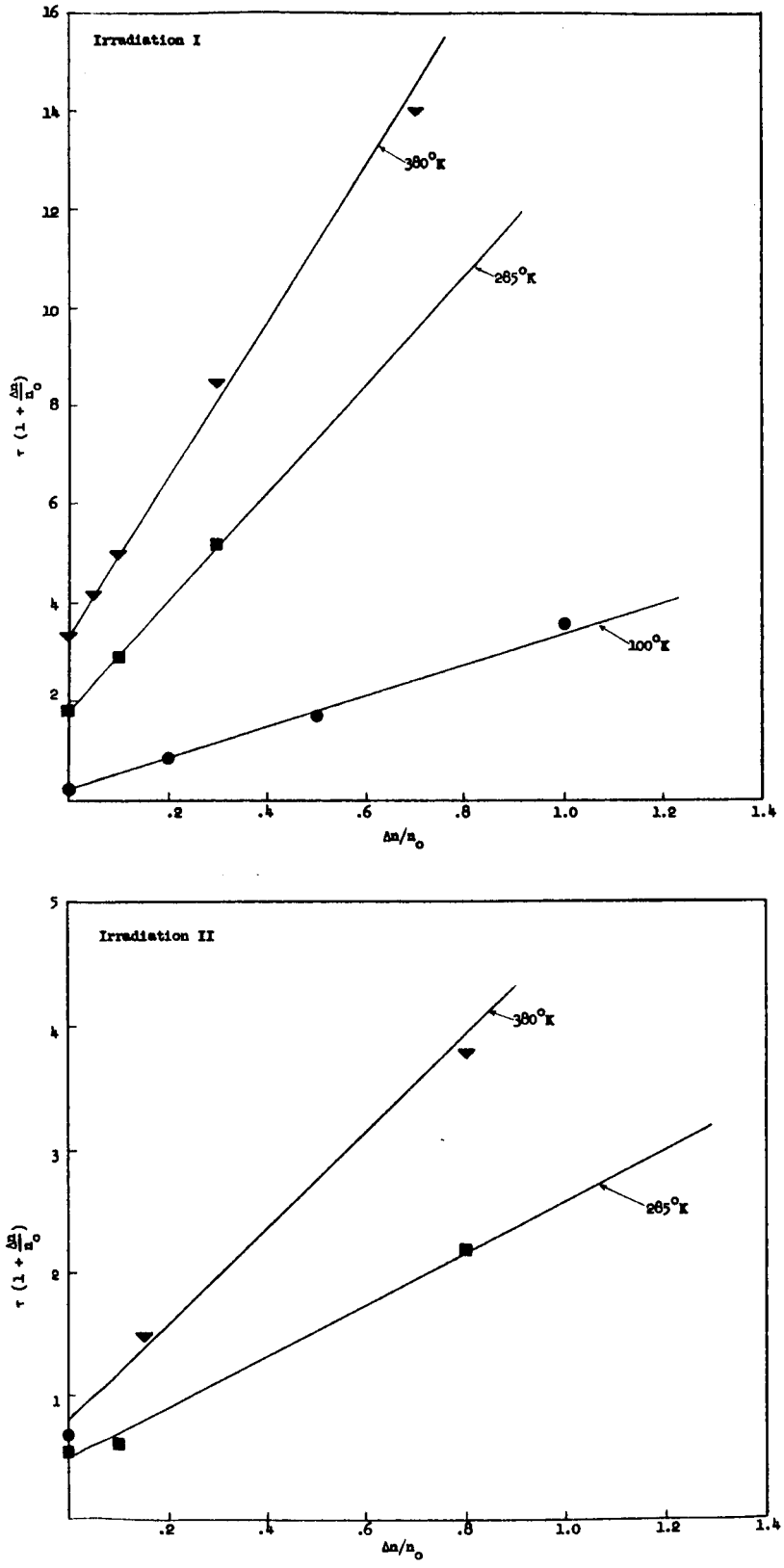

Fig. 41--Dependence of lifetime on excess carrier concentration - 10 ohm-cm FZ silicon

5.3 DISCUSSION

The most important features of the experimental data are the following:

1. The rate of change of lifetime during irradiation is approximately the same for QC and FZ materials.
2. It appears that the defects responsible for the lifetime changes in the vicinity of room temperature have an activation energy of approximately 0.11 ev, independent of the nature of production of the material.
3. Before irradiation, the lifetime is independent of excess-carrier concentration within the region $\Delta n/n_o = 10^{-3}$ to 1. Once the recombination is dominated by the radiation-induced recombination centers, however, the lifetime is a strong function of the excess-carrier concentration, especially in the vicinity of room temperature.

This latter observation, that the lifetime after irradiation is a strong function of excess carrier concentration, may assist in explaining some of the contraditory results from previous experimental measurements. It appears that the observed lifetime, as well as the temperature dependence, is a strong function of the concentration of excess carriers used to measure the lifetime. The technique used during this experimental program is ideal for maintaining accurate control over the excess-carrier concentration, and the data analysis procedures used enable us to plot out in detail the entire excess-carrier decay curve for analysis. The strong dependence of the excess-carrier lifetime on excess-carrier density is in agreement with measurements on silicon solar cells.[31] In this case, it was observed that, under higher illumination intensity, the effective minority carrier diffusion length, which is a measure of the recombination time, increased with increasing light intensity. Our observation that the carrier lifetime increases with increasing excess-carrier density is consistent with these results. It is also interesting to note that, within the information available, this effect does not seem to be as predominant for ~1-Mev electron irradiations as it is for either high-energy proton or higher-energy electron irradiations.

The values of the intercept and slopes of the plots of $\tau(1 + \Delta n/n_o)$ versus $\Delta n/n_o$ for the September 18 and October 12 irradiations have been summarized in Table 6. The activation energy, ϵ, corresponds to that activation energy calculated from the ratio in values at 285°K and the values at 380°K. The accuracy of this number is, of course, limited since it was determined from only two measurements. In interpreting this table, we must remember that the September 18 sample was a QC sample, whereas the October 12 data refers to an FZ sample. The

Table 6

ANALYSIS OF LIFETIME DATA

	$T(^{o}K)$	$\tau_{po}\left(1+\frac{n_1}{n_o}\right)$	ϵ (ev)	$(\tau_{no}+\tau_{po})$ (μsec)	ϵ (ev)	$\Phi(e/cm^2)$ ($\times 10^{12}$)
			QC Sample			
	380	5.8	0.09	19.9	0.09	5.2
I	285	2.4	"	8.2	"	
	100	2.5	"	9.8	"	
	380	1.9	0.08	11.0	0.10	17.0
II	285	0.9	"	3.9	"	
	100	0.8	"	2.2	"	
			FZ Sample			
	380	3.3	0.06	16.0	0.04	6.5
I	285	1.8	"	11.0	"	
	100	0.3	"	3.1	"	
	380	0.8	0.05	4.0	0.07	38.0
II	285	0.5	"	2.1	"	
	100	?				

following observations are significant:

1. At 100°K, the lifetime parameters for the QC silicon are essentially the same as those at 285°K. On the other hand, in the FZ silicon, both the intercept and slope of the lifetime plots are much smaller at 100°K than they are at 285°K.
2. It appears that the apparent activation energies for the intercept and the slope are essentially the same. This fact implies that it is quite likely that our interpretation of the rate of change of lifetime as a function of temperature in terms of the ionization energy of the recombination centers is doubtful. This interpretation is based upon the assumption that the quantity τ_{po} is approximately independent of temperature. However, it is shown that the quantity, $\tau_{no} + \tau_{po}$, measured by the slope of the curve of lifetime versus excess-carrier density, varies as rapidly as the quantity $\tau_{po}(1 + n_1/n_o)$. Hence, it is not necessarily correct to ascribe the only temperature dependence to the quantity n_1.

We have performed a quick survey of the literature to determine the status of the theoretical treatment of recombination lifetimes and the possibility of a temperature dependence. The appendix summarizes this information. In general, there appear to be severe difficulties in explaining theoretically the magnitude of the recombination cross section of impurity centers, and, therefore, the temperature dependence of these cross sections cannot be calculated with any certainty. The only reasonable agreement between experiment and theory has been secured at very low temperatures which are not applicable to our present problems. Further work in this area is needed. This observation does, however, provide further evidence for the factors that enter into the apparently conflicting interpretations ascribed to carrier lifetime data.

VI. ELECTRON SPIN RESONANCE MEASUREMENTS

6.1 THEORY

An electron in a dc magnetic field will have two energy states available to it due to the Zeeman interaction of its spin ($s = 1/2$) with the magnetic field. Electron spin resonance measurements determine the energy difference between these two states by measuring the energy required in a given magnetic field to excite an electron from the lower to the higher state.

In general, the magnetic field that an electron sees is a combination of the external field and any relevant internal fields, such as the fields due to other electron spins in the crystalline environment and the field caused by nuclear spins in the neighborhood of the electron (the hyperfine fields). Such fields can cause the original Zeeman levels to be either broadened or split. These effects can, in general, be orientation dependent. A further effect of the environment on the electron spin will be a perturbation of the Zeeman levels caused by the admixture to the pure spin states of orbital angular momentum states (spin-orbit coupling). Such effects can be described by assigning to the electron a g-value (the ratio of spin magnetic moment to angular momentum expressed in units of $e/2mc$) different from the free electron value of 2.0023. These spin-orbit effects can also be expected to be orientation dependent so that, in general, the g-value for an electron in a crystal must be described by a tensor.

It thus follows that measurement of electron spin resonance will serve to determine both the magnitudes of the local fields, due both to the dipole fields in the crystal and to the hyperfine interactions, and the effects of spin-orbit interaction. It can be expected that these effects will be different for electrons associated with different centers in a crystal because of positioned dependence.

It should be noted that spin resonance can be seen only for states which contain one of the two electrons allowed by the spin degeneracy. If both states are occupied, both Zeeman levels will contain an electron and hence no transition will be possible.

Considerable work has been done previously on the spin resonance of electrons associated with radiation produced centers in silicon.[16] As a specific example, for the silicon A center the g tensor has been

found by Watkins[5] to be

$$g_1 = 2.0093,$$
$$g_2 = 2.0025, \text{ and}$$
$$g_3 = 2.0031,$$

in a coordinate system oriented along the [011], [01$\bar{1}$] and [100] directions respectively and also oriented in a specific manner with respect to the A center. In addition, the hyperfine splitting, caused by interactions with the 4.7 percent abundant Si^{29}, helped greatly in identification of the structure of the center.

Use of spin resonance to monitor the number of A centers produced by irradiation is completely straightforward when the g tensor and splitting are known, since the A-center resonance is immediately identified. The area under the resonance curve is then proportional to the number of spins (and hence to the number of centers) participating. Measurement of the area of a marker sample resonance serves to calibrate the constant of proportionality.

6.2 EXPERIMENTAL RESULTS

Resonances were measured at 78 and 50°K with an incident microwave power of 1 mw. Data were taken in the dispersion mode with a modulation field of 0.5 gauss peak-to-peak. With a time constant of 10 sec the noise was approximately 2×10^{13} spins at 50°K.

The first sample in which A centers were seen, SiMoP-.5NZ1-D, showed the four-line structure typical of the A center g values with line widths of a few gauss.* Table 7 presents the data obtained from this and three subsequent samples. In addition, several other samples were irradiated at both higher and lower dose rates than those indicated in the table. In these samples no A-center resonance was seen above the noise.

All of the samples studied were irradiated at room temperature and subsequently cooled for resonance measurements.

---

*The orientation of the sample with respect to the dc magnetic field was not determined for this sample.

Table 7

ESR MEASUREMENTS OF A CENTER CONCENTRATION

Sample	Spins ($\times 10^{14}$)	E_o(Mev)	Dose (e/cm^2) ($\times 10^{16}$)
SiMoP-.5NZ1-D	20	10	2.5
SiMoP-.5NZ1-B	1	26	1.01
SiMoP-.5NZ1-A	7	26	1.58
SiMoP-.5NZ1-C	4	26	2.13

6.3 DISCUSSION

Although only a few measurements have thus far been made, the utility of using spin resonance to monitor the number of radiation-produced centers is evident. The range of flux over which A centers are produced at 30 Mev is much more limited than that at 1.5 Mev as reported by Watkins and Corbett.[8] At high doses, the explanation for this observation is evidently the production of acceptor-like defects at energies below that of the A center. These defects remove electrons from the A-center level, thus causing loss of the resonance signal. Evidently the production of such low-lying levels is much more rapid with irradiation at 30 Mev than at 1.5 Mev. A series of measurements of the magnitude of the A-center resonance as a function of dose, at several energies, will serve to verify this assumption.

As yet facilities for operation at liquid hydrogen temperatures have not been completed. Consequently the other known centers produced by irradiation and/or anneal have not been studied since relaxation times and level population considerations require that resonance measurements be made at temperatures lower than 50°K.

VII. OPTICAL MEASUREMENTS

7.1 THEORY

The investigation of radiation damage in silicon by infrared has been one of the most fruitful experimental procedures in the past. Studies of the near IR by a number of workers have revealed a large number of absorption and photoconductivity bands that are created by the introduction of lattice defects by irradiation (See Section 2.4). The only measurements performed under the program have been on interstitial oxygen and substitutional oxygen which are identified by bands at 9 microns and at 12 microns, respectively. It is believed that the absorption at 9 and 12 microns is associated with an asymmetric vibration mode of the oxygen atom. Unfortunately, the sensitivity of the measurements is fairly low and concentrations of centers in excess of $10^{16}/cm^3$ are required to achieve significant results. However, during this experimental program these measurements have been valuable in verifying the presence of interstitial oxygen in our QC material, and confirming the much lower concentration of oxygen in the FZ materials.

7.2 EXPERIMENTAL RESULTS

The absorption curve of a typical QC silicon sample of 0.5 ohm-cm initial resistivity is shown in Fig. 42. Absorption curves measured on the same sample after irradiation by approximately 2.3×10^{16} 30-Mev electrons/cm^2 is shown in Fig. 43. Within the accuracy of the measurements there is no appreciable difference between these two absorption curves. The large absorption of 9 microns only confirms the presence of approximately 5×10^{17} oxygen atoms/cm^3. A similar pair of curves on 0.5 ohm-cm QC silicon secured from a different manufacturer are shown in Figs. 44 and 45. In this case, the irradiation was much more extensive, amounting to 2.5×10^{17} electrons/cm^2. The sample was also thicker to increase the resolution of the optical measurements. Again there was no appreciable change in the transmission curve. In particular, the absorption in the vicinity of 12 microns was not appreciably enhanced by the irradiation. A pair of curves taken on FZ material is shown in Figs. 46 and 47. In this case the pre-irradiation absorption, shown in Fig. 46, exhibited some structure in the vicinity of 12.5 microns which was not apparent in any other samples. The effect of irradiation by 2.4×10^{17} electrons/cm^2 was to remove that structure and make the absorption curve more similar to those for the QC material. The much smaller absorption peak in the vicinity of 9 microns indicates that

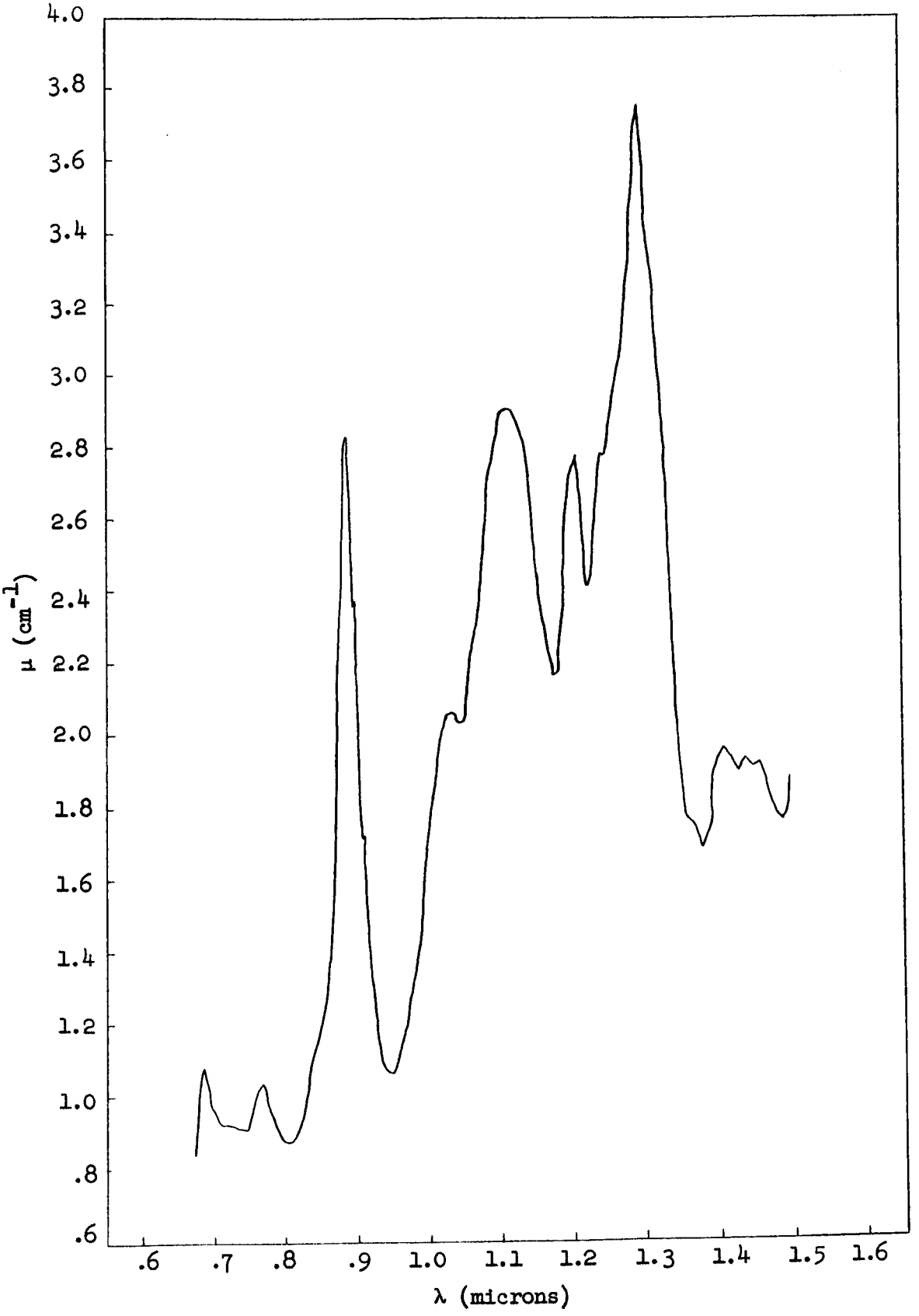

Fig. 42--Infrared absorption spectrum - 0.5 ohm-cm QC silicon before irradiation

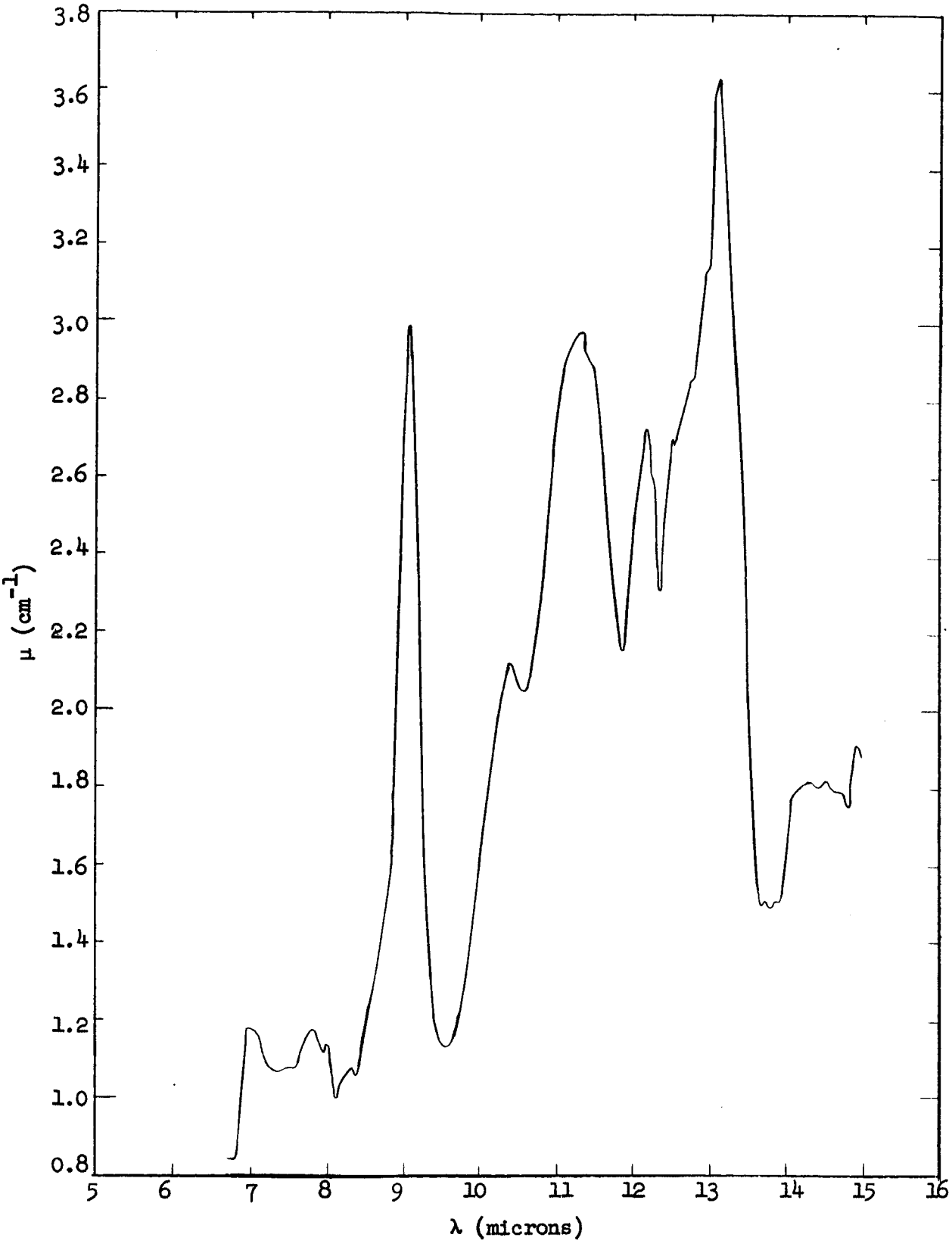

Fig. 43--Infrared absorption spectrum - 0.5 ohm-cm QC silicon (2.3×10^{16} electrons/cm^2)

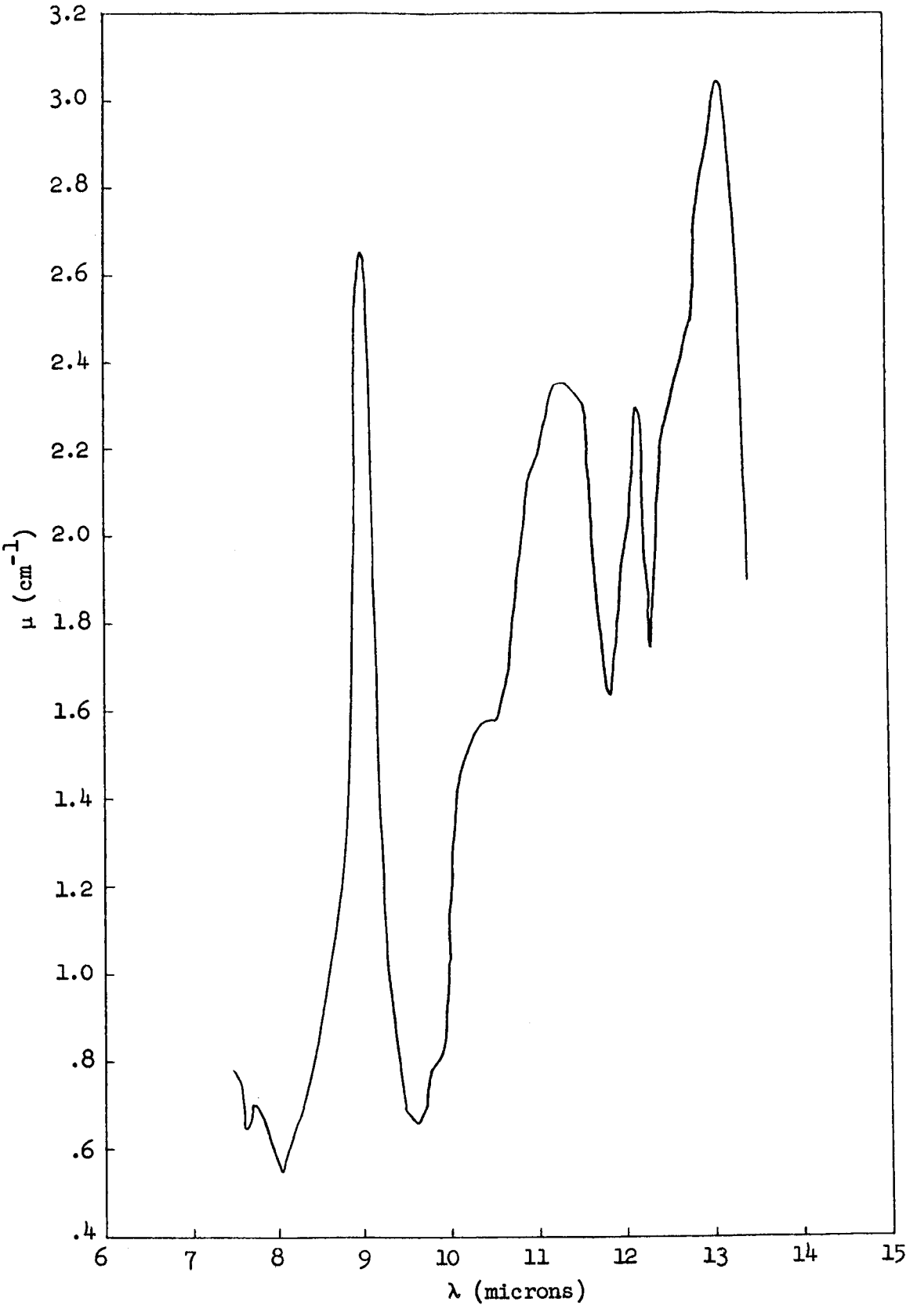

Fig. 44--Infrared absorption spectrum - 0.5 ohm-cm QC silicon before irradiation

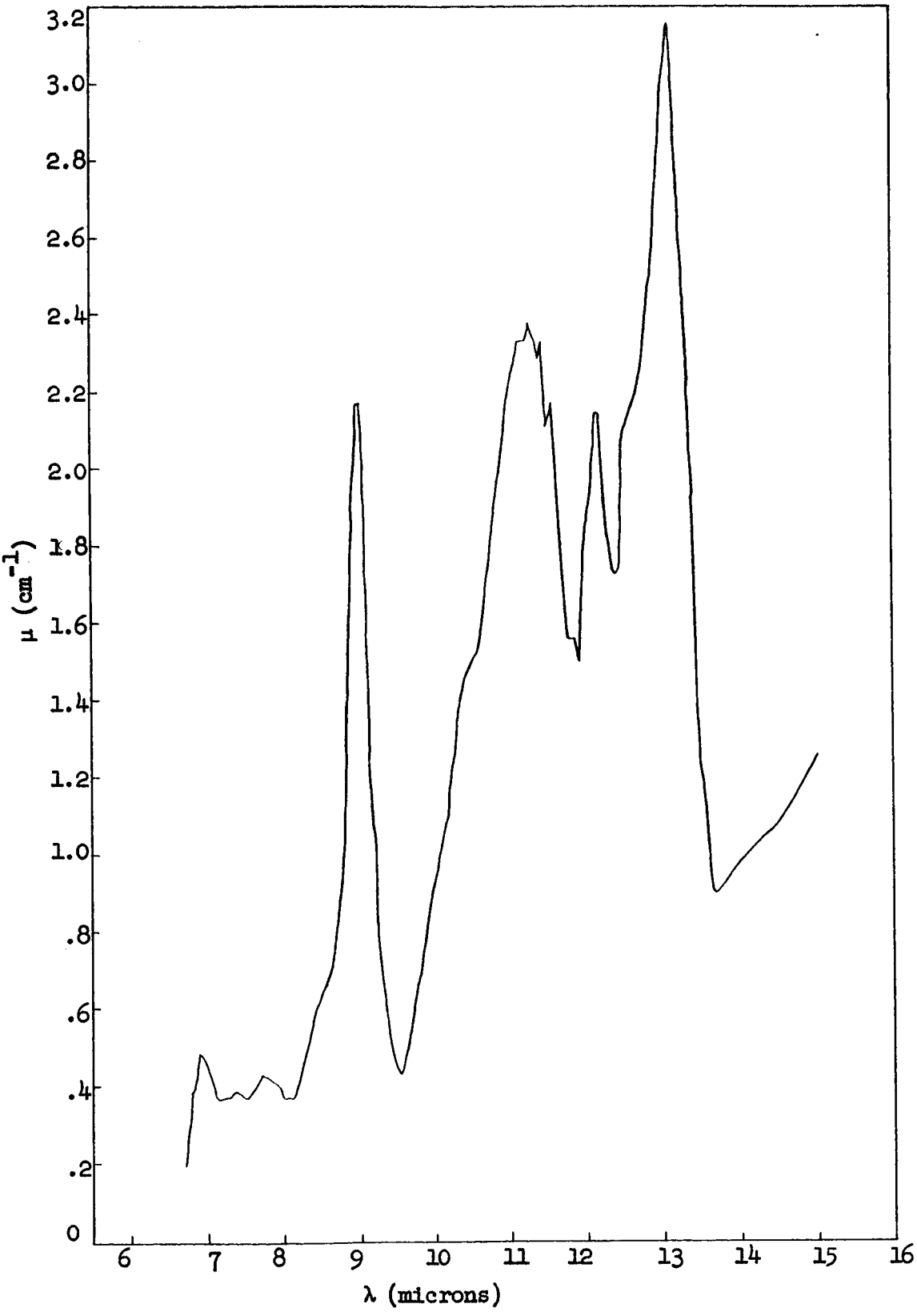

Fig. 45--Infrared absorption spectrum - 0.5 ohm-cm QC silicon (2.5×10^{17} electrons/cm^2)

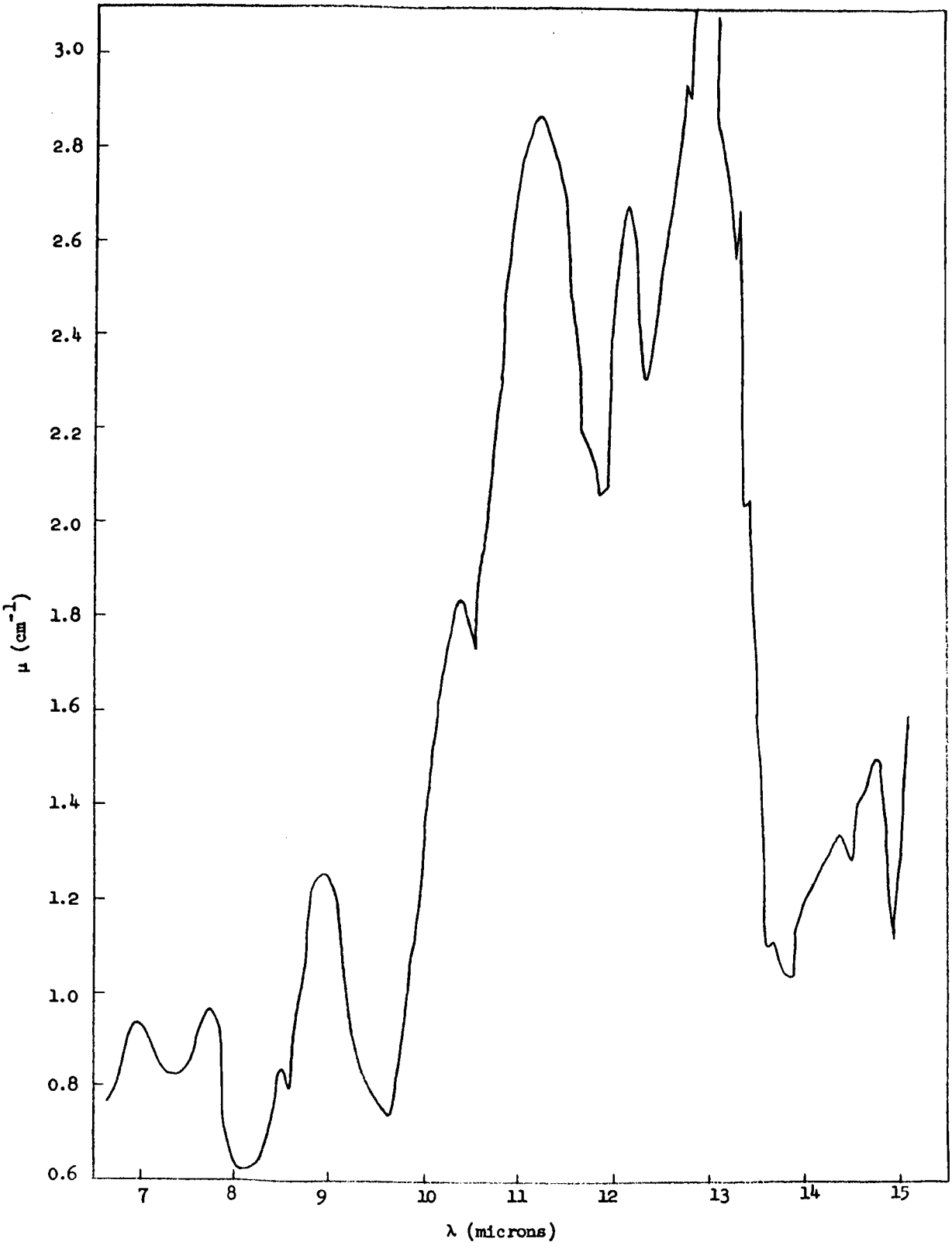

Fig. 46--Infrared absorption spectrum - 0.4 ohm-cm FZ silicon before irradiation

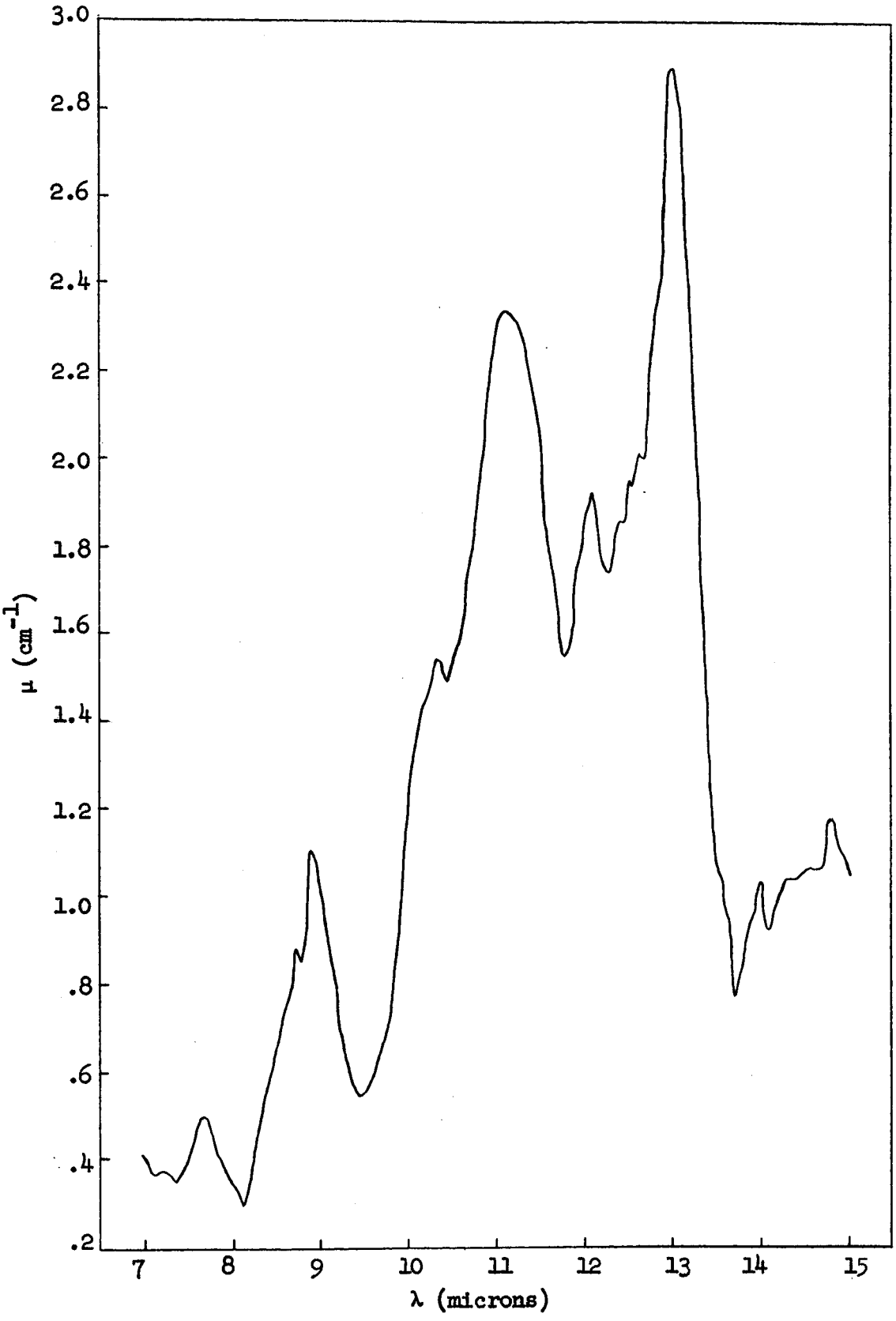

Fig. 47--Infrared absorption spectrum - 0.4 ohm-cm FZ silicon (2.4×10^{17} electrons/cm^2)

the oxygen concentration in this material was probably less than 10^{17} oxygen/cm^3.

7.3 DISCUSSION

It is apparent from the infrared absorption curves shown in Figs. 42 through 47 that there is no evidence of an increase in absorption in the vicinity of 12 microns associated with the production of substitutional oxygen (A centers). This lack of response was at first considered to be surprising until it was discovered that the galvanomagnetic measurements and the lifetime measurements did not reveal the presence of A centers either. Furthermore, the A centers which were finally identified by electron spin resonance measurements appeared to be in concentrations too small to be observed by the 12-micron absorption. All of these measurements seem to indicate that the irradiation by higher-energy electrons, which are similar to high-energy protons in producing small clusters of defects, does not produce a proportionately larger concentration of A centers. Instead, the clustering radiation appears to produce other defect centers, such as the center with an ionization energy of 0.12 ev which dominates the recombination property changes.

VIII. SUMMARY AND CONCLUSIONS

This research program has resulted in the development of techniques for measuring excess carrier recombination rates as a function of excess carrier density. These techniques are capable of yielding detailed insight into the nature of the defects responsible for the decrease in carrier lifetime in silicon as a result of irradiation. In addition, the following details have been added to our fund of knowledge concerning radiation effects:

1. The rate of change of minority carrier lifetimes upon irradiation in n-type materials prepared by floating-zone or quartz crucible growing are not appreciably different.
2. The defect level which dominates the excess carrier recombination in the vicinity of room temperature appears to have an ionization energy of 0.12 ev. A Hall coefficient measurement, which also reveals this level, suggests that it is an acceptor located approximately 0.12 ev below the conduction band. The nature of this level has not yet been established. Its apparent position may also be incorrect due to a temperature dependence of the capture cross sections.
3. Studies of the excess carrier recombination rates as a function of excess carrier concentrations indicate that there is a strong dependence of carrier lifetime on excess carrier density after irradiation. The form of this dependence suggests that, for either the electron or hole, a capture cross section is a strong function of temperature.
4. The observation that the excess carrier lifetime appears to increase suddenly in the vicinity of liquid nitrogen temperatures suggests that the recombination center dominant in this vicinity may be characterized by more than two charge states and hence undergoes a transition between the recombination and trapping behavior in this vicinity.
5. The possibility of doping silicon with a chemical defect that will act as a sink for the mobile vacancy to create secondary stable defects which are inactive as recombination centers, depends upon the nature of the 0.12 ev center. If it is identified as a secondary defect, this possibility remains and its implementation should be explored by studies of the temperature-dependent annealing behavior leading to the formation of the 0.12-ev center.

IX. PERSONNEL

The following personnel have participated in this research program. The principal investigator has been Dr. V. A. J. van Lint, head of the Radiation Effects Group, who has also conducted the carrier recombination studies. The galvanomagnetic measurements were conducted by Dr. E. G. Wikner, Mr. J. W. Harrity and Mr. H. Horiye. The development of the electron spin resonance equipment was supervised by Dr. D. M. J. Compton, assisted by Mr. M. E. Wyatt, Jr. The measurements were supervised by Dr. D. Snowden and performed by Mr. Wyatt. The infrared absorption measurements were supervised by Dr. S. Kurnick, assisted by Mr. R. F. Goff. Mr. D. K. Nichols assisted with the theoretical analysis in support of this work.

The data analysis for the carrier recombination studies were performed by Miss S. K. Boehm and Mrs. C. M. Faulkner. Miss Boehm also performed the modifications on the computer program necessary to perform the data reduction.

Support for the experimental program was provided by technicians from the Radiation Effects Group, including Messrs. R. Denson, H. Gomez, H. Güereña and G. B. Burns. Mrs. Nancy Hubble assisted with the preparation of the semiconductor samples.

We are indebted to Mr. G. M. Kelly for the design and construction of the semi-automatic film reader system and to the staff of the General Atomic Electron Linear Accelerator, who provided the accelerator beam with the required characteristics for performing these measurements.

REFERENCES

1. Abrahamson, A. A., R. D. Hatcher, and G. H. Vineyard, Phys. Rev. 121, 159 (1961).

2. Silsbee, R. H., J. Appl. Phys. 28, 1246 (1957).

3. Seitz, F., and J. S. Koehler, "Displacement of Atoms During Irradiation,", Solid State Physics, ed. F. Seitz and D. Turnbull, (Academic Press, New York, 1956) Vol. 2, pp. 305 ff..

4. Loferski, J. J., and P. Rappaport, Phys. Rev. 111, 432 (1958).

5. Watkins, G. D., and J. W. Corbett, Phys. Rev. 121, 1001 (1961).

6. Wertheim, G. K., Phys. Rev. 110, 1272 (1958).

7. Corbett, J. W., G. D. Watkins, et al., Phys. Rev. 121, 1015 (1961).

8. Watkins, G. D., J. W. Corbett, and R. M. Walker, Journ. Appl. Phys. 30, 1198 (1959).

9. Galkin, G. N., N. S. Rytova, and V. S. Vaviolov, Soviet Phys. Solid State 2, 1819 (1961).

10. Wertheim, G. K., Journ. Appl. Phys. 30 , 1166 (1959).

11. Bemski, B., and W. M. Augustyniak, Phys. Rev. 108, 645 (1957).

12. Sonder, E., and L. C. Templeton, Bull. Amer. Phys. Soc. 5, 196 (1960).

13. Ibid., 3, 375 (1958).

14. Wertheim, G. K., Phys. Rev. 115, 568 (1959).

15. Wertheim, G. K. and D. N. E. Buchanan, Journ. Appl. Phys. 30, 1232 (1959).

16. Watkins, G. D., and J. W. Corbett, Discussions Faraday Soc. 31, 86 (1961).

17. Wertheim, G. K., Phys. Rev. 105, 1730 (1957).

REFERENCES (CONT.)

18. Fan, H. Y., and A. K. Ramdas, Journ. Appl. Phys., 30, 1127 (1959).

19. Hill, D. E., Phys. Rev. 114, 1414 (1959).

20. Fan, H. Y., and A. K. Ramdas, Bull. Amer. Phys. Soc. 5, 197 (1960).

21. Sullivan, M. V., and R. M. Warner, Jr., "Ohmic Contacts to Silicon and Germanium," Transistor Technology, Vol. 3, F. S. Biondi, ed. (D. Van Nostrand Co., Inc., Princeton, New Jersey, 1958) pp. 163 ff.

22. For a complete discussion of this type of system, see, for instance, Feher, G., "Sensitivity in Microwave Paramagnetic Resonance Adsorption Techniques," Bell System Tech. J., 36, 449 (1957).

23. Conwell, E. M., Proc. IRE 46, 1281 (1958).

24. Rauch, C. J., J. J. Stickler, et al., Phys. Rev. 105, 525 (1957).

25. Long, D., Phys. Rev. 120, 2024 (1960).

26. Long, D., and J. Myers, Phys. Rev. 115, 1107 (1959).

27. Brooks, H., Phys. Rev. 83, 879 (1951).

28. Shockley, W., and W. T. Read, Jr., Phys. Rev. 87, 835 (1952).

29. Nomura, K. C., and J. S. Blakemore, Phys. Rev. 112, 1607 (1958).

30. Ibid., 121, 734 (1961).

31. Galkin, G. N., N. S. Rytova, and V. S. Vavilov, Soviet Phys. Solid State 2, 1819 (1961).

32. Denny, J. M., R. G. Downing, and G. W. Simon, Space Technology Laboratories, Inc., Report 8653-6008-KU-000 (1962).

33. See, for instance, Watkins, G. D., and J. W. Corbett, Discussion Faraday Soc. 31, 86 (1961).

34. Watkins, G. D., J. W. Corbett, and R. M. Walker, Journ. Appl. Phys. 30, 1198 (1959).

APPENDIX

TEMPERATURE DEPENDENCE OF CAPTURE CROSS SECTIONS

The temperature dependence of hole and electron capture cross sections for radiation-induced defects has only recently received attention. Analysis by Wertheim[1,2] and Curtis [3] determined values for electron and hole cross sections (σ_n and σ_p) in which the assumption was made that $1/\tau_{no} = N_t \sigma_{no} v$ and $1/\tau_{po} = N_t \sigma_{po} v$ are constants with temperature. Here τ_{no} and τ_{po} are the minority carrier lifetimes in highly n-type and p-type material, N_t is the number of recombination centers, and v is the thermal velocity of the free carriers. The temperature dependent data on lifetimes is then used to find the value of the cross section and a temperature-dependent trapping energy level. As Wertheim points out, the value for the energy level calculated in this manner is somewhat different from that calculated by Hall coefficient measurements and may be due to the assumption of a constant minority lifetime with its implicit assumption that $\sigma \propto T^{-1/2}$. The values of attractive cross sections range in Ge and Si between 10^{-13} to 10^{-15} cm^2 and those for neutral centers between 10^{-15} to 10^{-17} cm^2.

Galkin et al.[4] are apparently the only group who have explicitly determined the temperature dependence of radiation-induced cross sections. They report, for n-type silicon, that σ_p is constant and that $\sigma_n \propto T^{-n}$ where $n > 1$. However, their experimental set-up is such that these results are of questionable value.

As yet no theoretical treatment has been applied specifically to determine the temperature dependence of radiation defects and it is only recently that Ascarelli[5] and Lax[6] have succeeded in accounting for the giant cross sections for chemical impurities. Ascarelli's quantum-mechanical treatment indicates that, at low temperatures (3 - 10°K), $\sigma \propto T^{-2.5}$; this is in agreement with experimental data for chemical trapping centers. The possible extension of this theory to higher temperatures and radiation-induced defects is being studied.

References

1. G. K. Wertheim, Phys. Rev. 105, 1730 (1957).
2. G. K. Wertheim, Phys. Rev. 110, 1272 (1958).
3. O. L. Curtis, Journal Appl. Phys. 30, 1174 (1959).

4. G. N. Galkin, N. S. Rytova, and V. S. Vavilov, Fizika Tverdogo Telà 2, No. 9, 2025 (1960).

5. G. Ascarelli and S. Rodriguez, Phys. Rev. 124, 1321 (1961).

6. M. Lax, Phys. Rev. 119, 1502 (1960).